

Molecular Dynamics Simulations of
Amphiphilic Macromolecules at Interfaces

A Thesis

Submitted to The University of Manchester

For the Degree of

Doctor of Philosophy (PhD)

In The Faculty of Engineering and Physical Sciences

Selina Nawaz

School of Chemical Engineering and Analytical Science

2013

Contents

List of Figures	7
List of Tables	9
Abstract	11
Declaration	13
Copyright	15
Acknowledgments	17
1 Introduction	19
1.1 Motivation and Background.....	19
1.2 Thesis Overview.....	22
1.3 References.....	23
2 Molecular Dynamics Simulations	25
2.1 Introduction.....	25
2.2 Force Field.....	28
2.2.1 Non-bonded Interactions.....	30
2.2.2 Bonded Interactions.....	32
2.3 Periodic Boundary Conditions (PBC).....	33
2.4 Cut-off.....	34
2.5 Long Range Forces Particle Mesh Ewalds (PME).....	35
2.6 Ensembles.....	36
2.6.1 Thermostat.....	38
2.6.2 Barostat.....	39
2.7 Classical Mechanics.....	41
2.7.1 Finite Difference Methods.....	42
2.8 Constraint Algorithm.....	44
2.9 References.....	47

3	Stability of Amphiphilic Dendrimers at the Water/Air Interface	51
3.1	Introduction.....	51
3.2	Computational Details.....	53
3.3	Results.....	55
3.3.1	Structural Properties of the Dendrimer at the Interface.....	55
3.3.2	Hydrogen Bonds and Particle Stability.....	61
3.4	Summary and Conclusions.....	67
3.5	References.....	69
4	Interactions of PEO-PPO-PEO block copolymers with lipid membranes: a computational and experimental study linking membrane lysis with polymer structure	74
4.1	Introduction.....	74
4.2	Systems under Investigation.....	74
4.3	Methods.....	77
4.3.1	Simulations.....	77
4.3.2	Haemolysis assay.....	79
4.4	Analysis Performed.....	80
4.4.1	Order Parameter.....	80
4.4.2	Radius of Gyration.....	81
4.4.3	Mass Density Distribution.....	81
4.4.4	Head group P-N tilt angle.....	81
4.5	Results and Discussions.....	82
4.5.1	Validations of the force field parameters and polymer structure.....	82
4.5.2	Effect of Pluronics on the membrane structure stability.....	84
4.5.3	Area per lipid and membrane bending.....	84
4.5.4	Lipids order parameter and packing properties.....	89
4.5.5	Orientation of the lipid heads.....	95
4.5.6	Comparison between simulation and experimental results.....	96
4.6	Summary and Conclusions.....	98
4.7	References.....	100
4.8	Supporting Information.....	104

5	Biological Effects of PEO-PPO-PEO Block Copolymers: Relationship between Polymer Composition and their Interactions with Biological Membranes	111
5.1	Introduction.....	111
5.2	Materials and Methods.....	113
5.2.1	Materials.....	113
5.2.2	Cell Culture.....	113
5.2.3	MTS Metabolism Assay.....	113
5.2.4	LDH Release Assay.....	114
5.2.5	Determination of Polymer Membrane Binding Constants.....	115
5.2.6	Erythrocyte Protection Assay.....	116
5.2.7	JC-1 Mitochondrial Membrane Potential Assay.....	116
5.2.8	Molecular Modelling.....	117
5.2.9	Statistical Analysis.....	117
5.3	Results.....	117
5.3.1	MTS Metabolism Assay.....	117
5.3.2	LDH Release Assay.....	119
5.3.3	Haemolysis Assay.....	120
5.3.4	Erythrocyte Protection Assay.....	121
5.3.5	JC-1 Mitochondrial Membrane Potential Assay.....	122
5.4	Discussions.....	123
5.5	Conclusions.....	126
5.6	References.....	127
5.7	Supporting Information.....	130
6	Coarse Graining Poly-ethylene-oxide-Poly-propylene-oxide-Poly-ethylene-oxide (PEO-PPO-PEO) Block Copolymers using the MARTINI Force Field	133
6.1	Introduction.....	133
6.2	Computational Details.....	136
6.2.1	Atomistic Simulations.....	137
6.2.2	Coarse-grain Simulation.....	137
6.3	Development of the CG Model.....	138
6.3.1	Mapping Scheme.....	138
6.3.2	Parameterisation of the Bonded Part of the CG Potential.....	139

6.3.3	Parameterisation of the Non-bonded Part of the CG Potential.....	142
6.4	Results and Discussions.....	143
6.4.1	Homopolymer Validation.....	143
6.4.2	Pluronics.....	151
6.5	Conclusion.....	154
6.6	References.....	155
7	Conclusions and Future Work	161
7.1.	Conclusions.....	161
7.2.	Future Work.....	163
7.2.1	Atomistic Studies.....	163
7.2.2	Coarse-grain Model.....	164
7.3.	References.....	164
A	Reprint: Stability of Amphiphilic Dendrimers at the Water/Air Interface	166
B	Reprint: Interactions of PEO-PPO-PEO block copolymers with lipid membranes: a computational and experimental study linking membrane lysis with polymer structure	168
C	Reprint: Biological Effects of PEO-PPO-PEO Block Copolymers: Relationship between Polymer Composition and their Interactions with Biological Membranes	170
D	Radius of gyration values for PEO and PPO homopolymers	172

Word count: 41,279

List of Figures

1.1	Self-assembled structures formed by amphiphilic molecules.....	20
2.1	Multiscale modelling diagram.....	26
2.2	Bond stretching.....	31
2.3	Angle stretching.....	32
2.4	Dihedral bond.....	32
2.5	Two dimensional periodic system and spherical cut-off.....	33
2.6	Lennard Jones cut-off illustrating truncations, shift and switch methods.....	35
2.7	Leap frog integration method.....	44
2.8	Shake algorithm illustration.....	46
3.1	Poly(amino-amide) dendrimers.....	55
3.2	Degree of prolateness and surface area (SA) for the fully functionalised and Janus dendrimers at the interface.....	58
3.3	Snapshots of fully modified and Janus dendrimers at the interface.....	59
3.4	Mass density distributions for fully functionalised dendrimer and Janus dendrimer.....	60
3.5	Inter-dendron radial distribution function.....	61
3.6	Hydrogen bonds and short range coulomb energy for fully functionalised PAMAM dendrimer.....	63
3.7	Hydrogen bonds and short range coulomb energy for un-functionalised PAMAM dendrimer.....	63
3.8	Root mean square function of hydrogen atoms attached to the alkyl chain of the Janus and fully functionalised dendrimers when the dendrimer is in the water phase and when the dendrimer is at the interface.....	66
3.9	Area per dendrimer for fully functionalised dendrimer and Janus dendrimer	68
4.1	Average area per lipid for Pluronic membrane systems.....	88
4.2	Phosphor-phosphor (P-P) density profiles for Pluronic membrane systems...	89
4.3	Snapshots of Pluronic absorbed in DPPC bilayer membrane.....	90
4.4	Deuterium order parameter for DPPC tails.....	92
4.5	Free area profile for Pluronic in membrane systems.....	94
4.6	DPPC mass density profiles.....	95

4.7	Close packed area for Pluronics in membrane systems.....	95
4.8	Angle distribution of angle between the vector joining the P-N atoms of the DPPC lipids.....	98
4.9	Kinetics and haemolysis during exposure to Pluronics.....	100
5.1	Effect of Pluronics on MTS metabolism in Caco-2 cells.....	119
5.2	Effect of Pluronics on LDH release in HMEC-1 and Caco-2 cells.....	121
5.3	Affinity of Pluronics for erythrocyte membranes.....	122
5.4	Effect of Pluronic copolymers on erythrocyte lysis induced by hypotonic stress.....	123
5.5	Effect of Pluronic treatment on mitochondrial membrane potential in Caco-2 cells.....	123
5.6	Snapshot of L31 absorbed in DPPC bilayer after 200ns of a MD simulation..	127
6.1	Superposed description of an atomistic and CG Pluronic molecule.....	140
6.2	Bonded distributions for homopolymers, PEO and PPO.....	142
6.3	Bonded interactions for PEOPPO interconnecting beads in Pluronics.....	142
6.4	Radius of gyration of PEO homopolymers.....	146
6.5	Radius of gyration of PPO homopolymers.....	146
6.6	Flory characteristic ratio for PEO homopolymers.....	147
6.7	Flory characteristic ratio for PPO homopolymers.....	148
6.8	Temperature transferability of PEO30 in water.....	150
6.9	Temperature transferability of PPO30 in water.....	151
6.10	The radius of gyration.....	153
6.11	Temperature transferability of the OPLS-AA force field.....	154
6.12	Temperature transferability of the MARTINI force field.....	155

List of Tables

3.1 Dendrimer systems simulated.....	55
3.2 Radius of gyration (R_g), eigenvalues (λ_i) and aspect ratios (α) of the gyration tensor.....	57
4.1 Copolymer partial charge distribution from DFT calculations.....	79
4.2 Characteristics of Pluronic systems.....	83
4.3 Comparison between the values of radius of gyration of a single block copolymer chain simulated in hexane at 300K.....	84
4.4 Area per lipid and membrane thickness of DPPC membrane.....	87
5.1 Polymer composition and measured cytotoxicity endpoints.....	115
6.1 Characteristics of Pluronics investigated for the MARTINI force field model.....	138
6.2 Bonded interactions for the coarse-grain Pluronics.....	141
6.3 Non-bonded interactions for the coarse-grain Pluronics.....	144
6.4 Radius of gyration data for PEO and PPO homopolymers.....	145
6.5 Bulk density data for PEO dimers.....	148
6.6 Temperature transferability tested on PEO30.....	149
6.7 Temperature transferability tested on PPO30.....	150
6.8 Radius of gyration for varying lengths of PPO in hexane.....	152
6.9 Radius of gyration for Pluronics, L31, L61, L62 and L64 in solution.....	152

Molecular Dynamics Simulations of Amphiphilic Macromolecules at Interfaces

Selina Nawaz, The University of Manchester, 10th April 2013

Submitted for the degree of Doctor of Philosophy

Abstract

The aim of this thesis is to investigate the structural and thermodynamic properties of biologically and technological relevant macromolecules when placed at soft interfaces. In particular two amphiphilic macromolecules characterized by different topologies have been investigated namely amphiphilic dendrimers and linear block copolymers. This goal is achieved using a multiscale approach which includes all-atom, united atom and coarse grained models by means of molecular dynamic simulations.

Amphiphilic dendrimers have shown to be promising building blocks for a range of interfacial materials and can be used in applications such as surface-base sensors or surface nanopatterning. In this part of the thesis by means of all-atom molecular dynamics simulations, we investigated the structure and stability of alkyl-modified polyamido-amide (PAMAM) dendrimers at the air/water interface as a function of the number and the relative position of the modified end groups. We found that the PAMAM dendrimer with all terminal groups functionalized is more stable at the interface than the Janus dendrimer, where only half the amine groups are modified. These results indicate that monolayers of fully functionalized molecules could be as stable as (or more stable than) those self-assembled from Janus molecules.

The second part of the thesis is devoted to model a particular family of amphiphilic triblock copolymer sold as Pluronics, consisting of poly(ethylene oxide) (PEO) and poly(propylene oxide) (PPO) arranged as PEO–PPO–PEO. There is evidence that this class of amphiphilic materials can be used for different biological applications. A fuller understanding of the molecular mechanisms underpinning their interactions with living cells is essential for ensuring the polymers safety and efficacy in biomedical applications. Using united-atom molecular dynamics simulations and membrane lysis assays, we investigated the relationship between the molecular conformations of a subset of the Pluronic copolymers (L31, L61, L62 and L64) and their haemolytic activity. Our computational studies suggest that the hydrophilic blocks in these copolymers interact with the polar head groups of lipid molecules, resulting in a predicted modification of the structure of the membranes. Parallel membrane lysis assays in human erythrocytes indicate differences in the rates of haemolysis, as a result of incubation with these polymers, which correlate well with the predicted interactions from the atomistic simulations. The computational data thus provide a putative mechanism to rationalize the available experimental data on membrane lysis by these copolymers. The data quantitatively agree with haemoglobin release endpoints measured when copolymers with the same molecular weight and structure as of those modelled are incubated with erythrocytes. The data further suggest some new structure–function relationships at the nanoscale that are likely to be of importance in determining the biological activity of these otherwise inert copolymers.

In order to visualise the effect of Pluronics at a length and time scale closer to the experimental one, in the third part of the thesis we developed a coarse-grained model for the amphiphilic copolymers within the framework of the MARTINI force-field (Marrink *et al.*, *J. Phys. Chem. B*, 2007, **111**, 7812). The MARTINI force field is usually parameterized targeting thermodynamic properties. In addition to this, we further parameterized it based on atomistic simulations validating the parameters against structural properties of the copolymers. The ability of the model to predict several structural and thermodynamic properties of the atomistic system have been explored. The aim of this work is to be able to simulate the polymer/lipid interface at polymer concentration similar to the experimental one.

Declaration

The University of Manchester

PhD by published work Candidate Declaration

Candidate Name: Selina Nawaz

Faculty: Engineering and Physical Sciences

Thesis Title: Molecular Dynamics Simulations of Amphiphilic Macromolecules at Interfaces

Declaration to be completed by the candidate:

I declare that no portion of the work referred to in the thesis has been submitted in support of an application for another degree or qualification of this or any other university or other institute of learning.

Signed:

Date: 10th April 2013

Copyright

The author of this thesis (including any appendices and/or schedules to this thesis) owns certain copyright or related rights in it (the “Copyright”)¹ and s/he has given The University of Manchester certain rights to use such Copyright, including for administrative purposes.

Copies of this thesis, either in full or in extracts and whether in hard or electronic copy, may be made only in accordance with the Copyright, Designs and Patents Act 1988 (as amended) and regulations issued under it or, where appropriate, in accordance with licensing agreements which the University has from time to time. This page must form part of any such copies made.

The ownership of certain Copyright, patents, designs, trade marks and other intellectual property (the “Intellectual Property”) and any reproductions of copyright works in the thesis, for example graphs and tables (“Reproductions”), which may be described in this thesis, may not be owned by the author and may be owned by third parties. Such Intellectual Property and Reproductions cannot and must not be made available for use without the prior written permission of the owner(s) of the relevant Intellectual Property and/or Reproductions.

Further information on the conditions under which disclosure, publication and commercialisation of this thesis, the Copyright and any Intellectual Property and/or Reproductions described in it may take place is available in the University IP Policy (see <http://documents.manchester.ac.uk/DocuInfo.aspx?DocID=487>), in any relevant Thesis restriction declarations deposited in the University Library, The University Library’s regulations (see <http://www.manchester.ac.uk/library/aboutus/regulations>) and in The University’s policy on Presentation of Theses.

¹ This excludes material already printed in academic journals, for which the copyright belongs to said journal and publisher. Pages for which the author does not own the copyright are numbered differently from the rest of the thesis.

Acknowledgments

I would like to acknowledge and extend my heartfelt gratitude to my supervisor Dr Paola Carbone for her direction, assistance, and guidance. In particular, her recommendations and suggestions have been invaluable towards the studies carried out. She has made the achievements in this thesis possible.

I would also like to thank Martin Redhead, Guiseppe Mantovani, Cameron Alexander and Cynthia Bosquillon for the opportunity to work on an amazing collaboration project. The project began as a side project, but the tremendous prospects after publishing two high impact journal articles, soon brought this study to the frontline of my research. This project has opened many doors and is the beginning of a great long term research study. I would like to give a great appreciation to Professor Alessandro Troisi for performing DFT calculations for the systems studied in this project.

A special thank you to all my colleagues, past and present from C19 has to be made for their help and motivation. The lunchtime Bridge games and long natters are an important part of my PhD experience that I will never forget. I mustn't forget the non C19 members that also played a great role in making this process pleasurable. The academic staff from the department including Dr Leo Lue, Prof Andrew Masters and Dr Flor Siperstein whom supported my achievements and helped me through my struggles when I pestered them with obstacles I faced also must to be thanked for their patience and guidance.

I would like to thank all my family and friends and especially my best friend Vicky who encouraged, listened and supported me through the course of my PhD. I will never forget the support and patience she had towards me, especially at the times when I felt the whole world collapsed around me.

Finally, and most importantly I would like to thank my Mum and Dad who have supported me in many aspects and stood beside me. I would not be where I am today, if it was not for them. As a small token of gratitude and love, I would like to dedicate this thesis to them.

Ultimately God has made all things possible and I would just like to say thank you as opposed to always asking.

Chapter One

Introduction

This chapter outlines the background and motivation to the work presented in this thesis. It begins with the definition of amphiphilic macromolecules and continues with a brief introduction to the morphology of their self-assembled structures, alongside their potential vast application in a range of fields. The importance of studying the structural features of these molecules at interfaces is also discussed, with particular attention to the biological interface. Finally, the format and content of the remainder of this thesis are outlined.

1.1 Motivation and background

Amphiphiles are the fundamental components of living matter and important materials for various technologies [1-3]. The structure of amphiphilic molecules generally includes two chemically incompatible compounds, more specifically a water loving (hydrophilic) and water hating (hydrophobic) components which are structurally connected. Amphiphilic molecules can comprise of a wide variety of molecular structures including lipids, cholesterol, peptides and synthetic polymers in the form of block copolymers, star polymers and dendrimers. Amphiphilic molecules can also be defined as lyotropic as they forms liquid crystal phases due to the addition of a solvent [4]. The most important features of amphiphilic molecules is that they are able to alter interfacial properties of solid surfaces and liquid/liquid interfaces. When dissolved in polar or apolar solvent they in fact migrate at the interface and modify its structure and thermodynamic properties. When the concentration of amphiphiles increases above a certain threshold (known as critical micelle concentration, CMC) they have a propensity to microphase separate on the mesoscale and develop complex structures which in themselves contain many internal surfaces [5].

When mixed with polar solvent such as water, the process of self-assembly is driven by their hydrophobic effect. The self-assembled aggregates so formed are structured so that the hydrophobic parts of the amphiphiles are shielded from the aqueous surroundings by it hydrophilic counterpart. Amphiphilic molecules are able to form a wide variety of structures ranging from micelles, bilayer to bicontinuous cubic

structures. Lyotropic liquid crystalline phases are typically seen when the concentration of the amphiphiles are increased to a point where the micellar aggregates begin to arrange regularly in space. The change in concentration, temperature and other physicochemical parameters are what initiates the formation of complex liquid crystalline phases. The latter can range from micellar cubic to lamellar phases which incorporate stacks of bilayers [4-6]. The self-assembly properties shown by amphiphilic molecules are used in a wide variety of applications including in the formulation of personal to house care products, textiles and more recently even in pharmaceutical products [7].

Amphiphilic molecules are also of principle importance in biological processes. Lipid molecules are one example of a significant class of amphiphilic molecules. Their structure generally consists of polar hydrophilic head group usually attached to two very hydrophobic non polar tails. In polar solvents, i.e. water, they are able to self-assemble into a variety of structures ranging from small spherical micelles to large vesicles and even lamellae (Fig. 1.1).

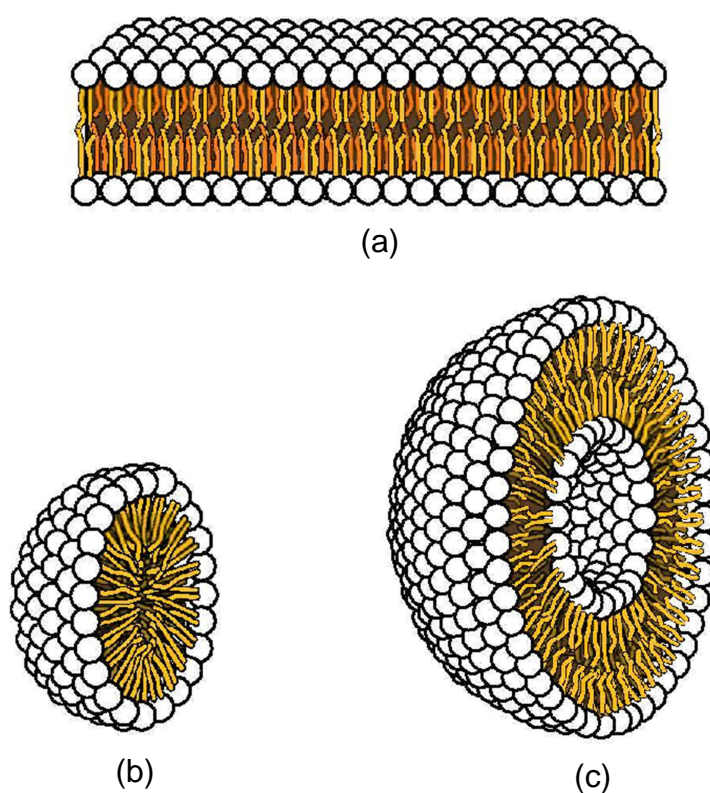


Figure 1.1: An example of self-assembled structures formed by amphiphilic molecules. (a) a bilayer, (b) a micelle and (c) a liposome vesicle [8].

A common element shared by many of these self-assembled structures is the lipid bilayer arranged in a smectic liquid crystal phase, which includes two opposing lipid monolayer sheets with the hydrophobic tails protected from water in the centre by the outer hydrophilic head groups. These bilayers flow like liquids yet exhibit crystal solid like orientational order. The membrane shape is preserved by their rigidity however this ordered structure regulates the transport of molecules in and out of the cell. Lipid bilayers provide the basic frame for biomembranes hence they play a central role in biophysics [9, 10].

An interface can be defined as a surface where there is a common boundary between two opposing phases such as two immiscible liquids, an insoluble solid with a liquid, a liquid with an insoluble gas or simple a liquid and vacuum. Interfaces can vary in size and shape, they can generally be considered as flat or spherical with finite or infinite radius. The size of the surface can reflect the effect of surface phenomena, and the importance of the interface depends on the system type under investigation. Processes that occur at the interface are ruled through the function of surface tension. Surface tension is significant in many common amphiphilic important matter including surfactants. The existence of interfaces in biological matter is an important area of study, for example to understand interactions between biomolecules and surfaces. Interfaces in biological matter can exist in conjunction with a number of matter, however a ubiquitous component of living cells are interfaces between biological membranes and water. The interfaces between water and membranes play an important role in many medical and pharmacological interesting phenomena. A range of biologically relevant processes occur in the proximity of these boundaries for example the transport of different chemical species like ions and nutrients, the mediation of immune response, transmission of neural signals and membrane fission. In drug delivery it is of fundamental importance to understand how small molecules interact and translocate across membranes. Understanding water membrane interfaces could answer many fundamental questions about the evolution of cells as it could be claimed that many essential bilayer functionalities may occur at these interfaces [11].

This thesis investigates the behaviour of different amphiphilic macromolecules at air/water and water/lipid interface focusing not only on the macromolecular properties but also on how its presence affects the interface itself.

1.2 Thesis Overview

This thesis is presented in an alternative format, according to the thesis submission guidelines allowed by The University of Manchester¹. As such, chapters throughout the thesis are presented in the format they were submitted or due for submission to refereed journals. Any original contribution of the author toward each chapter has been clearly identified at the beginning of each chapter. Finally Reprints of published work is included in the Appendices (see A-C).

The thesis is organised into two parts. The first part of this thesis (Chap. 2) introduces the background and theory of molecular dynamic (MD) simulations. A multiscale approach to MD simulations is discussed concentrating on the force fields that are used throughout the rest of the thesis. Furthermore the functions and parameters that are specifically adapted by the systems studied in following chapters are also presented in this chapter.

The second part of this thesis written in the form of journal articles then focuses on the actual systems under investigation (Chap. 3-7). Chapter 3 discusses the stability of amphiphilic dendrimers at water/air interface using an all-atom approach. Chapter 4 and 5 are based on a collaboration study with an experimental group from The University of Nottingham where the investigation into the cytotoxic effects of amphiphilic block copolymers (Pluronics) are evaluated. Chapter 4 uses united atom MD simulations and is primarily the work carried out by the author of this thesis, while chapter 5 is the experimental work done by the collaborators to integrate the computational work discussed in chapter 4. In chapter 6 the development of a coarse grain model for the Pluronics is presented. Finally a summary concluding the work throughout the thesis with directions and aspirations for future work is outlined in chapter 7.

¹ <http://www.socialsciences.manchester.ac.uk/intranet/pg/examprocess/documents/g-pres-theses-pgr.pdf>

1.3 References

1. Gompper, G., et al., *Phase Transitions and Critical Phenomena: Self-assembling amphiphilic systems*. 1994: Academic Press.
2. Israelachvili, J.N., *Intermolecular and surface forces*. 2nd Edition, ed. J. Israelachvili. 1991: Academic Press London.
3. Gelbart, W.M., et al., *Micelles, membranes, microemulsions, and monolayers*. 1994: Springer-Verlag.
4. Singh, D.A.D.a.S., *Liquid crystals: fundamentals*. 2002, Singapore: World Scientific Publishing Co. Pte. Ltd.
5. Goodwin, J., *Colloids and Interfaces with Surfactants and Polymers: An Introduction*. 2004: John Wiley & Sons.
6. Schmid, F., et al., *Amphiphiles at Interfaces: Simulation of Structure and Phase Behavior*, 2004.
7. Torchilin, V., *Targeted pharmaceutical nanocarriers for cancer therapy and imaging*. The AAPS Journal, 2007. **9**(2): p. E128-E147.
8. Villarreal, M.R., *Cross section of the different structures that phospholipids can take in a aqueous solution. The circles are the hydrophilic heads and the wavy lines are the fatty acyl side chains*, 2007.
9. Evans, D.F. and H. Wennerström, *The colloidal domain: where physics, chemistry, biology, and technology meet*. 1999: Wiley-VCH.
10. Cui, H., M.J. Webber, and S.I. Stupp, *Self-assembly of peptide amphiphiles: From molecules to nanostructures to biomaterials*. Peptide Science, 2010. **94**(1): p. 1-18.
11. Wilson, M.A. and A. Pohorille, *Molecular dynamics of a water-lipid bilayer interface*. Journal of the American Chemical Society, 1994. **116**(4): p. 1490-1501.

Molecular Dynamics Simulations

This chapter introduces some of the techniques used in molecular modelling and computational chemistry. The general formalism for molecular dynamics (MD) simulations is reviewed. A multiscale approach to MD simulations where coarse-grained models are developed from atomistic ones or experimental data is discussed. The molecular mechanics model is described focussing specifically on the functions and parameters that are used throughout this thesis. In particular several aspects of the algorithm typically implemented in a MD code are reviewed such as the use of periodic boundary conditions and the *ad-hoc* methods developed to treat long range interactions. The major role of classical mechanics in molecular dynamics simulations with particular focus on Newton's equation of motion and finite series method to tackle the many body problem is discussed together with the statistical mechanics relationship used to extract thermodynamic parameters such as temperature and pressure from the simulations. Finally the choice in time step and constraint algorithms is incorporated into the finite series method enabling the use of a larger time step and reducing computational time are also briefly described.

2.1 Introduction

Molecular modelling can be said to be a both an old and new concept in understanding the behaviour of systems at a molecular level. The foundation was laid with the development of quantum mechanics in the early parts of the twentieth century; however the implementation of the underlying framework into computational models and with the development of computational power in the last 35 years makes this also a fairly new concept. In general terms computational chemistry uses mathematical models to describe chemical processes and is important for explaining and predicting properties of materials complementing information produced experimentally which aims to help in reveal structural and thermodynamic properties. Molecular modelling can be used in many fields ranging from Chemistry, Pharmacology to Biology [1].

There are a number of simulation tools that can be used in molecular modelling, two of the most commonly utilized are Molecular Dynamics (MD) and Monte Carlo (MC) methods. Molecular simulations today still have many limitations, even with the advances in computational power. The time and length scale of a molecular system which can be modelled is dependent on the amount of degrees of freedom that are included in the model (Fig. 2.1). For example when the aim is to model with quantum theory a many body systems, the calculations are limited to very small time and length scale but the system is modelled with very high resolution revealing details about its electronic structure. The expansion of the time and length scale of the simulation can be achieved by reducing the degrees of freedom of the model ignoring, in the first approximation, the motion of the electrons and calculating the energy as a function of only the nuclear positions (classical simulations).

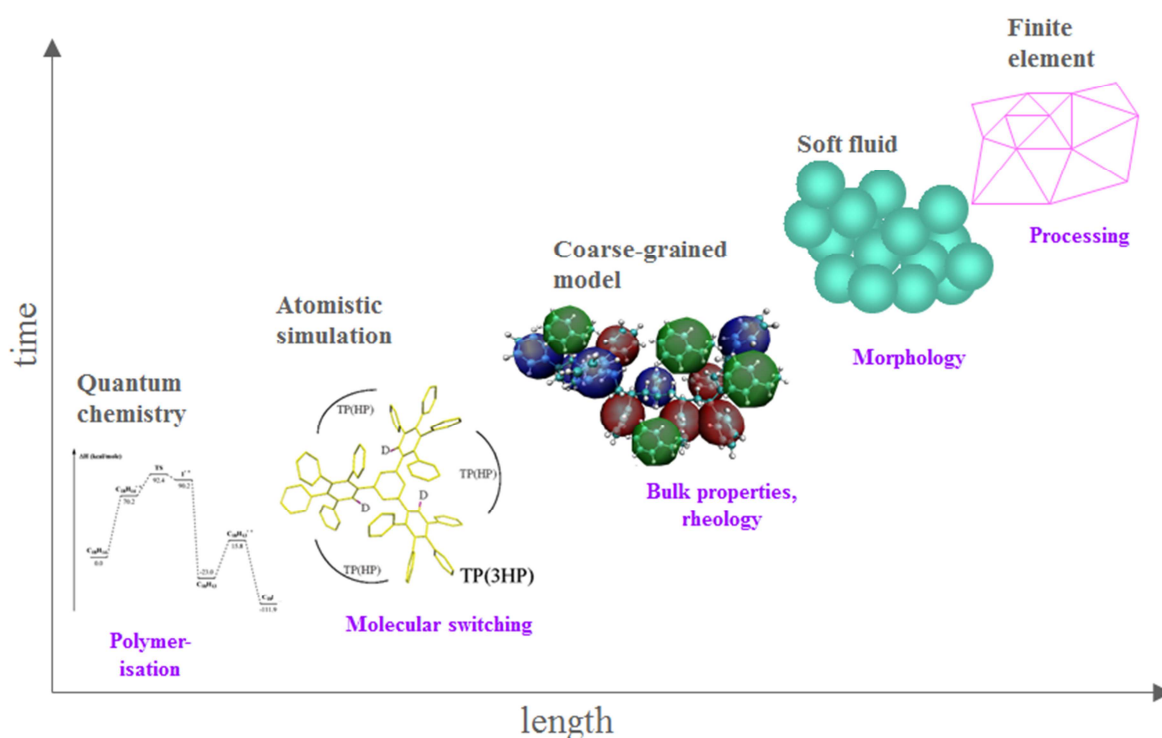


Figure 2.1: Multiscale modelling; the connection of time and length scale for molecular models illustrating the various levels of resolution

Molecular Dynamics (MD) was initially used to study simple models, for example the first was constructed to study the interaction of hard spheres by Alder and Wainwright in 1957 [2]. This model has led to the substantial understanding of the behaviour of simple liquids that has emerged from their studies. A crucial breakthrough

was in 1964 when the first simulation using a realistic potential from the liquid state of Argon was carried out by Rahman [3]. Rahman and Stillinger later carried out the simulation of water in 1974 which was the first molecular dynamics simulation of a realistic system [4]. It is more recent that molecular dynamics methods have been applied to more complex molecular systems due to the advancement of computational power [5]. In 1974 when the first protein model appeared with the simulation of the bovine pancreatic trypsin inhibitor (BPTI) [6]. If the literature was reviewed today, many studies related to molecular dynamics simulations of protein structure determination, protein-DNA complexes and even lipid systems can be found. Molecular dynamics simulations are nowadays routinely used to determine the structure, dynamics and thermodynamics of liquids and soft matter [7].

As mentioned before, classical simulations neglect the explicit treatment of the electrons and model the atoms as classical objects whose dynamics obeys to the Newton laws. This approximation enables to model molecular systems substantially larger than those treatable with quantum mechanics approaches even when semi empirical methods are used [8]. When a system is treated classically the interactions between the atoms are modelled with a specific set of mathematical functions and related parameters (known as force field). These sets of parameters encompass the quantum effects (mainly included in the two parameters used to describe the non-bonded interactions) and, while the mathematical functions are very often the same irrespectively to the simulated molecular system, they are usually specific for each chemical compound.

The functions and parameters associated to a force field can be derived from both experimental data such as XRD, NMR and high level quantum mechanical calculations performed on specific chemical systems. The outcome of a simulation controlled by the expressions for the total energy collectively is related to the force field. Generally in molecular simulations the interatomic potential is interpreted as the sum of bonded forces associated with chemical bonds, bond angles, dihedrals and non-bonded forces consisting of van der Waals and electrostatic forces. Depending whether the intermolecular potential describes the interactions between atoms or group of atoms, we can distinguish between all-atom, united atoms or coarse-grained force fields. In an all atom force field the parameters are assigned to each individual atom of the system; a united atom force field treats hydrogen's and carbons of methyl and methylene groups as a single interaction centre; and finally a coarse-grained force field reduces further the complexity of the system including several heavy atoms in single interaction centres [9].

2.2 Force Field

The selection of a force field depends on a number of choices subjecting to the molecular system under investigation and strictly depends on the size of the system, so small systems can be simulated in detail defining every atom in the system, however its simulation is then limited in the time scale. The simulation length and timescale can be increased when the number of interaction sites are decreased going from all-atoms to united atoms to coarse grained force fields. For the purpose of this research all three force fields are explored. The OPLS all atom [10], GROMOS united atom [11-13] and MARTINI coarse grained [14] force fields are used.

The OPLS (Optimized Potential for Liquid Simulations) comprises a set of functions and parameters developed at Purdue University and later at Yale University by Professor William L. Jorgensen's group and has been under development in his laboratories for almost 20 years [10]. This force field includes both united atom (OPLS-UA) and all atoms (OPLS-AA) force fields. A key characteristic feature of the OPLS parameters is that they were especially designed to fit the experimental properties of liquids for example density and boiling temperature of small organic molecules [15]. An extended literature can be found concerning the recent extension of the parameterization of the OPLS-AA force field for molecules of interest in the pharmaceutical industry [16].

The GROMOS (GRONingen MOlecular Simulation) united atom force field for molecular dynamics simulations was first developed at the University of Groningen and the laboratory for physical chemistry at the ETH in Zurich [11-13]. This force field is specifically developed for studying biomolecular systems such as proteins, nucleotides, sugars etc. The GROMOS force field has been validated against experimental data such as crystallographic and spectroscopic data for the bonded parameterisation and reproducing thermodynamic properties such as the density and the heat of vaporization for the non-bonded parameterisation [17]. The GROMOS force field has been also successfully applied to a range of chemical systems for example liquid crystals [18], polymers [19] and solutions of biomolecules [20]. The optimisation of the GROMOS force field has been performed for a number of systems ranging from proteins to fluid bilayers [21]. For the purpose of this thesis the GROMOS united atom force field with modifications from the work of Berger and co-workers (where they have altered the Lennard-Jones (LJ) parameters for the alkyl hydrocarbon chains in a

dipalmitolphosphatidylcholine bilayer to match accurate experimental density and heat of vaporisation values) has been used [22].

In order to develop force fields for models even coarser than the united atoms, different techniques can be used [23]. The MARTINI coarse grained force field [14] developed by Marrink and co-workers uses experimental thermodynamic data for the parameterisation process. These are determined by reproducing bulk densities and free energies of partitioning between polar and apolar phases [24]. Originally this force field was developed mainly to model phospholipids forming the biological membranes [14, 24], but it was later extended to model other chemical systems such as proteins [25], carbohydrates [26] and fullerene molecules [27]. The MARTINI coarse grain force field overcomes time and length scale limitations typical of the atomistic and united atoms simulations by grouping a cluster of atoms into a single particle or bead, reducing the overall number of particles in the system. In order to retain the chemical specificities of the system in the model, information coming from both experimental and detailed atomistic simulations are used to develop the potential interactions acting between the beads.

Molecular interactions are modelled using functional forms and related parameters which determine the systems internal energy. In molecular modelling the total internal energy (E_{tot}) of the system is usually written as the sum of the bonded (E_{bonded}) and non-bonded ($E_{\text{nonbonded}}$) components.

$$E_{\text{tot}} = E_{\text{nonbonded}} + E_{\text{bonded}} \quad (2.2.1)$$

The non-bonded energy is calculated as the sum of the electrostatic and weak dispersive interactions (van der Waals) acting among atoms that are separated by at least three covalent bonds. In most typical force fields, the non-bonded term is usually computed using a Coulomb and a Lennard-Jones potential to model the electrostatic interactions and the van der Waals interactions respectively. The non-bonded terms are typically parameterised for a range of functions which are obtained from liquid state calculations and performed for both intermolecular and intramolecular interactions. The bonded energy includes bond stretching, angle bending and torsional energy. The bonded interactions are usually parameterised from experimental data such as XRD and NMR experiments. The parameters for these terms are generally fitted to quantum chemical calculations, which have been systematically upgraded over the years for the force fields.

2.2.1 Non-bonded Interactions

The non-bonded van der Waals potential includes a combination of attractive forces due to dipole-dipole interactions and empirical repulsive forces due to Pauli repulsion. These non-bonded parameters can be fitted to reproduce experimental data or accurate quantum chemistry calculations. In some instances the Lennard-Jones parameters are customized empirically to match the experimental densities and enthalpies of vaporization. The atomic partial charges are usually obtained from geometry optimization calculations. The partial charges so obtained are generally fixed during molecular dynamics simulations unless a polarizable force field is used. The electrostatic potential is then fitted to obtain the charges.

The Lennard-Jones potential 12-6 ($V_{LJ}(r)$) is generally used to describe the van der Waals interactions (Eq. 2.2.2) and the Coulomb potential (V_c) is used to describe the charge charge interaction (Eq. 2.2.3).

$$V_{LJ}(r) = \sum_{i=1}^N \sum_{j=i+1}^N \left(4\epsilon_{ij} \left[\left(\frac{\sigma_{ij}}{r_{ij}} \right)^{12} - \left(\frac{\sigma_{ij}}{r_{ij}} \right)^6 \right] \right) \quad (2.2.2)$$

where the depth of the potential well is described as ϵ , the distance at which the inter-particle interaction is zero is σ , r is the distance between the particles, N is the total number of particles in the system and i and j are the particle pair for which the potential is calculated.

$$V_c = \frac{1}{4\pi\epsilon_0} \frac{q_i q_j}{r_{ij}} \quad (2.2.3)$$

where q_i and q_j are the partial charges of two particles i and j and r is the distance between two particles.

The non-bonded parameters are usually developed for every individual particle in the force field and combination rules are used to derive the pair potentials. The interactions between particles in the OPLS all atom force field uses the combination rule $\epsilon_{ij} = \sqrt{\epsilon_{ii}\epsilon_{jj}}$ and $\sigma_{ij} = \sqrt{\sigma_{ii}\sigma_{jj}}$ known as the Lorentz Berthelot rule [28]. This intramolecular non-bonded interaction is applied to atoms three bonds or more apart. Two atoms involved in a torsion interacting via the torsional potential (Eq. 2.2.7) can interact also via the LJ interaction. The GROMOS united atom force field uses a geometric combination rule $C12 = \sqrt{C12_{ij}C12_{ij}}$ and $C6 = \sqrt{C6_{ij}C6_{ij}}$ where $C6$ is $4\epsilon_i\sigma_i^6$

and C12 is $4\epsilon_i\sigma_i^{12}$. Finally the MARTINI force field doesn't use a particular mixing rule but instead develops one by one the mixing parameters between each pair of particles during the force field parameterization.

2.2.2 Bonded Interactions

The parameters which define the equilibrium values for bonds and angles are usually taken from experimental X-ray data and values for the force constants are derived by fitting infra-red (IR) experimental vibrational frequency data. Dihedrals can be derived in two ways using *ab initio* methods: the first optimises the dihedral potential on a very simple molecule and then generalises it over larger molecules containing the same dihedral type. The second optimises the dihedral potential for a large number of molecules with different chemical specificities.

Bond stretching

Bonds are defined between two covalently bonded atoms and described by a harmonic potential (Eq. 2.2.5).

$$E_{\text{bonds}} = \sum_{\text{bonds}} \frac{1}{2} K_r (r - r_{\text{eq}})^2 \quad (2.2.5)$$

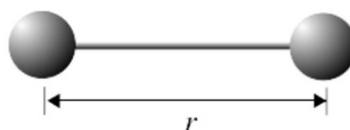


Figure 2.2: A figure illustrating bond stretching

where K_r is the force constant, r is the bond length and the r_{eq} is the equilibrium bond length. The sum runs over all the bonds within the system.

Angle bending

Angles are calculated among every three atoms chemically bonded. The bending energy for angles is obtained in accordance to the following harmonic potential (Eq. 2.2.6).

$$E_{\text{angles}} = \sum_{\text{angles}} \frac{1}{2} K_{\theta} (\theta - \theta_{\text{eq}})^2 \quad (2.2.6)$$

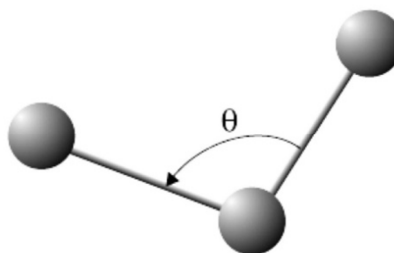


Figure 2.3: A figure illustrating angle stretching

where K_{θ} is the force constant, θ is the angle among three atoms and θ_{eq} is the equilibrium angle.

Dihedral Potential

The dihedral potential defines the interaction between atoms connected by a torsional angle. The mathematical representations for dihedrals used include the proper dihedral function and the Ryckaert-Bellemans function described below.

$$E_{\text{dihedrals}} = \sum_{n=0}^5 C_n (\cos(\varphi))^n \quad (2.2.7)$$

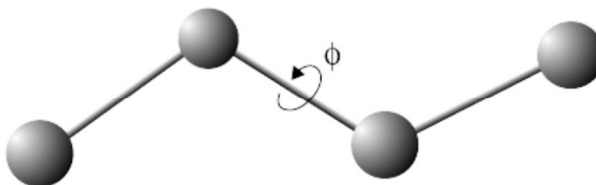


Figure 2.4: A figure illustrating the dihedral bond

where $\varphi = \phi - 180^\circ$, C_n is the force constant in kJmol^{-1} and ϕ is the torsion angle. n in (Eq. 2.2.7) is the multiplicity; its value represents the number of minimum points in the function as the bond rotates through 360° .

2.3 Periodic Boundary Conditions (PBC)

Real systems are usually not confined and must be simulated as infinite large system. Of course it is impossible to simulate a molecular system of infinite size. To overcome this problem the period boundary conditions (PBC) are commonly implemented in molecular modelling. With the PBC a large system is simulated by modelling a small part of it and replicating it in the three dimensions of the space. To minimize the problem of surface effects of atoms on the edge of a system, usually the PBC are implemented together with the minimum image convention. Under the minimum image convention when the particle in the original system moves through a simulation box, the exact same movement is observed in its periodic image in each of the neighbouring boxes. So say if a molecule leaves the central simulation box, its image will reappear in the opposite face. Hence there are no walls on the central box and no surface particles [29].The short range non-bonded interactions are considered using only the closest image of each particle. Fig. 2.5 illustrates (in two dimensions) how particles can enter and leave the simulation box across each of the four faces. A three dimensional system would allow the entering and leaving of a molecules on all faces, for example on a cubic system the molecules would be able to enter and leave across all 26 faces.

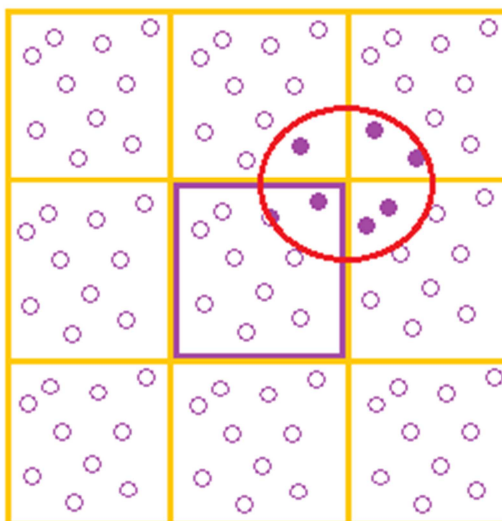


Figure 2.5: A two dimensional periodic system and spherical cut-off

In Fig. 2.5 the central simulation system originally prepared is the purple box highlighted. The filled purple particles illustrate how they can leave and re-enter the central box. The exact same move is taking place in all the surrounding boxes therefore can be said to have identical simulation boxes surrounding the original simulation box

in three dimensions [30]. According to the shape and dimensions of a system, for example in the case of the bilayer system where an orthorhombic box is utilized and an infinite system can be reproduced.

2.4 Cut-off

To calculate the interactions between all the particles in the system is computationally very expensive and physically not necessary, therefore a non-bonded spherical cut-off can be applied to the minimum image convention (Fig. 2.5). When a cut-off is applied the interactions between all the pairs of atoms beyond this distance are not calculated. The choice in the cut-off value has to be decided carefully: it should not be too large that the particle can see its own image, or indeed the same molecule dually, but it cannot be too small to neglect interactions between particles. The size of the box limits the cut-off distance which cannot be larger than the half the length of the shortest side of a box $r_c \leq \frac{1}{2}L$ [9]. Thus, the potential energy beyond the cut-off distance fades out to zero. Several methods can be used to bring the potential energy to zero: a simple truncation method can be used which involves simply setting the interaction to zero for interatomic distances that are greater than the cut-off distance defining the potential energy as:

$$U(r) = \begin{cases} U(r) & r \leq r_c \\ 0 & r \geq r_c \end{cases} \quad (2.4.1)$$

This method is not commonly used as it can lead to large fluctuations in energy [31] and introduces discontinuity in the potential and force that leads to problems especially in molecular dynamics simulations where energy conservation is required. To resolve this problem the shift and switching cut-off methods can be used which are described below. The shift cut-off method basically involves the shifting of the entire potential energy surface so that at the cut-off distance the potential is zero. There is a small disadvantage to this method as it can slightly decrease equilibrium distances [32]. Another popular method is the switching method which adjusts the potential over a certain predefined range of distances. So the potential is kept the same up to the first cut-off value and then slowly switched to zero within a distance range. This method is generally used only for large molecules for example coarse grain particles that require larger cut-off values. The switching method on smaller particles for example individual

atoms can perturb the equilibrium structure since it suffers from strong forces in the switching region [9]. Fig. 2.6 graphically shows the different Lennard-Jones cut-off methods discussed.

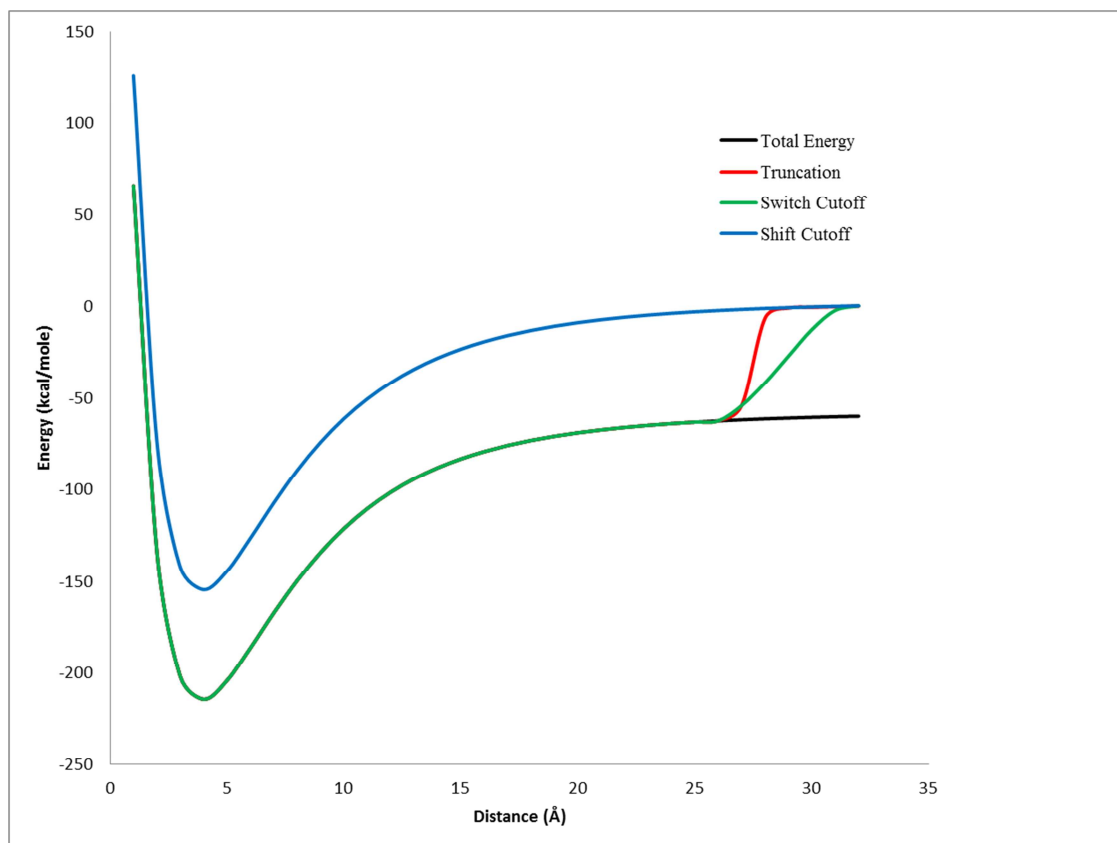


Figure 2.6: Lennard Jones cut-off illustrating truncation, shift and switch methods

2.5 Long Range Forces Particle Mesh Ewald (PME)

As explained above, the van der Waals potential can be confidently used to calculate pair potentials by simply truncating the potential for distances larger than the cut-off, however the electrostatics potential cannot be treated in the same manner outside the cut-off region, especially when charged species are modelled, for example electrolytes, and ad-hoc methods need to be developed to treat long range interactions. The Ewald summation [33] technique for the treatment of long range electrostatic interactions including boundary conditions is considered efficient [28]. Particle Mesh Ewald (PME) is a variation of the original Ewald method for the periodic systems [34].

In the particle mesh Ewald summation method, the generic interaction potential $\varphi(\mathbf{r})$ is defined by two terms:

$$\varphi(\mathbf{r}) = \varphi_{\text{sr}}(\mathbf{r}) + \varphi_{\text{lr}}(\mathbf{r}) \quad (2.5.1)$$

where the $\varphi_{\text{sr}}(\mathbf{r})$ accounts for the short range interaction potential and $\varphi_{\text{lr}}(\mathbf{r})$ is the long range interaction one.

The basic idea for PME is to replace the direct summation of interaction energies between point particles with two summations: the summation of the short range potential performed in real space (φ_{sr}) and the summation in Fourier space for the long range part performed in the reciprocal space (φ_{lr}):

$$\varphi(\mathbf{r}) = \sum_{i,j} \varphi(\mathbf{r}_j - \mathbf{r}_i) = E_{\text{sr}} + E_{\text{lr}} \quad (2.5.2)$$

$$\varphi_{\text{sr}} = \sum_{i,j} \varphi_{\text{sr}}(\mathbf{r}_j - \mathbf{r}_i) \quad (2.5.3)$$

$$\varphi_{\text{lr}} = \sum_{\mathbf{k}} \tilde{\Phi}_{\text{lr}}(\mathbf{k}) |\tilde{\rho}(\mathbf{k})|^2 \quad (2.5.4)$$

where $\tilde{\Phi}_{\text{lr}}$ and $\tilde{\rho}(\mathbf{k})$ represents the Fourier transform of the potential and the charge density respectively, \mathbf{r}_i and \mathbf{r}_j are the position of the charge i and j in the real space.

The short range summation defines the particle part of the PME, whereas the long range interaction is the Ewald part. Evaluating the Fourier transformation $\tilde{\rho}(\mathbf{k})$ of the charge density field efficiently, the density field is evaluated on a discrete lattice in space using the Fast Fourier transform which can be recalled as the mesh part.

2.6 Ensembles

One of the most important results that can be monitored with molecular simulations are the thermodynamic properties of the system simulated. A small set of parameters which include temperature (T), pressure (P) and the number of particles (N) are usually used to define the thermodynamic state. Equations of state and fundamental thermodynamic equations can be used to derive other important thermodynamic properties that are not directly available such as density and free energy of a system. Computer simulations allow to study directly the instantaneous properties of the system, whereas experiments measure typically averaged properties over particles and

time. Therefore for a reliable comparison with experiments, we must know what kind of averages we should compute. The Ergodic hypothesis clarifies this as it states that statistical ensembles averages are equal to time averages of the system i.e:

$$\langle A_{\text{obs}} \rangle_{\text{time}} = \langle A_{\text{obs}} \rangle_{\text{ensemble}} \quad [32] \quad (2.6.1)$$

where A is the observable (macroscopic property).

Coordinates in a multidimensional space (phase space) represented by the atomic positions (\mathbf{r}) and momenta (\mathbf{p}) define the mechanical or microscopic state of a system. There are $6N$ dimensions for systems with N particles. An ensemble is a collection of all possible systems which have different microscopic states but have an identical macroscopic (thermodynamic) state. In molecular dynamics simulations, a sequence of particles in phase space over time which represents different conformations of the system and their momenta belong to one ensemble. The equivalence reported in (Eq. 2.6.1) is satisfied if the system will eventually pass through all possible states producing enough representative states [9, 31]. The macroscopic property A_{obs} experimentally observed is the time average of its instantaneous value in a specific point of the phase space $A(\Gamma)$.

$$A_{\text{obs}} = \langle A \rangle_{\text{time}} = \langle A(\Gamma(t)) \rangle_{\text{time}} = \lim_{t_{\text{obs}} \rightarrow \infty} \frac{1}{t_{\text{obs}}} \int_0^{t_{\text{obs}}} A(\Gamma(t)) dt \quad (2.6.2)$$

The time evolution of A in a simple classical system is governed by Newton's equation. The integration over time cannot be extended to infinite time but might be solved over a long finite time t_{obs} which represents the length of the MD simulation.

From a continuous description to a discrete one, the equation of motion is solved on a step by step basis with (summation) using a large finite number of steps (τ_{obs}) of a length $\delta t = t_{\text{obs}}/\tau_{\text{obs}}$

$$A_{\text{obs}} = \langle A \rangle_{\text{time}} = \frac{1}{\tau_{\text{obs}}} \sum_{\tau=1}^{\tau_{\text{obs}}} A(\Gamma(\tau)) \quad (2.6.3)$$

Here we assume that for τ_{obs} is sufficiently long that the time average does not depend on the initial coordinates (initial \mathbf{r}_0 and \mathbf{p}_0).

Ensembles with a number of different characteristics that have different microscopic states but do not change their macroscopic or thermodynamic state include the microcanonical ensemble (NVE), that is used traditionally to model isolated

systems in molecular dynamics. A fixed number of particles, N , fixed volume, V , and fixed energy E , is what characterizes the thermodynamic state. The canonical ensemble (NVT) characterizes the thermodynamic state by using a fixed number of particles, N , a fixed volume, V and a fixed temperature, T . Another thermodynamically important ensemble is the isobaric-isothermal (NPT), where the number of particles, N , pressure, P , and temperature, T , are all kept constant through the simulation. Finally the grand canonical ensemble (μVT) characterizes the thermodynamic state by fixing the chemical potential, μ , at a constant volume and temperature [31].

Thermostats and barostats can be used in simulations to ensure the temperature and pressure of the system sample the correct ensemble. When the system is coupled with weak thermostat and barostat, the temperature of the system is regulated by manipulating the velocities of the atoms conserving the kinetic energy of the system while the pressure is modulated by modifying the box vectors of a simulation box and scaling the coordinates within the system.

2.6.1 Thermostat

The temperature, T in a system relates directly to its average kinetic energy and the systems degrees of freedom N_{dof} . The instantaneous temperature $T(t)$ can be defined as

$$T(t) = \frac{1}{N_{\text{dof}}k_B} \sum_{i=1}^N M_i v_i^2(t) \quad (2.6.4)$$

where k_B is the Boltzmann constant, M_i and v_i are the mass and the velocity of the i th particle respectively and N is the total number of particles in the system. In simulations the temperature is effectively a time average $T = \langle T \rangle$ averaged over a long enough time interval.

To be able to perform simulations at certain temperatures, it is important to be able to set an initial temperature and then control it through the simulation. Initially random velocities with a Maxwell-Boltzmann distribution are assigned to each particle to set the initial temperature of the system. The requirement to control the temperature is necessary as the temperature can undergo large fluctuations due to force truncations and round-off errors in the integration algorithm. There are a number of coupling schemes that can be adopted to correct the temperature through the simulation. The

Berendsen [35] coupling scheme and an extended-ensemble Nosé Hoover scheme [36, 37] are thermostats that can be used.

The Berendsen algorithm mimics the weak coupling of a system that has a fixed temperature using an external heat bath. Depending on the temperature, the bath adds or removes heat from the system. Using a reference temperature T_0 , the system temperature is slowly corrected according to

$$\frac{dT(t)}{dt} = \frac{1}{\tau} (T_0 - T(t)) \quad (2.6.5)$$

where τ is the coupling parameter or time constant which determines the strength of the coupling amongst the bath and the system.

An exponential decay of the systems temperature is obtained from this method until a reference temperature is reached. The velocities of the particles are scaled every time step using a time-dependant factor λ , represented as

$$\lambda = \left[1 + \frac{\Delta t}{\tau} \left(\frac{T_0}{T(t)} - 1 \right) \right]^{1/2} \quad (2.6.6)$$

The time constant τ can be adjusted to vary the strength of coupling according to the requirements. The Berendsen weak coupling scheme holds the disadvantage that it cannot generate rigorous canonical averages. So there can be temperature differences when rescaling the velocities. Coupling separately for different components of a system can aid in avoiding this problem.

Another temperature coupling scheme that can be used is the extended-ensemble approach by Nosé [36] and Hoover [37] which incorporates a thermal reservoir integrated into the system. This reservoir is represented by an additional degree of freedom approaching the temperature using an oscillatory relaxation. The Nose-Hoover algorithm conserves the desired temperature enabling a correct canonical ensemble simulation, however the computational expense is far greater compared with the weak coupling time method.

2.6.2 Barostat

Many measurements are usually carried out under constant temperature and pressure conditions, thus in molecular dynamics simulations the ability to maintain the

pressure as well as the temperature at target values is desirable. The pressure is maintained by changing the volume of the simulation box. The fluctuation of the volume is related to the isothermal compressibility κ as:

$$\kappa = -\frac{1}{V} \left(\frac{\partial V}{\partial P} \right)_T \quad (2.6.7)$$

where V is the volume of the simulation box, P is the pressure and T is the temperature of the system.

Substances that are easily compressible have a large κ value resulting in larger fluctuations for a specific pressure value than substances that are more incompressible. The energy fluctuations can be related to the pressure analogue of the heat capacity known as the isothermal compressibility.

In an isobaric system, the volume can be changed in all directions or selectively in one or two directions only. In a typical system of constant pressure simulation, it is instructive to consider the range of changes in volume one may expect to observe. The isothermal compressibility is directly related to the mean square volume displacement by:

$$\kappa = \frac{1}{k_B T} \frac{\langle V^2 \rangle \langle V \rangle^2}{\langle V^2 \rangle} \quad (2.6.8)$$

Controlling the pressure includes many methods that are analogous to the temperature thermostat in a simulation. Thus, a constant value for the pressure can be maintained by basically scaling the simulation box volume using a barostat.

Analogous to the temperature bath, using a Berendsen [35] barostat using a pressure bath can be utilised to control the system pressure in a simulation. The rate in change of pressure can be calculated as:

$$\frac{dP(t)}{dt} = \frac{1}{\tau_P} (P_{\text{bath}} - P(t)) \quad (2.6.9)$$

where τ_P is the coupling constant, P_{bath} is the pressure of the bath and the actual pressure at time t is defined as $P(t)$.

A scaling factor λ that is equivalent to the scaling of the particles coordinates by a factor of $\lambda^{1/3}$ and can be used to scale the volume of the simulation box by:

$$\lambda = 1 - \kappa \frac{dt}{\tau_P} (P - P_{\text{bath}}) \quad (2.6.10)$$

The new positions for the atomic coordinates are then given by:

$$\mathbf{r}'_i = \lambda^{1/3} \mathbf{r}'_i \quad (2.6.11)$$

The change in the box size can be applied both using isotropic pressure coupling, where the simulation box is uniformly modified in all the three cartesian directions, and a semi-isotropic pressure coupling scheme where the x-y and z dimensions are changed independently. Finally a completely anisotropic pressure coupling can also be applied independantly in all directions.

2.7 Classical Mechanics

In a molecular dynamics simulation, incremental configurations are generated by integrating the Newton's law of motion. Positions and velocities of particles in a system vary with time; these positions are specified in trajectories produced after simulations [38]. The Newton's law of motion can be stated as: 1) in the absence of exertion of any force on the centre of mass on a particle, the particle shall move in a straight line at constant velocity; 2) force is equal to the rate of change of momentum and 3) if a force is exerted on the particle, to every action there is an equal and opposite reaction [9].

Molecular dynamics trajectories (i.e. the collection of configurations of the system) are obtained when the differential equation of motion of Newton's second law ($F = ma$) is solved (Eq. 2.7.1). The positions (\mathbf{r}), velocities ($d\mathbf{r}/dt$) and accelerations ($d^2\mathbf{r}/dt^2$) of the particles as they vary with time are collected into the trajectories files from which the average values of several properties can be determined:

$$\frac{d^2\mathbf{r}_i}{dt^2} = \frac{\mathbf{F}_{\mathbf{r}_i}}{m_i} \quad (2.7.1)$$

where \mathbf{m}_i is the mass of the particle; \mathbf{r}_i is the position of the particle along one coordinate and $\mathbf{F}_{\mathbf{r}_i}$ is the force exerted on the particle that direction. The change in the motion of the particle is proportional to the force applied and so changed in the direction the force is applied [39].

2.7.1 Finite Difference Methods

In realistic molecular models where intermolecular interactions occur, the change in the position of the particles, or if any other particles interact with it changes the force. In a molecular dynamics simulation with continuous potentials where the motions of all particles are coupled together, a many body problem arises which cannot be solved analytically. For this reason the equations of motion are integrated with the aid of finite difference methods. The basic idea of the finite difference approach is that the integration can be broken down into a number of small steps, where each step in time is separated by a fixed time δt . At time t the force on each particle in the system is calculated as the sum of the forces arising from the interaction of that particle with all the others in the system. From the knowledge of the force values at time t one can determine the acceleration associated to each particle which can then be combined with its position and velocity enabling the calculation of position and velocity at $t + \delta t$. During every step, the force is assumed to be constant [9].

There are a number of algorithms that have been developed for numerically integrating the equations of motion in molecular dynamics simulations using finite difference techniques; the most commons include the Verlet algorithm, leap-from algorithm, the velocity Verlet method and the Beeman's algorithm. Ideally the numerical methods should be computationally efficient and allow the use of a long integration time step; moreover they have to conserve energy and momentum. All algorithms normally employed estimate positions, velocities and acceleration at time $t + \delta t$ using their Taylor series expansion [29]:

$$\mathbf{r}(t + \delta t) = \mathbf{r}(t) + \delta t \mathbf{v}(t) + \frac{1}{2} \delta t^2 \mathbf{a}(t) + \frac{1}{6} \delta t^3 \mathbf{b}(t) + \dots \quad (2.7.2)$$

$$\mathbf{v}(t + \delta t) = \mathbf{v}(t) + \delta t \mathbf{a}(t) + \frac{1}{2} \delta t^2 \mathbf{b}(t) + \dots \quad (2.7.3)$$

$$\mathbf{a}(t + \delta t) = \mathbf{a}(t) + \delta t \mathbf{b}(t) + \dots \quad (2.7.4)$$

where \mathbf{r} is the position of the vectors at time t , \mathbf{v} is the velocity (the first derivative of the particles with respect to time), the second derivative is acceleration (\mathbf{a}), the second derivative is \mathbf{b} , and so on.

Verlet algorithm

The Verlet algorithm [6] is probably the most widely used numerical method for integrating the equation of motion in a molecular dynamics simulation. The Verlet algorithm calculates positions of successive time steps using the positions of the previous and current timestep. To derive the Verlet algorithm, the Taylor expansions of the position vectors $\mathbf{r}(t)$ at time $t+\delta t$ and $t-\delta t$ are used [29].

$$\mathbf{r}(t + \delta t) = \mathbf{r}(t) + \delta t \mathbf{v}(t) + \frac{1}{2} \delta t^2 \mathbf{a}(t) \dots \quad (2.7.5)$$

$$\mathbf{r}(t - \delta t) = \mathbf{r}(t) - \delta t \mathbf{v}(t) + \frac{1}{2} \delta t^2 \mathbf{a}(t) \dots \quad (2.7.6)$$

Adding Eq. 2.7.5 to Eq. 2.7.6 gives:

$$\mathbf{r}(t + \delta t) = 2\mathbf{r}(t) - \mathbf{r}(t - \delta t) + \mathbf{a}(t)\delta t^2 \dots \quad (2.7.7)$$

The Verlet algorithm does not use any specific velocities; however they can be calculated in a number of ways. A simple way is exploiting the definition of velocity dividing the difference of the positions at time $t + \delta t$ and $t - \delta t$ by $2\delta t$ [9]:

$$\mathbf{v}(t) = [\mathbf{r}(t + \delta t) - \mathbf{r}(t - \delta t)]/2\delta t \quad (2.7.8)$$

The Verlet algorithm has the advantage over other algorithms that it is straightforward and has modest storage requirements; however it also has its disadvantages; there is a loss in precision of the positions $\mathbf{r}(t + \delta t)$ obtained from the addition of a small term ($\delta t^2 \mathbf{a}(t)$) to the difference of two much larger terms, $2\mathbf{r}(t)$ and $\mathbf{r}(t - \delta t)$. There is also the problem that velocities are unobtainable before the positions are computed at the next step [9].

Leap-Frog Algorithm

The Leap frog algorithm is a valid alternative to the Verlet one. [40] Instead of the Verlet, the leap-frog numerical integration method uses the positions and velocities at time t and $t-\delta t/2$ to calculate the positions at time $t+ \delta t$, moreover the velocities are explicitly calculated during the numerical integration, [41].

$$\mathbf{r}(t + \delta t) = \mathbf{r}(t) + \mathbf{v}(t + 1/2 \delta t)\delta t \quad (2.7.9)$$

$$\mathbf{v}(t + 1/2 \delta t) = \mathbf{v}(t - 1/2 \delta t) + \mathbf{a}(t)\delta t \quad (2.7.10)$$

With this algorithm the velocities are calculated first at time $t + 1/2 \delta t$, these are then used to calculate the positions \mathbf{r} at time $t + \delta t$. Hence the velocities leap over the positions, and then the positions leap over the velocities (Fig. 2.7).

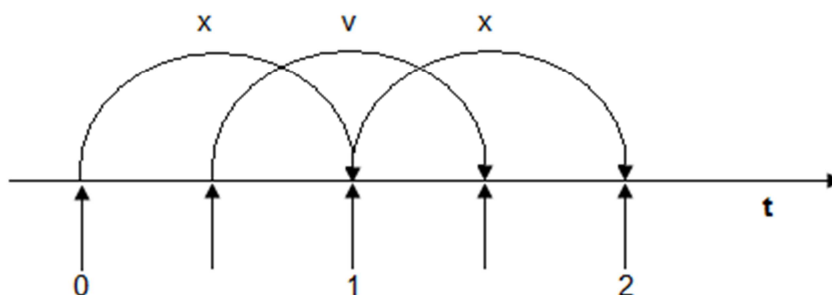


Figure 2.7: An illustration of the leap-frog integration method

This illustrates the reasoning for this algorithm being called the leap-frog because \mathbf{r} and \mathbf{v} are leaping over each other like frogs over each other's back. Velocities at time t can be approximated by the relationship (equation 2.4.11):

$$\mathbf{v}(t) = 1/2 [\mathbf{v}(t - 1/2 \delta t) + \mathbf{v}(t + 1/2 \delta t)] \quad (2.7.11)$$

One of the main advantages of the Leap-frog method is that the velocities explicitly appear in the integration scheme and calculated directly therefore it does not require the calculation of the differences of large numbers. However the disadvantage of the Leap-frog algorithm is that it does not synchronise the calculation of the velocities and positions [42].

2.8 Constraint algorithm

A timestep in a molecular dynamics simulation should be chosen so that it is not too short to be able to sample portions of phase space and not too long to prevent unphysical fluctuations of the energy system. The choice of timestep is dependent on the frequency of motion of particles that are simulated. The highest frequency of motion present in a classical atomistic system is the bond vibration, and for example the fastest vibrational energy in an aliphatic molecule is the C-H bond having a value of 3000cm^{-1} .

Converting the latter to time predicts a 1fs time step allowance enabling to sample all possible motions in the system efficiently. If the frequency of motion is decreased then a larger time step can be adopted. The major conformational changes in a system usually occurs at lower frequency motion and higher frequency motions can be eliminated by treating bonds as rigid or constraining them using constraint algorithms.

Constraint algorithms can be used to restrain bond lengths in simulations allowing the use of a larger timestep. In one of the most commonly used method for constraining bond lengths (known as SHAKE [5]) the imposed constraints are satisfied simultaneously when the equations of motion is solved. During this constrained dynamics the coordinates of all the particles are still included in the equation of motion connected in each coordinate direction while satisfying the imposed constraints. The degrees of freedom for the motion of the system containing N particles have 3N independent coordinates or degrees of freedom. The SHAKE algorithm uses holonomic constraints which can be expressed as:

$$f(\mathbf{r}_1, \mathbf{r}_2, \mathbf{r}_3, \dots, \dots, t) = 0 \quad (2.8.1)$$

where $\mathbf{r}_1, \mathbf{r}_2$, etc are the coordinates of the particles

A holonomic constraint is where the motion of particles is constrained to lie on the surface of a sphere. A holonomic sphere that keeps a particle on the surface of a sphere can be represented as:

$$R^2 - a^2 = 0 \quad (2.8.2)$$

where R is the distance of the particle from the centre where the sphere of a radius a is centered.

The numbers of degrees of freedom of the system are reduced to $3N - k$ according to the number of holonomic k constraints that are present. In a constrained system there are two types of forces that are involved in the equation of motion. Firstly the usual forces from the intra and inter-molecular interactions and secondly the forces arising from the constraints. \mathbf{G}_i describes the constraint forces defined as:

$$\mathbf{G}_i = - \sum_{k=1}^K \lambda_k \frac{\partial \sigma_k}{\partial \mathbf{r}_i} \quad (2.8.3)$$

where the number of constraints is defined as K and Lagrange multipliers λ_k have to be solved to fulfil the constraint algorithm and σ_k which requires the bond between the

position of two atoms to remain fixed. Thus, when a force is exerted on atom i the equation of motion for a constrained system includes two types of forces where the forces arising from intra and intermolecular interaction is \mathbf{F}_i and \mathbf{F}'_i is the forces due to the constraints defined as:

$$\mathbf{F}'_i = \mathbf{F}_i + \mathbf{G}_i = -\frac{\partial}{\partial \mathbf{r}_i} (V(\mathbf{r}) + \sum_{k=1}^K \lambda_k \sigma_k) \quad (2.8.4)$$

The Verlet algorithm can then incorporate this expression by

$$\mathbf{r}_i(t + \Delta t) \approx -\mathbf{r}_i(t - \Delta t) + 2\mathbf{r}_i(t) + \Delta t^2 \frac{\mathbf{F}_i}{m_i} + \Delta t^2 \frac{\mathbf{G}_i}{m_i} \quad (2.8.5)$$

The displacement is then $(\mathbf{G}_i/m_i)(\Delta t)^2$ due to the constraint forces. An imposed distance constraint are fulfilled when the Lagrange multipliers are solved in the constrained equation of motion, and the SHAKE algorithm constrains a set of unconstrained coordinates from \mathbf{r}' to constrained coordinates \mathbf{r}'' (Fig. 2.8). SHAKE iteratively solves the equation as one constraint can cause another constraint to become violated, therefore it becomes necessary for the iteration process satisfying a set tolerance values.

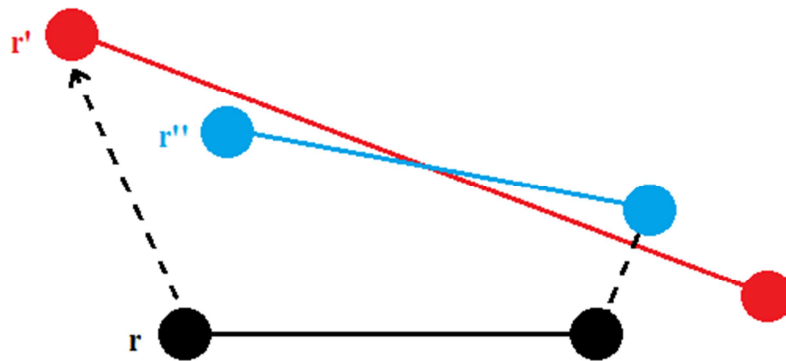


Figure 2.8: Shake algorithm illustration showing the changing of a set of unconstrained coordinates from \mathbf{r}' to \mathbf{r}'' .

There are a number of similar algorithms that can be used, for example SETTLE [43] which is an algorithm that is generally used to constrain small molecules such as water molecules in simulations. LINCS [44] is another constraint algorithm that can be used which resets bond distances to their correct lengths following an unconstrained update. This algorithm is a non-iterative procedure as the constraints themselves are reset instead of derivatives of the constraints, therefore eliminating drift. Although the

LINCS algorithm is faster and more stable than SHAKE, it is limited by the fact that it can only be used with bond constraint and isolated angle constraint. When the LINCS algorithm cannot reset the constraints, it generates a conformation fulfilling the constraint as close as possible, therefore the LINCS algorithm will never crash.

2.9 References

1. Clark, G., *The Molecular World (Molecular modelling and Bonding)*, ed. E.A. Moore. Vol. 4. 2002: Royal Society of Chemistry.
2. Alder, B.J. and T.E. Wainwright, *Phase Transition for a Hard Sphere System*. The Journal of Chemical Physics, 1957. **27**(5): p. 1208-1209.
3. Rahman, A., *Correlations in the Motion of Atoms in Liquid Argon*. Physical Review, 1964. **136**(2A): p. A405.
4. Stillinger, F.H. and A. Rahman, *Improved simulation of liquid water by molecular dynamics*. The Journal of Chemical Physics, 1974. **60**(4): p. 1545-1557.
5. Ryckaert, J.-P., G. Ciccotti, and H.J.C. Berendsen, *Numerical integration of the cartesian equations of motion of a system with constraints: molecular dynamics of n-alkanes*. Journal of Computational Physics, 1977. **23**(3): p. 327-341.
6. McCammon, J.A., B.R. Gelin, and M. Karplus, *Dynamics of folded proteins*. Nature, 1977. **267**(5612): p. 585-590.
7. Lin, J.-H., et al., *Computational Drug Design Accommodating Receptor Flexibility: The Relaxed Complex Scheme*. Journal of the American Chemical Society, 2002. **124**(20): p. 5632-5633.
8. Fréchet, J.M.J., *Dendrimers and supramolecular chemistry*. Proceedings of the National Academy of Sciences, 2002. **99**(8): p. 4782-4787.
9. Leach, A.R., *Molecular Modelling Principles and Applications*. Second ed. 2001, Essex: Pearson Education Limited.
10. Jorgensen, W.L., D.S. Maxwell, and J. Tirado-Rives, *Development and Testing of the OPLS All-Atom Force Field on Conformational Energetics and Properties of Organic Liquids*. Journal of the American Chemical Society, 1996. **118**(45): p. 11225-11236.
11. Tokuhisa, H. and R.M. Crooks, *Interactions between Organized, Surface-Confined Monolayers and Vapor-Phase Probe Molecules. 12. Two New Methods for Surface-Immobilization and Functionalization of Chemically Sensitive Dendrimer Surfaces*. Langmuir, 1997. **13**(21): p. 5608-5612.
12. Pericet-Camara, R., et al., *Nano-patterning of solid substrates by adsorbed dendrimers*. Chemical Communications, 2007(3): p. 266-268.
13. Sui, G., et al., *A Structural Study of Amphiphilic PAMAM (Poly(amido amine)) Dendrimers in Langmuir and Langmuir-Blodgett Films*. Journal of Colloid and Interface Science, 2002. **250**(2): p. 364-370.

14. Marrink, S.J., et al., *The MARTINI Force Field: Coarse Grained Model for Biomolecular Simulations*. The Journal of Physical Chemistry B, 2007. **111**(27): p. 7812-7824.
15. Martin, M.G. and J.I. Siepmann, *Transferable Potentials for Phase Equilibria. 1. United-Atom Description of n-Alkanes*. The Journal of Physical Chemistry B, 1998. **102**(14): p. 2569-2577.
16. Shoichet, J.A.a.B., *Virtual Screening in Drug Discovery*. 2005: CRC Press, Taylor and Francis Group.
17. Gunsteren, W.F.v. and A.E. Mark, *Validation of molecular dynamics simulation*. The Journal of Chemical Physics, 1998. **108**(15): p. 6109-6116.
18. Chooi, K.W., et al., *The Molecular Shape of Poly(propylenimine) Dendrimer Amphiphiles Has a Profound Effect on Their Self Assembly*. Langmuir, 2009. **26**(4): p. 2301-2316.
19. Esfand, R. and D.A. Tomalia, *Poly(amidoamine) (PAMAM) dendrimers: from biomimicry to drug delivery and biomedical applications*. Drug Discovery Today, 2001. **6**(8): p. 427-436.
20. Rosen, B.M., et al., *Dendron-Mediated Self-Assembly, Disassembly, and Self-Organization of Complex Systems*. Chemical Reviews, 2009. **109**(11): p. 6275-6540.
21. Huang, W., Z. Lin, and W.F. van Gunsteren, *Validation of the GROMOS 54A7 Force Field with Respect to β -Peptide Folding*. Journal of Chemical Theory and Computation, 2011. **7**(5): p. 1237-1243.
22. Berger, O., O. Edholm, and F. Jähnig, *Molecular dynamics simulations of a fluid bilayer of dipalmitoylphosphatidylcholine at full hydration, constant pressure, and constant temperature*. Biophysical Journal, 1997. **72**(5): p. 2002-2013.
23. Percec, V., et al., *Self-assembly of Janus dendrimers into uniform dendrimersomes and other complex architectures*. Science (New York, N.Y.), 2010. **328**(5981): p. 1009-1014.
24. Marrink, S.J., A.H. de Vries, and A.E. Mark, *Coarse Grained Model for Semiquantitative Lipid Simulations*. The Journal of Physical Chemistry B, 2003. **108**(2): p. 750-760.
25. Monticelli, L., et al., *The MARTINI Coarse-Grained Force Field: Extension to Proteins*. Journal of Chemical Theory and Computation, 2008. **4**(5): p. 819-834.
26. López, C.A., et al., *Martini Coarse-Grained Force Field: Extension to Carbohydrates*. Journal of Chemical Theory and Computation, 2009. **5**(12): p. 3195-3210.
27. Wong-Ekkabut, J., et al., *Computer simulation study of fullerene translocation through lipid membranes*, 2008, NATURE PUBLISHING GROUP.
28. Tildesley, M.P.A.a.D.J., *Computer Simulation of Liquids*, ed. Clarendon. 1989, Great Britain: Oxford 385.
29. Tildeseley, M.P.A.D.J., *Computer Simulation of Liquids*. 1987: Clarendon Press Oxford.
30. Iacovella, C.R., *Periodic boundary conditions*. Glotzer group. Depts of Chemical Engineering, Materials Science & Engineering, 2006.
31. Smit, D.F.B., *Understanding Molecular Simulation From Algorithms to Applications*, ed. A. Press. Vol. 1. 2002, London: Academic Press.

32. M. P. Allen, D.J.T., *Computer Simulations of Liquids*. 1987, New York: Oxford University Press Inc.
33. Ewald, P.P., *Die Berechnung optischer und elektrostatischer Gitterpotentiale*. Annalen der Physik, 1921. **369**(3): p. 253-287.
34. Darden, T., D. York, and L. Pedersen, *Particle mesh Ewald: An $N \log(N)$ method for Ewald sums in large systems*. The Journal of Chemical Physics, 1993. **98**(12): p. 10089-10092.
35. Berendsen, H.J.C., et al., *Molecular dynamics with coupling to an external bath*. The Journal of Chemical Physics, 1984. **81**(8): p. 3684-3690.
36. Nose, S., *A unified formulation of the constant temperature molecular dynamics methods*. The Journal of Chemical Physics, 1984. **81**(1): p. 511-519.
37. Hoover, W.G., *Canonical dynamics: Equilibrium phase-space distributions*. Physical Review A, 1985. **31**(3): p. 1695-1697.
38. Andersen, H.C., *Molecular dynamics simulations at constant pressure and/or temperature*. The Journal of Chemical Physics, 1980. **72**(4): p. 2384-2393.
39. Newton, S.I., *Mathematical Principles of Natural Philosophy*, ed. A. Motte. Vol. 1. 1803: Benjamin Matte.
40. Van Gunsteren, W.F. and H.J.C. Berendsen, *A Leap-frog Algorithm for Stochastic Dynamics*. Molecular Simulation, 1988. **1**(3): p. 173 - 185.
41. Thomas DeGrande, C.D., *Lattice methods for quantum chromodynamics*. 2006, Singapore: World Scientific Publishing Co. Pte. Ltd. 3.
42. Wu, Z., *Lecture Notes on Computational Structural Biology*. 2008, Singapore: World Scientific. 1.
43. Miyamoto, S. and P.A. Kollman, *Settle: An analytical version of the SHAKE and RATTLE algorithm for rigid water models*. Journal of Computational Chemistry, 1992. **13**(8): p. 952-962.
44. Berk, H., et al., *LINCS: A Linear Constraint Solver for Molecular Simulations*.

Stability of Amphiphilic Dendrimers at the Water/Air Interface

This chapter is published in The Journal of Physical Chemistry B (see Appendix A)

Authors: Selina Nawaz, Paola Carbone

3.1 Introduction

In recent years amphiphilic dendrimers have shown to be promising building blocks for a large range of interfacial materials. In fact, tailor made dendrimers show interesting self-assembly properties when strong dispersive, polar or hydrogen bonding intermolecular forces are present [1, 2]. In particular, alkyl modified hydrophilic dendrimers such as poly-(amino amide) (PAMAM) or poly-(propylene imine) form a Langmuir-Blodgett monolayer at surface or interface that, due to the large number of functionalities present in their hydrophilic core, can show high stability. Indeed, amphiphilic dendrimers can bind at the interface more efficiently than classical surfactants and, because of dendrimers unique topology, their monolayers find a wide number of applications such as surface-based sensors or surface nanopatterning [3, 4]. Recently, the physical characterization of the Langmuir-Blodgett monolayer formed at the air-water interface by amphiphilic PAMAMs fully functionalized with long aliphatic chains, has been the subject of intensive experimental investigations [5-7]. Amphiphilic dendrimers can also self-assemble in aqueous media forming micelles whose stability is function of the shape of the functionalized dendrimer molecules [2].

Moreover, through a specific synthetic route, dendrimers can be also modified targeting specifically one side of the molecule. This type of synthetic procedure allows the preparation of amphiphilic “Janus” dendrimers, where the hydrophobic chains are attached only to part of the end-monomers breaking the symmetry of the macromolecule (see Fig. 3.1) [8-11]. In this case, the bipolar nature of the molecules allows the formation in water of a large variety of self assembled structures that can be exploited for several applications such as encapsulation or delivery of drugs. The Janus dendrimers can be seen as an example of Janus nanoparticle whose properties and

applications have been foreseen as very innovative due to the dual nature of the particle that, especially at interfaces, can bind different substrates [12].

Computer simulations can help in predicting the behaviour of amphiphilic molecules both in bulk and at the interface. Using simplified models, it is possible for example to calculate the free energy profile of ideal nanoparticles at the interface predicting their stability as a function of shape, orientation and distance from the interface [13-15]. Similar simplified models have also been used to study the strength of the interaction between a spherical model Janus nanoparticle at an ideal fluid interface studying how the particle-interface stability is controlled by changing the difference in affinities between the two particle regions and their relative sizes [16]. Moreover, in the particular case of dendrimers, using simplified models it has been predicted that amphiphilic dendrimers interacting via a purely repulsive Gaussian potential crystallize into cubic lattice with density-independent lattice constants [17]. However, while simplified models are very useful to gain properties common to a large family of molecules [18], atomistic models are needed when one wants to investigate the specific chemical interactions responsible, for example, for molecular aggregation [19] or intramolecular rearrangements [19, 20]. Despite this, besides the simplified models that idealize the nanoparticle as compact impenetrable sphere, simulations of nanoparticles at the interface that use an atomistic description of the molecules, are almost absent in literature. The only work we are aware of is that of Tay and Bresme [21] who reported the results of atomistic molecular dynamics simulations performed on alkythiol passivated gold nanoparticle absorbed at the air-water interface predicting the contact angle, particle shape and orientational order of the water molecules.

This paper aims at covering partially this gap clarifying and predicting the stability of single amphiphilic PAMAM dendrimer (fully modified and Janus dendrimer) at the air/water interface by means of atomistic molecular dynamics simulations. The structural properties of the molecule at the interface, the molecular interactions responsible of the diffusion of the dendrimer toward the interface and the interface stability are investigated also in term of wetting properties and particle shape and compared with the thermodynamic model predictions. The ultimate goal of this investigation is to help in the design of new dendrimeric molecular structures with target properties rationalizing the different non bonded interactions responsible for the molecular aggregations.

3.2 Computational Details

One PAMAM dendrimer molecule of second generation (16 terminal groups) is functionalized with either 16 (pure amphiphilic dendrimer) or 8 (Janus dendrimer) n-decane chains. In the Janus dendrimer the eight n-decane chains are attached in a symmetric fashion in order to have the aliphatic chains attached to the terminal NH_2 groups belonging to the same side of the amine dendrimer core (see Fig. 3.1). The functionalized dendrimer models are obtained adding 16 (fully functionalized) or 8 (Janus) n-decane chains to the NH_2 primary amine terminal groups of well equilibrated un-functionalized PAMAM dendrimer models [19]. The force field parameters and the steps followed to equilibrate the un-functionalized models are reported in reference [19] and here only briefly described. The force field employed during the simulations is the OPLS-AA force field developed specifically for primary amines [22] and amides [23]. The OPLS-AA force field has shown to be a reliable force field for polyamides characterized by different topologies being able to reproduce their thermodynamic (density, glass transition temperature, thermal expansion coefficient) [19] [24] and structural (radius of gyration, hydrogen bonds) [25] [26] experimental properties.

The un-functionalized PAMAM models are initially pre-equilibrated in vacuum using a Monte Carlo algorithm and then put randomly oriented in a simulation box of large size. The bulk system is then subjected to a series of energy minimization and soft core MD runs until the proper density is reached. From this well equilibrated PAMAM dendrimer bulk one molecule is extracted and functionalized adding either 16 (fully functionalized dendrimer) or 8 (Janus dendrimer) n-decane chains. The molecule is then subjected to energy minimization in order to initially equilibrate the structure. Four different systems are set up and simulated. The dendrimer model (both fully functionalized and Janus) is put either inside the water phase or at the air/water interface. The interface is built simulating a cubic water box with 4000 molecules of SPC water [27] for 1 ns in NPT (constant temperature and pressure) ensemble until the correct density of liquid water at room temperature and atmospheric pressure is reached. The simulation box is then increased in the Z-direction and the dendrimer is immersed into the water phase (or placed at the interface) removing all the water molecules whose atoms overlap the dendrimer ones. The system is then further minimized before starting the simulations.

Two different starting configurations for each system are used. Table 1 summarizes the characteristics of the simulated systems. The simulations where the

dendrimer molecule is placed into the water phase are carried out to investigate the time scale and the molecular mechanism responsible for the migration of the dendrimer toward interface. For the equilibration and production runs the very high-frequency bond stretching vibrations are removed using rigid constraints which allow to use an integration time step of $\Delta t = 2$ fs. Long simulations (up to 40 ns) in NVT (constant temperature and volume) at 300 K are run with a thermostat coupling time of 0.1 ps and a cut off of 1.0 nm. The long range electrostatic interactions are treated using the reaction field method using the dielectric constant of the water (72) for the continuum. [28] The simulations are carried out with the GROMACS package [29-32].

Table 3.1: List of the simulated systems.

Model	Position of the dendrimer model	Number of water molecules	Simulation box size (nm)	Simulations length
Fully functionalized	Inside the water phase	3798	5.0 5.0 15.0	25 ns
Fully functionalized	At the air/water interface	3784	5.0 5.0 15.0	40 ns
Janus	Inside the water phase	3886	5.0 5.0 15.0	25 ns
Janus	At the air/water interface	3882	5.0 5.0 15.0	40 ns

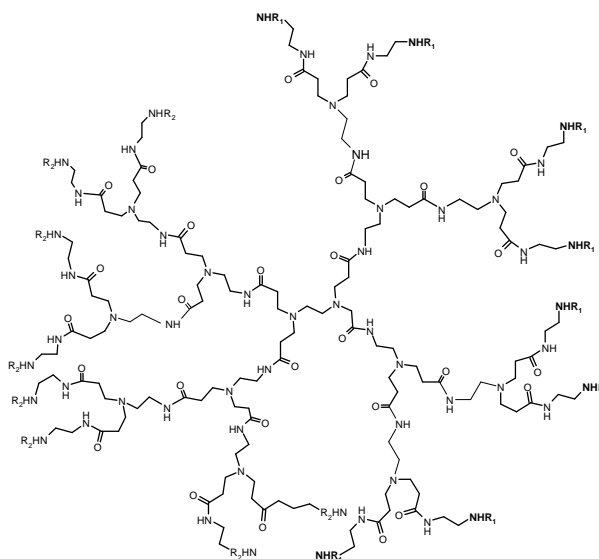


Figure 3.1: Poly(amino-amide) dendrimer of second generation. In the fully functionalized dendrimer $R_1=R_2=C_{10}H_{23}$. In the Janus dendrimer $R_1=C_{10}H_{23}$ while $R_2=H$. In the unmodified dendrimer $R_1=R_2=H$.

3.3 Results

3.3.1 Structural Properties of the Dendrimer at the Interface

Analytical studies based on thermodynamic models predict that the stability of a generic nanoparticle at the interface depends upon a complicated interplay between particle shape, line tension and particle orientation. In general, elongated (prolate) nanoparticles show a reduced stability compared with spherical and oblate ones although for a small interval of aspect ratio α ($1 < \alpha < 1.904$), being α the ratio between the two semi axis, the prolate particles show to be stable. Moreover, oblate particle whose symmetry axis is parallel to the normal vector of the interface show the highest stability while the prolate particles with the symmetry axis perpendicular to the vector normal to the interface have higher stability than those whose symmetry axis is parallel to it [13].

Detailed atomistic simulations enable to monitor the change in the 3D molecular shape by the calculation of the second moment of the atomic distribution (the gyration tensor) which is defined as [33]

$$\mathbf{R}_{\alpha,\beta}^2 = \frac{1}{N} \sum_{i=1}^N (\mathbf{r}_{\alpha}^i - \mathbf{r}_{\alpha}^M)(\mathbf{r}_{\beta}^i - \mathbf{r}_{\beta}^M) \quad \alpha, \beta = x, y, z \quad (3.1)$$

where N is the number of atoms in the molecule, \mathbf{r}_{α}^i is the position of the i -th atom and \mathbf{r}_{α}^M is the position of the dendrimer's geometrical center. The eigenvalues of the gyration tensor (λ_1^2 , λ_2^2 and λ_3^2) represent the characteristic lengths of the equivalent ellipsoid with which the dendrimer is described. From the knowledge of the λ_i it is possible to calculate the degree of prolateness that can be measured through the parameter S where $S = \frac{(\lambda_1 - \bar{\lambda})(\lambda_2 - \bar{\lambda})(\lambda_3 - \bar{\lambda})}{\bar{\lambda}^3}$ and $\bar{\lambda}$ is the mean eigenvalue of the gyration tensor [34]. For prolate rod-like shape $S = 2$ (being $\lambda_1 \neq \lambda_2; \lambda_3 = 0$), $S = 1/4$ for oblate disk-like object (where $\lambda_1 = \lambda_2; \lambda_3 = 0$) and $S = 0$ for spherical shape (where $\lambda_1 = \lambda_2 = \lambda_3$). In general $S > 0$ for prolate ellipsoid-like molecules and $S < 0$ for the oblate ones. Table 3.2 reports the values for the gyration radius and the corresponding eigenvalues averaged over the last 20 ns of the two set of simulations carried out for each system simulated, while Fig. 2a shows how the value of S , calculated for the fully functionalized and Janus dendrimers placed at the interface, changes during simulation.

From the plots in Fig. 3.2a we observe that the approximated 3D shape of both dendrimer models oscillates between the two most stable configurations predicted by the theory (oblate and prolate). Table 3.2 reports also the value of the aspect ratio α_{12} and α_{13} calculated using either the smallest eigenvalue (λ_3) or the middle one (λ_2). The aspect ratios are also in good agreement with the interval of stability predicted by the theory ($1 < \alpha < 1.904$). Unlike the surface area of a sphere, the surface area of a general ellipsoid cannot be expressed exactly by an elementary function; however, knowing the eigenvalues (λ_i) of the gyration tensor, it is possible to calculate its approximated Surface Area (SA) through the following formula:

$$SA \approx 4\pi \left(\frac{\lambda_1^p \lambda_2^p \lambda_1^p \lambda_3^p \lambda_2^p \lambda_3^p}{3} \right)^{1/p} \quad (3.2)$$

where p is a constant. This approximation has the least relative error ($\pm 1.061\%$ in the worst case) when $p = 1.6075$ [35] [36]. Fig. 3.2b shows the SA calculated using Eq. 3.2 for the two models placed at the interface along with the top view of the fully functionalized and Janus dendrimer at the end of the simulation. It is interesting to notice that while for the fully modified PAMAM the rearrangement of the hydrophobic chains increases the total SA of the molecule, for the Janus model this rearrangement leads to a decrease of its SA. In fact, as we will show with more details below, during the simulation, the fully functionalized dendrimer changes its global shape adopting a conformation that enables large part of the polar atoms of the hydrophilic dendrimer core to interact with the water increasing in this way its interfacial area.

Table 3.2: Radius of gyration (R_g), eigenvalues (λ_i) and aspect ratios (α) of the gyration tensor with the corresponding standard deviations. The average is performed over the last 10 ns of the trajectory for two different starting configurations.

Model	R_g (nm)	λ_1 (nm)	λ_2 (nm)	λ_3 (nm)	$\alpha_{12} = \lambda_1/\lambda_2$	$\alpha_{13} = \lambda_1/\lambda_3$
Janus	1.05 ± 0.02	0.77 ± 0.03	0.57 ± 0.03	0.41 ± 0.02	1.35 ± 0.07	1.88 ± 0.08
Fully functionalized	1.18 ± 0.03	0.86 ± 0.03	0.66 ± 0.04	0.46 ± 0.03	1.30 ± 0.08	1.88 ± 0.09

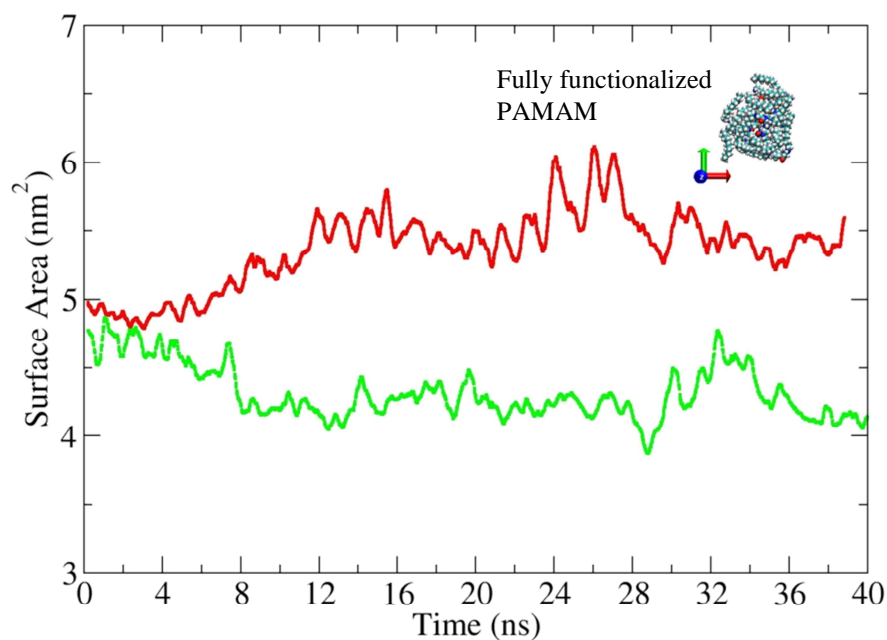
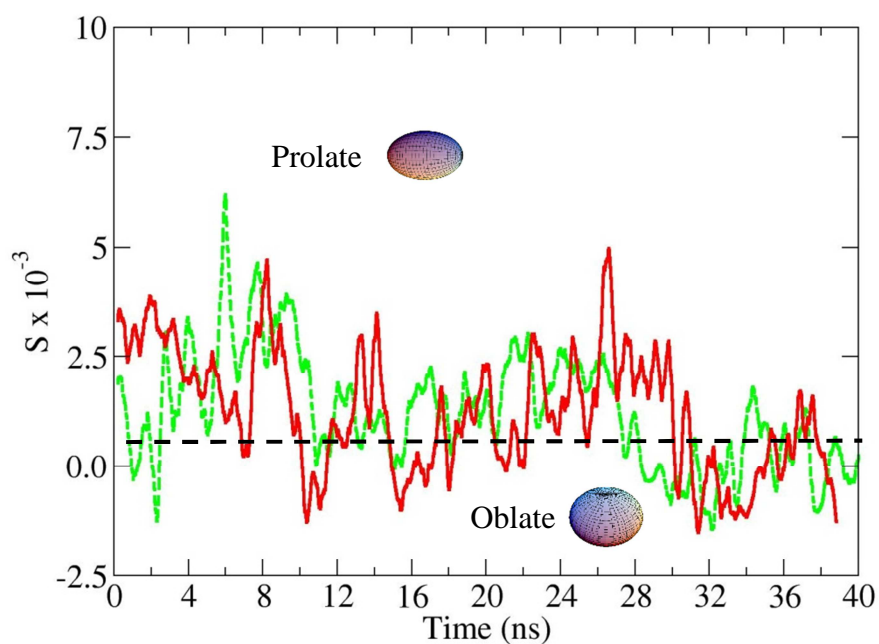


Figure 3.2: Degree of prolatness (S) and Surface Area (SA) for the fully functionalized (solid red line) and Janus (dashed green line) dendrimer at the interface. The results are shown for only one of the two simulations run for each model. In the molecular structures (Low panel): the oxygen, nitrogen and carbon atoms are depicted in red, blue and cyan respectively. Water molecules are omitted for clarity. The vision of the molecule is from the top along the Z-axis in the vacuum phase

Although, due to the intrinsic flexibility of the molecular structure, both the Janus and the fully functionalized dendrimers modify their shape, their orientation at the interface agrees with the analytical predictions [15]. The value of the angle between the Z-axis (perpendicular to the interface plane) and the eigenvector (Λ) corresponding to the highest eigenvalue of the gyration tensor oscillates in fact around 90 degrees ($90^\circ \pm 20^\circ$ averaged over the last 20 ns of the simulations). This result can be inferred also from Fig. 3.3 that depicts the structure of the models after 200 ps and at the end of the simulation. From the figure it can be seen that the fully functionalized dendrimer initially rotates slightly at the interface and changes its relative orientation from perpendicular to the interface to parallel to it. The Janus dendrimer rotates as well from a tilted conformation to a parallel one. From the Figure it appears also clear that in both models the hydrophilic amide groups and the hydrophobic aliphatic chains tend to segregate within the molecule.

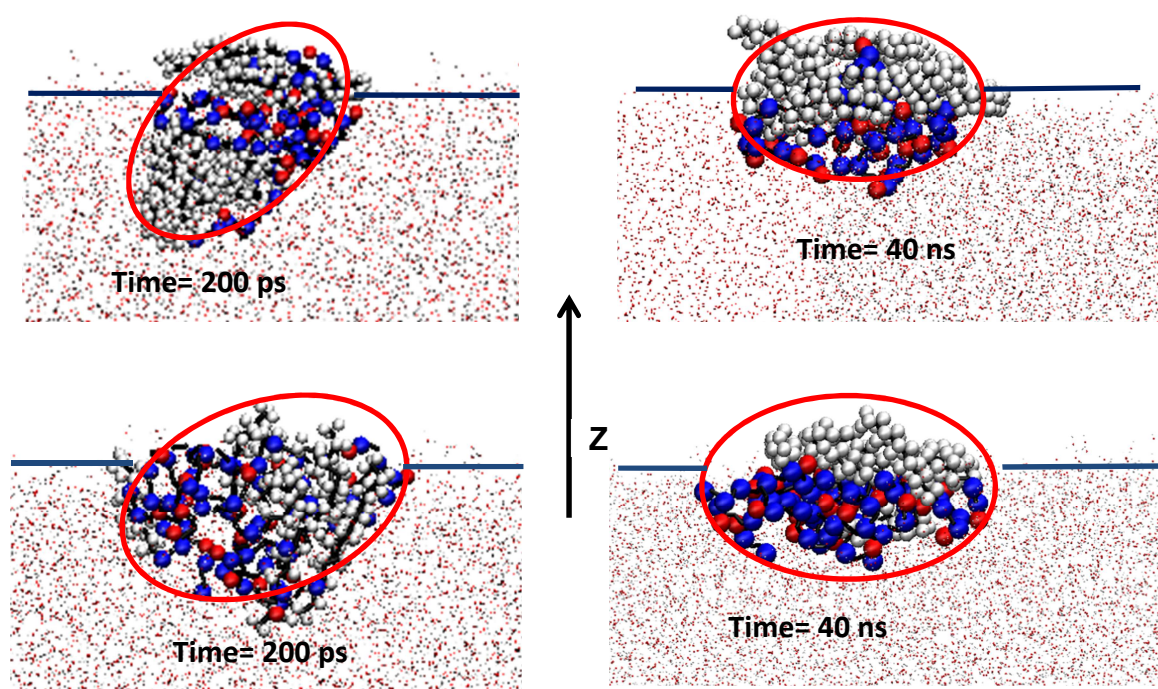


Figure 3.3: Snapshots of the fully modified (top panel) and Janus (lower panel) dendrimer at the interface at the beginning and end of the simulation. The ellipse is drawn to help to visualize the orientation of the molecule with respect to the Z- axis. For the molecular structure: the oxygen, nitrogen atoms are depicted in red and blue respectively; the only the hydrogen atoms bonded to the alkyl chains are pictured (white); the water molecules are pictured as points.

We can quantify this segregation calculating the atomic mass density distribution across the simulation box (in the Z-direction). Fig. 4 shows the change of the density distributions of the apolar atoms (carbon atoms of the alkyl chain) and polar atoms (defined as the nitrogen and oxygen of the amide groups) during the simulation. What appears clearly from the density profiles is that the fully modified dendrimer, when initially placed inside the water phase, cannot expose its hydrophilic part to the water molecules due to the presence of the aliphatic chains that form a hydrophobic layer around it. However, approaching the interface the hydrocarbon chains unwrap revealing the dual nature of the molecule. Fig. 3.4a shows that, when the fully functionalized PAMAM dendrimer is inside the water phase, the polar and apolar atoms distribution is symmetric with respect to the Z-axis. However, when the dendrimer approaches the interface this symmetry is broken and the aliphatic chains extend toward the air while the hydrophilic part of the dendrimer is more exposed to the water.

On the contrary, the Janus dendrimer, due to the distribution of the alkyl chains within the molecule, shows a clear separation between the hydrophilic and hydrophobic parts even when it is immersed into the water phase. When the molecule reaches the interface the separation becomes more evident, however, in contrast with what happens for the fully functionalized molecule, large part of the aliphatic chains is either still in contact with the water or partially immersed in it (Fig. 3.4b).

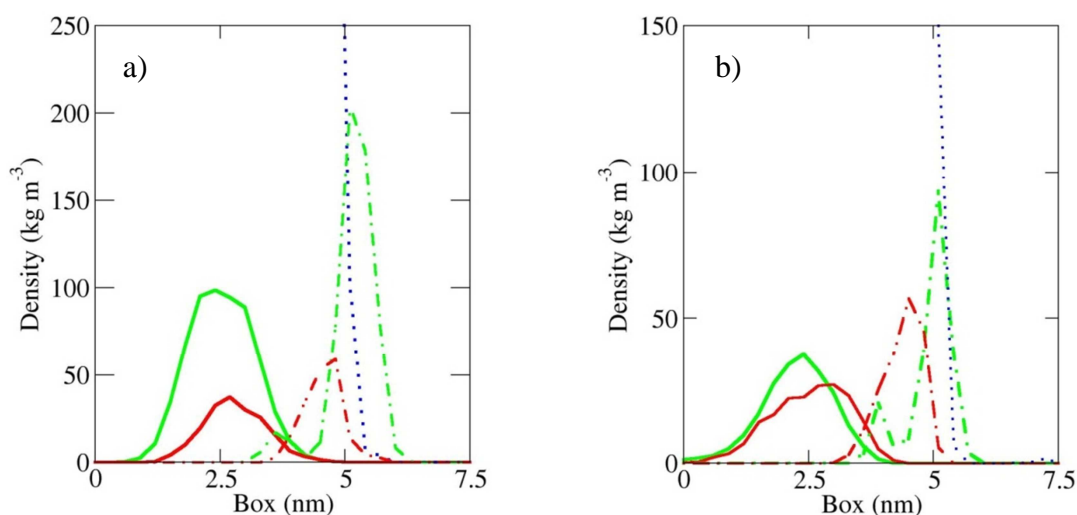


Figure 3.4: Mass density distribution calculated across the interface of the apolar atoms (i.e. carbon atoms of the aliphatic chain) (green line), polar atoms (i.e. nitrogen and oxygen atoms) (red line) and water molecules (dotted blue line) when inside the water phase (solid lines) and when at the interface (point-dashed lines). (a) the fully functionalized dendrimer; (b) the Janus dendrimer.

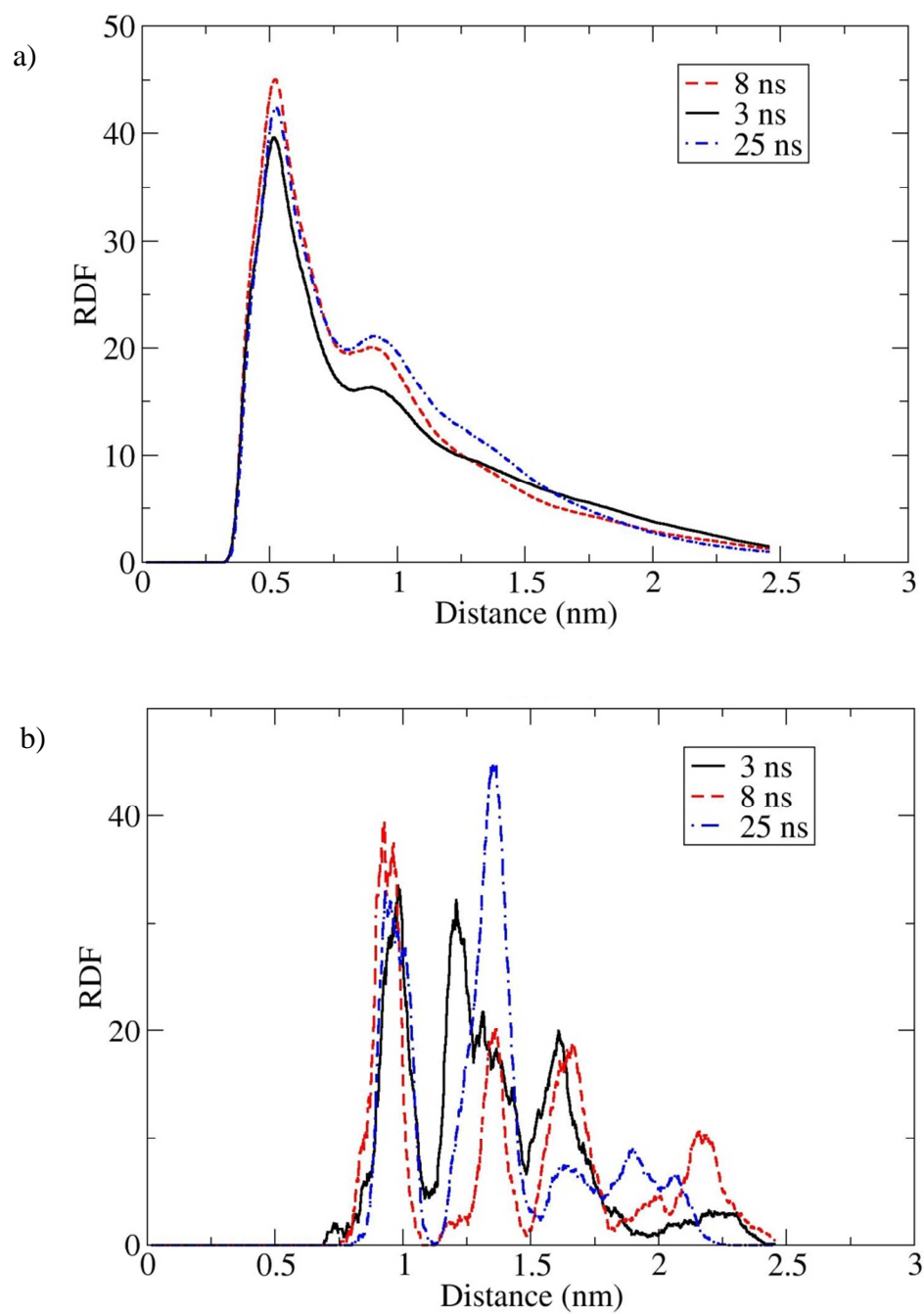


Figure 3.5: Inter-dendron radial distribution function (RDF) calculated for the carbon atoms belonging to the alkyl chains (a) and for the tertiary amine nitrogen atoms (b) of the fully functionalized dendrimer. The RDFs are calculated between the 2-3 ns, 7-8 ns and 24-25 ns.

3.3.2 Hydrogen Bonds and Particle Stability

In this section of the paper we investigate whether the intra dendrimer or dendrimer-water hydrogen bonds (HBs) affect the stability of the molecule at the interface and whether their number changes following the change in the global conformation of the dendrimer molecules. The HBs have been identified following the geometrical criteria reported in references [19] [37] that showed to be able to provide results in agreement with X-ray experimental data. To consider a donor (X_d) -acceptor (X_a) couple hydrogen-bonded the distance between them has to be below 0.3 nm (d_{HB}) and the donor-hydrogen-acceptor ($X_d \cdots H \cdots X_a$) angle above 130° (θ_{HB}). These criteria are broad enough to include all possible HBs formed in the model and are consistent with the NMR findings [19].

Fig. 6a reports the number of HBs calculated from the simulation of the fully functionalized dendrimer when the molecule is initially placed into the water phase. During the 25 ns of the simulation the dendrimer moves toward the interface and approaches it after 10 ns ca. Here it is important to notice that this time scale is typical for this particular simulation and that different starting configurations lead to slightly different time scales. For example in our second simulation the dendrimer reaches the interface after 15 ns ca. However, although the time required for the dendrimer to approach the interface can vary, the variation in the number of HBs with the time is the same in our two simulations: while the dendrimer migrates toward the interface, the number of dendrimer-water HBs constantly increases until reaching a plateau value around which it oscillates, while the number of intra dendrimer HBs slightly decreases. The plateau value, reached in the case reported in Fig. 3.6a after 5 ns ca, is the same for the two simulations carried out on the fully functionalized dendrimer and corresponds to 57 ± 4 . It is appear clear from these results that initially the presence of the aliphatic chains wrapped around the hydrophilic dendrimer core prevents the formation of HBs between the amide groups of the dendrimer whose number, however, increases within the first 5 ns ca. of the simulation.

These results are in agreement with what observed from the RDFs reported in Fig. 3.5a, which shows that approaching the interface the alkyl chains self assemble trying to minimize their contact with the water while the hydrophilic “core” of the dendrimer opens up allowing the formation of HBs with the water molecules. When the dendrimer is directly placed at the interface the number of HBs (both intra dendrimer and dendrimer-solvent) does not change during the entire simulation time (not showed

and their numbers (10 ± 3 and 58 ± 4 respectively) are consistent with the plateau values that can be inferred from Fig. 6a.

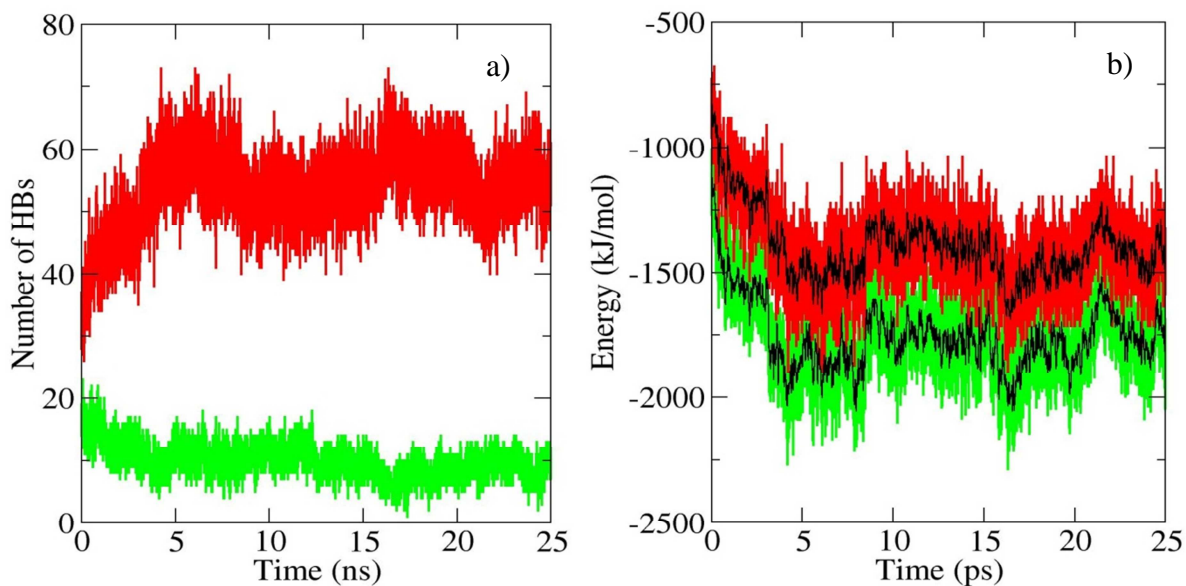


Figure 3.6: Fully functionalized PAMAM dendrimer: a) number of dendrimer-dendrimer (green) and dendrimer-water (red) hydrogen bonds; b) short range Coulomb energy (calculated among atoms whose distance is less than or equal to 1.1 nm) (green) and HBs energy (red). The black line shows the running average (averaged every 20 ps).

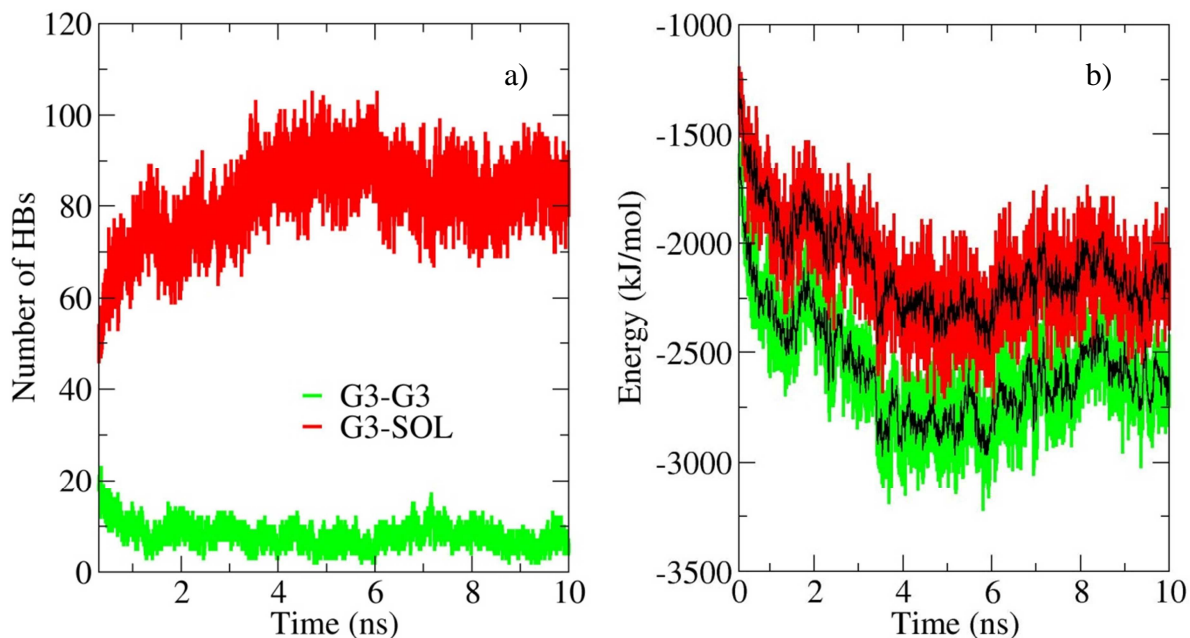


Figure 3.7: Un-functionalized PAMAM dendrimer: a) number of dendrimer-dendrimer (green) and dendrimer-water (red) hydrogen bonds; b) short range Coulomb energy (calculated among atoms whose distance is less than or equal to 1.1 nm) (green) and HBs energy (red). The black line shows the running average (averaged every 20 ps)

Monitoring the different components of the total internal energy of the system while the dendrimer approaches the interface, it can be noticed that the short range (calculated among atoms whose distance is less than or equal to 1.1 nm) electrostatic energy calculated between the dendrimer and the water molecules, shows the largest variation (500 kJ/mol ca.). The energy component initially constantly decreases (see Fig. 6b) and then reaches a plateau. Interestingly, the number of dendrimer-water HBs and the short-range Coulomb energy change with the time in a similar fashion: an increase in the number of HBs corresponds to a decrease in the short range coulomb energy. To make this relation more clear we can associate an energy value to the formation of each HB. Quantum chemical calculations have shown that an averaged value of -26 kJ/mol [38] can be associated to the formation of one HB between an amide group and a water molecule. We can then calculate the total energy due to the creation of the HBs multiplying the number of HBs reported in Fig. 3.6a by -26 kJ/mol. Fig. 6b reports the energy obtained in such way and compares it with the change in the short range Coulomb energy. The two energy profiles follow indeed the exact same pattern.

In order to further analyze the effect of the HBs on the position of the dendrimer with respect to the interface, a new simulation with un-modified PAMAM dendrimer ($R_1=R_2=H$ in Fig. 3.1) of second generation is set up. The simulation is carried out following the procedure described in the previous section. The dendrimer is placed at the air-water interface and a NVT simulation ($T=300K$) is run for 10 ns. After 3 ns ca. the dendrimer has completely moved into the water phase. At this point we also calculate the radius of gyration of the un-functionalised dendrimer in the water phase in order to further verify our force field choice. The R_g obtained (0.92 ± 0.01) agrees well with previous computational and experimental studies [39-41]. Also in this case the major change in the internal energy of the system is due to the decrease of the dendrimer-water short range Coulomb interactions during the first 3 ns of the simulation. Fig. 3.7b shows the short range (atomic distance less than or equal to 1.1 nm) Coulomb energy calculated among the dendrimer and the water molecules and the corresponding HBs energy considering again that each HB corresponds to a -26 kJ/mol. The two energy profiles perfectly match also in this case.

These results show that the major contribution to the change (decrease) in the total internal energy of the system is due to the formation of the dendrimer-water HBs whose number increases when the alkyl chains self-assemble. They also show that the HBs drive the migration of the dendrimer toward the air-water interface and that the

corresponding energy represents the major component of the short range Coulomb interactions. Moreover, Fig. 3.6b proves that the OPLS-AA force field [22, 23] is a reliable inter-atomic potential for polyamides being able to reproduce the correct energy for the amide-water HBs. Similar calculations are performed on the Janus dendrimer. In this case the number of HBs (63 ± 5) does not change when the dendrimer travels toward the interface showing that the aliphatic chains, being attached only to one side of the molecule, do not hinder the formation of HBs between the water and the amide groups whose number is slightly higher than that of the fully functionalized PAMAM. However, this also shows that the amide groups belonging to the arms functionalized with the n-decane are restrained in their conformation probably for steric reasons.

To verify this hypothesis, we calculate the root mean squared fluctuation (RMSF) of the position of the hydrogen atoms attached to the alkyl chains around the averaged structure. Fig. 3.8 shows that, at the beginning of the simulation (1.5-3.5 ns) the aliphatic chains attached to the Janus dendrimer are on average less mobile than those attached to the fully functionalized one, but once the aliphatic chains have rearranged, their relative mobility is reversed and the chains attached to the fully modified PAMAM become on average less mobile than those of the Janus molecule. This fact can be explained considering that in the water phase the aliphatic chains surrounding the amphiphilic “core” of the fully modified dendrimer try to avoid the contact with the water molecules while the amide groups of the core form HBs as soon as they are enough close to them. This metastable situation leads to frequent intramolecular conformational changes.

Once the dendrimer is at the interface the segregation of the apolar and polar parts of the molecule imparts a peculiar conformation to the dendrimer that tries to maximize the energetic favourable contacts. All the aliphatic chains tend to separate from the water interface and segregate as much as the topology of the molecule allows. This creates a very crowded environment around the aliphatic carbons (and so around the hydrogen covalently bonded to them) that hampers the motion of the atoms. In the case of the Janus dendrimer, on the contrary, the fact that the polar and apolar parts of the molecule are separated topologically makes energetically more stable the dendrimer into the water phase. In fact, in the water solution the amide groups belonging to the unfunctionalized dendrons form HBs with the water, while the others form intradendrimer HBs. Once the dendrimer reaches the interface, the aliphatic chains that extend out from the interface show a less restrained dynamics than that of the fully

functionalized dendrimer. In fact, being their number half of the number of the fully functionalized dendrimer, they are less sterically constrained.

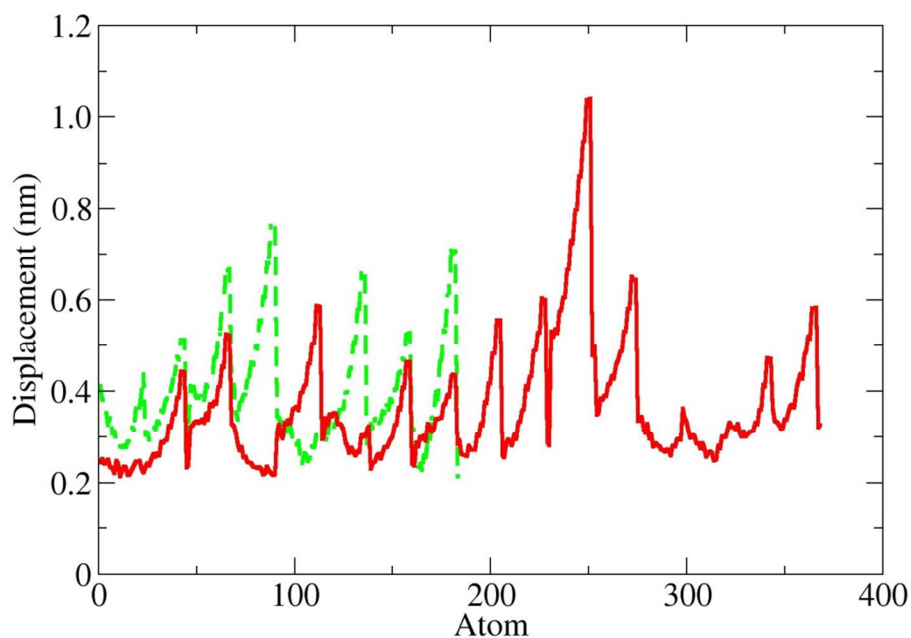
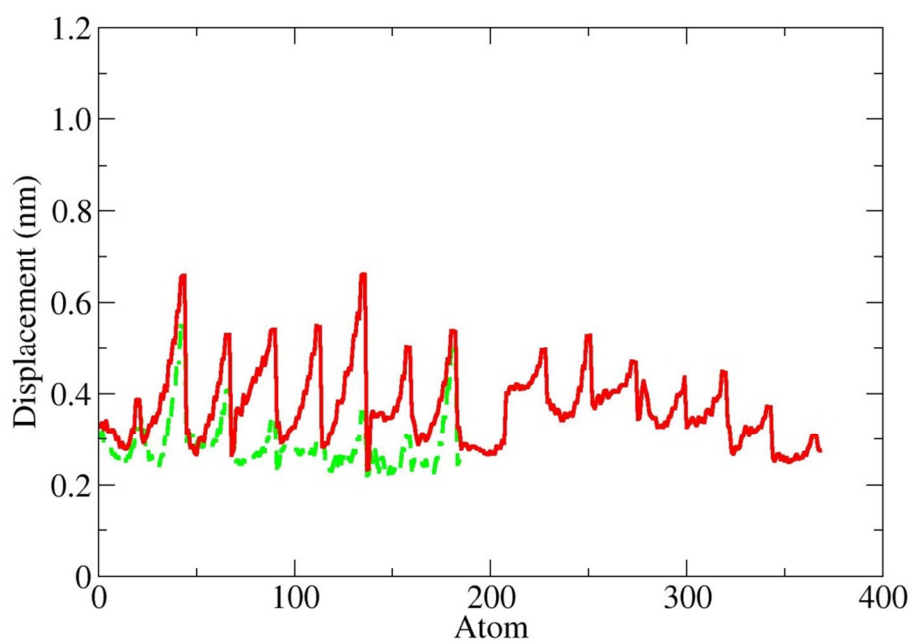


Figure 3.8: Root mean square fluctuation (RMSF) of the hydrogen atoms attached to the alkyl chains of the Janus (green dashed line) and fully functionalized (red solid line) dendrimer, when the dendrimer is in the water phase (first part of the simulation) (top) and when it is at the interface (bottom).

As described in the previous section, both amphiphilic dendrimers investigated here adopt at the interface either a oblate or prolate shape with the highest eigenvector of the gyration tensor perpendicular to the Z-axis (see Fig. 3.3 and 3.4). Moreover we have showed that large part of the alkyl chains of the fully functionalized dendrimer emerged from the water phase extending into the vacuum, while for the Janus molecule the apolar chains are largely submerged by the water molecule.

We can further analyse the stability of dendrimers at the interface by looking at their wetting properties such as the contact area. In fact, particles with large contact area show higher stability than those with smaller one. From our simulations we can calculate the area of the dendrimer at the water-air interface slicing the dendrimer in the Z direction and taking only those atoms whose centres of mass lie at the interface (that corresponds to $z=0$ nm). In order to calculate the area a 2D grid is built around the portion of the molecule in contact with the interface (see Fig. 3.9). The mesh of the grid is tune until the resulting area converges. For the fully functionalized dendrimer, the area calculated in such way and averaged over the last 2 ns of the simulation is $780 \pm 20 \text{ \AA}^2$. This result can be reasonably compared with the experimental limiting molecular area obtained for PAMAM dendrimer of generation 3 (16 end-groups) but modified with lauroyl chloride ($\text{C}_{11}\text{H}_{23}\text{COCl}$) that is $676 \pm 1 \text{ \AA}^2$ [6]. It is, in fact, expected the experimental value to be smaller than the simulated one as the data are extrapolated at zero surface pressure under maximum packing conditions.

The same calculation using the last 2 ns of the simulation of the Janus dendrimer gives an area of $660 \pm 7 \text{ \AA}^2$. The fact that the Janus dendrimer shows a smaller area at the interface compared with the fully modified one agrees with the results obtained from the calculation of the surface area and degree of prolatness and may indicate that, surprisingly, the topologic dual nature of the Janus molecule does not increase its stability at the interface. In fact, the flexible structure of the dendrimer and its symmetric topology allow the fully modified molecule to change its behaviour depending on which environment it is placed in.

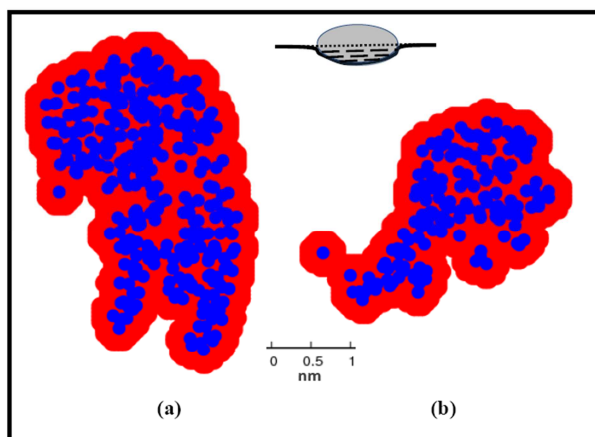


Figure 3.9: Area per dendrimer (red) at the interface calculated using the geometrical method as reported in the text for (a) the fully modified dendrimer; (b) the Janus dendrimer. The atom positions are showed in blue and correspond to the configuration after 10 ns of simulation. In the figure the prolate nanoparticle at the interface is also schematically represented in 2D. The volume calculated in the text corresponds to the dashed area.

3.4 Summary and Conclusions

By means of atomistic molecular dynamics simulation we have investigated the stability of alkyl modified polyamino-amide dendrimer (PAMAM) at the air-water interface as a function of the number and relative position of the functionalized terminal amine groups. In particular we have simulated two types of amphiphilic dendrimers one where all the amine terminal groups are modified with n-decane and another where only half of the terminal groups (in a symmetric fashion) are functionalized (Janus particle). We used our simulations to test the most recent thermodynamic theories developed for nanoparticles at interfaces and to compare the relative stability of two macromolecules characterized by different topological structure.

We found that both our models follow the theoretical predictions in terms of particle orientation and particle shape. In fact, the dendrimers are oriented with their longest axis perpendicular to the normal of the interface line. Due to the topology of the molecule, its shape oscillates between the predicted two most stable shapes (oblate and prolate) with their aspect ratio α is also in agreement with the theoretical value.

The dendrimer mass density distribution calculated across the interface showed that the Janus dendrimer is largely submerged by the water molecules while the alkyl

chains of the fully functionalized PAMAM stand out from the water phase and extend toward the vacuum.

We observed that in the case of the fully functionalized model the molecular interactions that govern the migration of the dendrimer toward the interface are the dendrimer-water hydrogen bonds (HBs). Similar simulations performed on unmodified PAMAM dendrimer of the same generation showed that the dendrimer-water HBs are also responsible for the motion of the hydrophilic dendrimer from the air-water interface into the water phase.

We showed that when the amphiphilic dendrimer is into the water phase, the long aliphatic chains are initially wrapped around the hydrophilic part of the dendrimer and hinder the formation of the intermolecular HBs. Within the first 10-15 nanoseconds the alkyl chains unwrap and segregate avoiding the contact with the water solvent and the dendrimer migrates toward the interface.

We noticed that the clustering of the alkyl chains starts when the dendrimer is still submerged by the water and leads to a more ordered structure for the hydrophilic dendrimer “core” which opens up and form HBs with the water solvent. On the contrary, in the case of the Janus dendrimer, the number of HBs when the molecule is at the interface does not differ from their number when the molecule is into the water phase showing that the asymmetric topology of the dendrimer does not require any major changes to minimize its energy.

Calculating the interfacial contact area between the dendrimer and the water, we observed that the fully modified PAMAM molecule shows a higher contact area than the Janus one confirming that the former is characterized by a more oblate 3D shape than the latter.

These results indicate that, due to the topology of the molecule and the flexibility of its dendrons, the fully functionalized dendrimer show better stability at the interface than the Janus one. This latter result may indicate that monolayers of fully modified dendrimers are characterized by the same or higher stability than monolayer of Janus dendrimer, confirming the extraordinary versatility of dendrimeric molecules and the necessity of atomistic molecular modelling to gain a complete picture of their behaviour.

3.5 References

1. Tully, D.C. and J.M.J. Frechet, *Dendrimers at surfaces and interfaces: chemistry and applications*. Chemical Communications, 2001(14): p. 1229-1239.
2. Frechet, J.M.J., *Dendrimers and supramolecular chemistry*. Proceedings of the National Academy of Sciences of the United States of America, 2002. **99**(8): p. 4782-4787.
3. Pericet-Camara, R., et al., *Nano-patterning of solid substrates by adsorbed dendrimers*. Chemical Communications, 2007(3): p. 266-268.
4. Tokuhisa, H. and R.M. Crooks, *Interactions between organized, surface-confined monolayers and vapor-phase probe molecules .12. Two new methods for surface-immobilization and functionalization of chemically sensitive dendrimer surfaces*. Langmuir, 1997. **13**(21): p. 5608-5612.
5. Sui, G., et al., *A structural study of amphiphilic PAMAM (poly(amido amine)) dendrimers in Langmuir and Langmuir-Blodgett films*. Journal of Colloid and Interface Science, 2002. **250**(2): p. 364-370.
6. Zhang, T., P.R. Dvornic, and S.N. Kaganove, *A comparative study of Amphiphilic PAMAM dendrimers at the air-water interface with different hydrophobe attachment groups*. Langmuir, 2007. **23**(21): p. 10589-10597.
7. Chooi, K.W., et al., *The Molecular Shape of Poly(propylenimine) Dendrimer Amphiphiles Has a Profound Effect on Their Self Assembly*. Langmuir, 2010. **26**(4): p. 2301-2316.
8. Esfand, R. and D.A. Tomalia, *Poly(amidoamine) (PAMAM) dendrimers: from biomimicry to drug delivery and biomedical applications*. Drug Discovery Today, 2001. **6**(8): p. 427-436.
9. Lee, C.C., et al., *Designing dendrimers for biological applications*. Nature Biotechnology, 2005. **23**(12): p. 1517-1526.
10. Rosen, B.M., et al., *Dendron-Mediated Self-Assembly, Disassembly, and Self-Organization of Complex Systems*. Chemical Reviews, 2009. **109**(11): p. 6275-6540.
11. Percec, V., et al., *Self-Assembly of Janus Dendrimers into Uniform Dendrimerosomes and Other Complex Architectures*. Science, 2010. **328**(5981): p. 1009-1014.

12. Walther, A. and A.H.E. Muller, *Janus particles*. *Soft Matter*, 2008. **4**(4): p. 663-668.
13. Faraudo, J. and F. Bresme, *Stability of particles adsorbed at liquid/fluid interfaces: Shape effects induced by line tension*. *Journal of Chemical Physics*, 2003. **118**(14): p. 6518-6528.
14. Cheung, D.L. and S.A.F. Bon, *Interaction of Nanoparticles with Ideal Liquid-Liquid Interfaces*. *Physical Review Letters*, 2009. **102**(6): p. 066103-066107.
15. Bresme, F. and M. Oettel, *Nanoparticles at fluid interfaces*. *Journal of Physics-Condensed Matter*, 2007. **19**(41): p. 413101-413134.
16. Cheung, D.L. and S.A.F. Bon, *Stability of Janus nanoparticles at fluid interfaces*. *Soft Matter*, 2009. **5**(20): p. 3969-3976.
17. Mladek, B.M., G. Kahl, and C.N. Likos, *Computer assembly of cluster-forming amphiphilic dendrimers*. *Physical Review Letters*, 2008. **100**(2): p. 028301-028305.
18. Carbone, P. and L. Lue, *Prediction of Bulk Density and Molecular Packing in Model Dendrimers with Different Chain Stiffness*. *Macromolecules*, 2010. **43**(21): p. 9191-9197.
19. Carbone, P. and F. Müller-Plathe, *Molecular dynamics simulations of polyaminoamide (PAMAM) dendrimer aggregates: molecular shape, hydrogen bonds and local dynamics*. *Soft Matter*, 2009. **5**(13): p. 2638-2647.
20. Carbone, P., et al., *Shape persistence and bistability of planar three-fold core polyphenylene dendrimers: A molecular dynamics study*. *J. Phys. Chem. A*, 2006. **110**(6): p. 2214-2224.
21. Tay, K.A. and F. Bresme, *Wetting properties of passivated metal nanocrystals at liquid-vapor interfaces: A computer simulation study*. *Journal of the American Chemical Society*, 2006. **128**(43): p. 14166-14175.
22. Rizzo, R.C. and W.L. Jorgensen, *OPLS all-atom model for amines: Resolution of the amine hydration problem*. *Journal of the American Chemical Society*, 1999. **121**(20): p. 4827-4836.
23. Jorgensen, W.L., D.S. Maxwell, and J. TiradoRives, *Development and testing of the OPLS all-atom force field on conformational energetics and properties of organic liquids*. *J. Am. Chem. Soc.*, 1996. **118**(45): p. 11225-11236.
24. Goudeau, S., M. Charlot, and F. Muller-Plathe, *Mobility Enhancement in Amorphous Polyamide 6,6 Induced by Water Sorption: A Molecular Dynamics*

- Simulation Study*. The Journal of Physical Chemistry B, 2004. **108**(48): p. 18779-18788.
25. Roberts, B.P., et al., *Molecular Dynamics of Variegated Polyamide Dendrimers*. Macromolecules, 2009. **42**(7): p. 2784-2794.
 26. Karimi-Varzaneh, H.A., P. Carbone, and F. Muller-Plathe, *Hydrogen Bonding and Dynamic Crossover in Polyamide-66: A Molecular Dynamics Simulation Study*. Macromolecules, 2008. **41**(19): p. 7211-7218.
 27. Berendsen, H.J.C., J.R. Grigera, and T.P. Straatsma, The Missing Term In Effective Pair Potentials. Journal of Physical Chemistry, 1987. **91**(24): p. 6269-6271.
 28. Tironi, I.G., Sperb, R., Smith, P. E., van Gunsteren, W. F., *A generalized reaction field method for molecular dynamics simulations*. Journal of Chemical Physics, 1995. **102**: p. 5451–5459.
 29. Berendsen, H.J.C., et al., Molecular Dynamics with Coupling to an External Bath Journal of Chemical Physics, 1984. **81**(8): p. 3684-3690
 30. Berendsen, H.J.C., D. van der Spoel, and R. van Drunen, *GROMACS: A message-passing parallel molecular dynamics implementation*. Comp. Phys. Comm., 1995(91): p. 43-56.
 31. Lindahl, E., B. Hess, and D. Van Der Spoel, *GROMACS 3.0: a package for molecular simulation and trajectory analysis*. Journal of Molecular Modeling, 2001. **7**(8): p. 306-317.
 32. Van der Spoel, D., et al., *GROMACS: Fast, flexible, and free*. Journal of Computational Chemistry, 2005. **26**(16): p. 1701-1718.
 33. Theodorou, D.N. and U.W. Suter, *Rg*. Macromolecules, 1985. **18**: p. 1206-14.
 34. Blavatska, V. and W. Janke, *Shape anisotropy of polymers in disordered environment*. Journal of Chemical Physics, 2010. **133**(18): p. 184903-184910.
 35. Klamkin, M.S., *Elementary Approximations to the Area of N-Dimensional Ellipsoids*. The American Mathematical Monthly, 1971. **78**(3): p. 280-283.
 36. Klamkin, M.S., The American Mathematical Monthly, 1976. **83**(6): p. 478.
 37. Karimi-Varzaneh, H.A., P. Carbone, and F. Muller-Plathe, *Hydrogen Bonding and Dynamic Crossover in Polyamide-66: A Molecular Dynamics Simulation Study*. Macromolecules, 2008. **41**(19): p. 7211-7218.
 38. Mitchell, J.B.O. and S.L. Price, On the Relative Strengths of Amide-Amide and Amide-Water Hydrogen Bonds. Chemical Physics Letters, 1991. **180**(6): p. 517-523.

39. Maiti, P.K., et al., *Structure of PAMAM dendrimers: Generations 1 through 11*. *Macromolecules*, 2004. **37**(16): p. 6236-6254.
40. Maiti, P.K., et al., *Structure of polyamidoamide dendrimers up to limiting generations: A mesoscale description*. *Journal of Chemical Physics*, 2009. **130**(14): p. 10.
41. Rathgeber, S., et al., *Dynamics of star-burst dendrimers in solution in relation to their structural properties*. *Journal of Chemical Physics*, 2002. **117**(8): p. 4047-4062.

Interactions of PEO-PPO-PEO block copolymers with lipid membranes: a computational and experimental study linking membrane lysis with polymer structure

This chapter has been published in Soft Matter (see Appendix B)

Authors: Selina Nawaz, Martin Redhead, Guiseppe Mantovani, Cameron Alexander, Cynthia Bosquillon and Paola Carbone

This Chapter is primarily the work of S. Nawaz based on a collaboration study with M. Redhead from the University of Nottingham who performed the experimental study associated to the work.

4.1 Introduction

The development of self-assembled nanostructures formed by amphiphilic macromolecules and their evaluation as nano-devices or as means to alter the cell membrane properties has dramatically increased in recent years [1, 2]. Such amphiphiles can interact strongly with the cell membrane and, depending on their concentration and molecular structure, modify its mechanical properties [3]. Block copolymers sold as PluronicsTM are a specific class of triblock amphiphilic copolymers whose structure consists of hydrophilic, poly(ethylene oxide) (PEO), and hydrophobic, poly(propylene oxide) (PPO), blocks arranged in A-B-A (PEO-PPO-PEO) tri-block structure. These polymers can be used as surface coating for nanoparticles [4], or, exploiting their ability to self-assemble in polar solvents, as drug or gene “nano carriers” [5, 6]. Recently, some PEO-PPO-PEO copolymers within the Pluronic class also have been shown to elicit biological responses both *in vitro* and *in vivo* increasing the susceptibility of multi drug resistant cancer cells to chemotherapeutic agents such as doxorubicin [7] and in enhancing gene transcription [8]. Because these copolymers are designed to interact with and target specific organs within the human body, it is

important to understand the molecular mechanism underpinning their association with lipid bilayers in order to avoid toxicity and to inform future rational polymer design. Although numerous experimental studies have been conducted to understand the association and incorporation of selected Pluronics with the lipid membrane, a detailed picture of the interaction mechanism has not been achieved. Indeed, the complex interplay between the chemical interactions can be assessed by the fact that experimental studies employing different models of the lipid membrane such as monolayers [9], bilayers [10] or unilamellar vesicles [11] have showed contradictory results. The data have suggested that in some cases the amphiphilic copolymers are able to heal a damaged membrane by stabilizing its structure [9], but in other cases, that the presence of the copolymers disturbs the lipid packing and enhances membrane permeability [12]. The polymer insertion and expulsion mechanisms in and out the membrane are themselves still unclear. Similarly, which block of the copolymer chain penetrates inside the membrane, e.g. whether it is only the hydrophobic block or the whole copolymer chain, remains uncertain. It is however clear that these copolymers, depending on their architecture and hydrophilic:hydrophobic block lengths and ratios, can bind tightly to a lipid membrane and be translocated across it [13]. Several experiments have also shown that, depending on the nature of the binding interaction (hydrophobic or hydrophilic) the copolymers, when inside the bilayers, induce local disorder and accelerate the flip-flop of lipids [14].

Even though computational chemistry is an important tool to gain a detailed picture of the molecular interactions, it has been applied only recently to simulate synthetic-biological material interfaces [15-18]. In particular, recently several computational studies have reported interesting results about the interaction mechanism between hydrophilic polymers such as PEG (poly ethylene glycol) and model lipid membranes when the polymer is in physical contact with or covalently bonded to (PEGylated membrane) phospholipid membranes [19-22]. Using coarse-grained and mesoscopic models the interactions between amphiphilic copolymers and both solid support [23] and model membranes [24] have also been simulated. However, despite their widespread use as drug delivery nanocarriers, the effects that amphiphilic copolymers have on the structure of the lipid bilayers have been studied only by means of coarse-grained models [25, 26] while, to the best of our knowledge, atomistic simulations of amphiphilic copolymers such as the Pluronics embedded in model lipid membranes have not been reported yet.

In this paper we investigate how the presence of selected amphiphilic PEO-PPO-PEO block copolymers, spanning a range hydrophilic/hydrophobic contents and different overall molar masses, affects the internal structure of model lipid membranes. We present the simulation results along with new experimental haemolysis data obtained by using copolymers with the same size and architecture of those simulated. Our computational results provide a molecular picture of the interactions between amphiphilic copolymers and lipid membranes and suggest a clear structure-function relationship between amphiphilic block copolymer microstructure and their membrane disruptive effects.

4.2 Systems under Investigation

The Pluronic copolymers investigated in this manuscript were L31, L61, L62, L64, and the key features of these polymers are reported in Table 4.2. The simulations were performed on model lipid membrane consisting of 128 dipalmitoylphosphatidylcholine (DPPC) phospholipids, 64 lipids per monolayer, hydrated with 3655 water molecules incorporating one polymer chain. In this study we assume that the polymer chain has already translocated across the lipid bilayer and the triblock copolymer is added directly into the central part of the bilayer membrane. The assumption that the Pluronics investigated in this work can translocate into the membrane is justified considering their experimental water-hexane partition coefficients [14] and the high experimental binding constants (the latter reported in Table 4.2). These values in fact indicate, respectively, that these Pluronics are hydrophobic enough to translocate across the membrane and bind to it. To further test this assumption, four simulations where the copolymer chains reported in Table 4.2 are initially placed outside the membrane, i.e. in the water phase, have been set up and run for 300 ns. In all cases we see the passive migration of the whole copolymer inside the membrane (see supporting information: Fig. 1S).

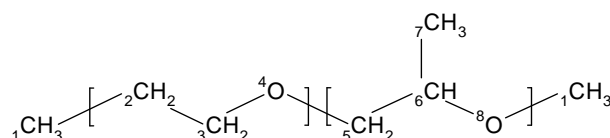
4.3 Methods

4.3.1 Simulations

The starting configuration, force field parameters and GROMACS type topology files for the DPPC bilayer have been downloaded from Biocomputing group at the University of Calgary [27]. The lipids were modelled using the GROMOS [28] united atom force field with modifications from the work of Berger and co-workers [29] and the SPC model [30] was used for the water in the systems. To model the poly(ethylene-oxide)-poly(propylene-oxide)-poly(ethylene-oxide) triblock copolymers two different force fields have been used. Firstly we tested the unmodified GROMOS force field with ad-hoc set of partial charges specific for the copolymer chain obtained from DFT calculations using Gaussian 03 [31] software performed with the B3LYP functional form and with 6-311+G** as basis set. The quantum mechanical calculations were performed on short oligomers of PEO (two monomers) and PPO (three monomers) capped with methyl groups (see the structural formula associated with Table 4.1). After a geometry optimization the charges were calculated using the CHelpG method. [32] The final charges (after few small modifications in order to neutralize the monomer) used during the simulation are reported in Table 4.1. Then we also tested a new GROMOS-type atomistic force field recently developed by Hezaveh et al. [33] specifically developed for the ethylene-oxide and propylene-oxide monomers.

Table 4.1: Copolymer partial charges distribution obtained from DFT calculations. Atom types are those used in the GROMOS force field [28].

Atom number	Atom type	Charge[C]
1	CH3	0.006
2	CH2	0.200
3	CH2	0.200
4	OS	-0.406
5	CH2	0.190
6	CH	0.280
7	CH3	-0.020
8	OS	-0.450



Due to the flexibility of the copolymer chain, for the two copolymers with intermediate length (L61 and L62), three different starting configurations are considered. In two of these starting points, the polymer main chain assumes an extended conformation with each PEO block interacting with a different membrane leaflet (see Fig. 4.3). One of the three starting configurations considers instead that the copolymer could assume a U-shape conformation where both PEO blocks are in contact with the same leaflet (see Fig. 4.3). The initial configurations were obtained following the procedure described below. Each copolymer chain was initially separately energy minimized using steepest decent method and then briefly simulated (300 ps) in vacuum to accelerate the coiling up of the chain. Each polymer was then placed in the centre of the DPPC membrane within the hydrocarbon region. The final (polymer-membrane) systems were then energy minimised to reduce any residual unfavourable steric interactions and then equilibrated. During the equilibration the polymer assumed either

an extended conformation or a U-shape conformation and maintained that configuration during the length of the simulation (see supporting information Fig. 2-3S).

Three different simulations were run for the two copolymers with intermediate length (L61 and L62) while two starting configurations have been used for the shortest and the longest copolymers (L31 and L64).

All simulations were performed using the GROMACS software package (version 4.5.2) [34]. Bond lengths were constrained using the LINCS algorithm [35] and a 2fs timestep was employed. The particle-mesh Ewald summation [36, 37] was used to calculate the long range electrostatic interactions with a Fourier spacing of 0.12 nm and a fourth order interpolation. The coulomb cutoff and the van der Waals cutoff were set to 0.9 nm and 1.2 nm respectively. The neighbour list was updated every 10 steps using a grid with 0.9 nm cutoff distance. The NpT ensemble was adopted where the temperature was maintained at 325 K, well above the phase transition temperature of DPPC (315 K) [38], with a Berendsen thermostat with one single coupling time of 0.1 ps used for the whole system [39]. Semiisotropic pressure coupling was used where the simulation box in the bilayer normal (z-axis) and the cross sectional area of the box in the x-y plane can vary independently using Berendsen barostat [39] with a reference pressure of 1 bar, coupling time of 1.0 ps and compressibility to $4.5 \times 10^{-5} \text{ bar}^{-1}$.

4.3.2 Haemolysis assay

Fresh blood was collected from healthy adult male volunteers (ethical approval was obtained from the University of Nottingham Medical School Ethics Committee) and the erythrocytes were separated by centrifugation. For determination of the membrane binding constant (K_b), suspensions containing erythrocytes at hematocrits between 0.03%-0.3% were prepared in Phosphate Buffered Saline (PBS). These were added to 96 well plates containing solutions of the Pluronics at concentrations ranging from 0.0005M to 0.1 M. Untreated erythrocytes (spontaneous lysis), erythrocytes treated with 4% Triton X-100 (100% lysis) and solutions of each polymer without erythrocytes (background absorbance) were used as controls. After four hours of incubation, the plates were centrifuged and the supernatant was placed in a fresh plate. The absorbance was read at 410nm in a TECAN colorimetric plate reader (2 sets of 6 replicates). Dose response curves showing haemolysis normalised for controls against polymer concentration were produced and the analysis of Lichtenberg et al [40] was

followed to obtain K_b [41, 42].

For the kinetics study, erythrocytes at a haematocrit of 0.6% in PBS were added to test tubes containing 1 M Pluronic solutions, resulting in a final haematocrit of 0.3% and a Pluronic concentration of 0.5 M. The tubes were incubated at 37 °C. Every 15 minutes over a two hour time period, tubes were collected and centrifuged at 600 g for 5 minutes. The supernatant was transferred into a 96 well plate and the absorbance was read at 410 nm.

Absorbance values were compared to those obtained with erythrocytes treated with 4% (w/v) Triton X-100 (100% lysis) or PBS (0% lysis) and Pluronic solutions without erythrocytes (background absorbance). Percentage haemolysis values were plotted against the time of incubation and the time needed to achieve 50% lysis (T50) was determined.

4.4 Analysis performed

4.4.1 Order Parameter

As a measure of the degree of order within the DPPC bilayer, the deuterium order parameter S_{CD} were calculated for the acyl chains. As there are no explicit hydrogen atoms in the simulations, the order parameters were calculated from the positions of the carbon atoms along the chain.

The orientation of the ordering of the phospholipid tails in the bilayer with respect to the bilayer normal per atom was calculated using the following expression

$$S_z = \frac{3}{2} \langle \cos^2 \theta_z \rangle - \frac{1}{2} \quad (4.1)$$

where θ_z is the angle between the molecular vector defined by the vector from C_{n+1} to C_{n-1} and the z axis which is parallel to the bilayer normal. The value of S_z obtained from eq. 4.1 for united atoms models can be then compared with the experimental values (S_{CD}) obtained from NMR on deuterated DPPC considering that $S_{CD} = -1/2 S_z$ [43].

4.4.2 Radius of Gyration

Detailed atomistic simulations enable to monitor the change in the 3D molecular shape by the calculation of the second moment of the atomic distribution (the gyration tensor) which is defined as

$$\mathbf{R}_{\alpha,\beta}^2 = \frac{1}{N} \sum_{i=1}^N (\mathbf{r}_{\alpha}^i - \mathbf{r}_{\alpha}^M)(\mathbf{r}_{\beta}^i - \mathbf{r}_{\beta}^M) \quad \alpha, \beta = x, y, z \quad (4.2)$$

where N is the number of atoms in the molecule, \mathbf{r}_{α}^i is the position of the i -th atom and \mathbf{r}_{α}^M is the position of the molecule's geometrical centre.

4.4.3 Mass Density Distribution

The heterogeneity of the system was analysed by calculating the mass density distribution across the bilayer. The mass density is calculated for the DPPC bilayer, the copolymer and the solvent molecules and for certain groups of atoms. The distance, D_{P-P} , calculated between the two phosphorus-phosphorus atom density distributions calculated separately for the two individual monolayers, is used to determine the thickness of the bilayer.

4.4.4 Head group P-N tilt angle

The orientation of the lipid head group orientation is analysed calculating the distribution of the angle θ defined as the angle between the phosphorus-nitrogen (P-N) vector and the outward normal of each leaflet which is assumed to be parallel to the z axis of the simulation box.

4.5 Results and Discussions

4.5.1 Validation of the force parameters and polymer structure

Experimentally different Pluronics show different levels of biological activity depending on the copolymer structure and molecular weight. In particular, our recent studies [41, 42] highlighted that a relationship exists between the length of both the hydrophilic (PEO) and hydrophobic (PPO) blocks, the experimental membrane binding constant (K_b) and the cytotoxic effect of the copolymers. The data suggest that as the membrane-polymer interaction increases (i.e. increasing value of K_b), the higher is the cytotoxicity of the copolymer as measured by MTS and LDH assays. Therefore, for our simulations we choose four different Pluronics exhibiting different experimental K_b values and spanning a range of hydrophobic and hydrophilic block lengths. Table 4.2 summarizes the characteristics of the systems simulated and the length of the simulations. The table also reports the experimental binding constant (K_b) values that indicate the strength of the polymer-membrane interactions and have been generated from haemolysis assay [41, 42].

Table 4.2: Characteristics of the simulated systems. ${}^a N_m$ represents the number of PO repeating units in the PPO core. ${}^b N_n$ indicates the number of EO repeating units on each side of the PEO-PPO-PEO triblock copolymers. For example, L31 ($N_m=16$ and $N_n=2$) corresponds to a $EO_2-PO_{16}-EO_2$ triblock copolymer. c Experimental binding constants determined by haemolysis assay [41, 42].

Pluronics name	${}^a N_m$ PPO	${}^b N_n$ PEO	Simulation time (ns)	${}^c K_b$ (M^{-3})
L31	16	2	200	0.13
L61	31	3	200	0.97
L62	31	6	200	-
L64	31	14	300	1.66

It is known that the GROMOS force field should be used with caution to simulate in water polymers containing ether oxygen atoms as it might underestimate the polymer hydrophilicity. Simulations of poly(ethylene-oxide) in water have in fact showed that the radius of gyration of homopolymer composed by more than 40 monomers is underestimated by 30% ca. at room temperature [44]. Therefore in order to

test whether the GROMOS force field can be used to model PEO-PPO copolymers in apolar environments (that correspond to the environment inside the lipid membrane) we initially simulated the four Pluronics reported in Table 4.2 in hexane and compared the resulting polymer radius of gyration (R_g) with the corresponding values obtained employing a new united atom models compatible with the GROMOS force field recently developed specifically for the ethylene-oxide and propylene-oxide monomers [33].

Table 4.3 reports the values of R_g obtained for the different copolymer models after 50 ns of molecular dynamics simulation performed at room temperature (300 K). From the good agreement between the R_g values reported in the table it appears clear that the GROMOS force field can be confidently used to simulate in apolar solvent the Pluronic copolymers investigated in this study. Moreover to further test the original GROMOS force field we calculated the bulk density of dimers of the PO (i.e. 2-[2-methoxy propoxy] butane). The simulation was run at 300K at 1 atm for 10 ns. The resulting density, $0.879 \pm 0.05 \text{ g/cm}^3$ is in good agreement with the value of 0.865 g/cm^3 obtained from previous atomistic simulations (and validated against experimental data) performed on 1,2-dimethoxy propane at the same temperature [45].

Table 4.3. Comparison between the values of the radius of gyration (R_g) of single block copolymer chain simulated in hexane at 300 K.

Model	R_g [nm]	R_g [nm]
	GROMOS original [28, 29]	Hezaveh et al. [33]
L31	0.72 ± 0.05	0.71 ± 0.08
L61	0.77 ± 0.04	0.75 ± 0.03
L62	0.89 ± 0.08	0.82 ± 0.05
L64	0.91 ± 0.06	0.89 ± 0.07

Finally in order to verify that the strength of the interactions between the polar heads of the lipid molecules and the oxygen atoms of the copolymer chain were properly modelled by the GROMOS force field, simulations with one chain of the L64 and L31 copolymer chain interacting with the lipid membrane have been also carried out using the force field developed by Hezaveh et al [33]. The results obtained using the

two force fields were comparable. All the results presented in the subsequent sections of the paper have been obtained using the unmodified GROMOS force field.

4.5.2 Effect of Pluronics on the membrane structure and stability

Experimentally we have observed that all the polymer models investigated in this paper show some degree of cytotoxicity resulting from cell membrane damage [41, 42]. Accordingly, our simulations show that the presence of the copolymer chain inside the bilayer visibly affects its structure leading, in some cases, to an evident bending of the membrane already after 30 ns of simulation. These structural changes are early signs of the initiation of a hydrophilic pore [46, 47] whose formation is however not observed within our longest simulation (300 ns). The reason why the deformation of the membrane is such a slow process in this case might be ascribed to the mild hydrophilic nature of the PEO groups that do not exert the strong hydrophilic interactions with the water molecules from the opposite leaflet which generally trigger rapid pore formation. The flexible structure of the polymer that enables it to assume different local configurations might also play a role in slowing down the rate of the membrane deformation. Moreover, although the copolymer molecule is large enough to span the entire bilayer, it is possible that a cooperative process where more than one polymer chain involved is necessary to trigger the lysis of the membrane.

The change in the mechanical properties of the DPPC membrane upon the insertion of the PEO-PPO-PEO chain is monitored by calculating the area per lipid, the thickness, the order parameter of the membrane, its packing properties and the orientation of the head groups, and comparing these values with those obtained from the simulation of the pure DPPC membrane.

4.5.3 Area per lipid and membrane bending

Fig. 4.1 and Table 4.4 show that upon insertion of the copolymer the area per lipid is reduced slightly from the value of 0.65 obtained for the pure DPPC (value in agreement with previous simulation results [48] [49]) to 0.62 for the shortest copolymer model. It is interesting to notice that the major effect on the area per lipid is shown by the polymer chains with the smallest PEO content (L62, L61 and L31). A similar

correlation between the degree of the structural membrane modifications and the PEO content is also shown by the value of the bilayer thickness. Table 4.4 reports the bilayer thickness calculated for all systems defined in Table 4.2 including a pure DPPC membrane system. In order to highlight the effect exerted by the polymer chain, the lipid molecules are distinguished accordingly to their distance from the polymer centre of mass. Lipids whose centres of mass lie at a distance less or equal to 1.5 nm from the centre of mass of the copolymer are considered adjacent to the copolymer chain and their structural properties are calculated separately from the other lipids (to which we will refer as “far” from now on).

From Table 4.4, it can be observed that the largest effect on membrane thickness in comparison to pure DPPC is shown by systems containing the shortest PEO block (L31, L61 and L62). In fact, from the calculations of the partial density of the phosphorus atoms across the membrane (Fig. 4.2) and visual inspections (Fig. 4.3) it can be seen that the two hydrophilic blocks of the copolymer chain (PEO) anchor to the polar heads of the lipid molecules and pull them toward the centre of the membrane causing its visible bending. Therefore the membrane shows a reduced thickness in the region close to where the polymer has been inserted. However, away from the copolymer chain, the membrane becomes thicker with a reduced interdigitation among the acyl chains belonging to the two leaflets. Moreover, overall the phosphorus atoms distributions show broader peaks compared with those obtained from the pure DPPC simulation (Fig. 4.2) showing that the leaflets are subjected to a tension due to the interactions with the PEO blocks of the polymer.

Table 4.4: Area per lipid (calculated as the total area of the simulation box in the xy plane divided the number of lipids in each leaflet) and the membrane thickness (calculated as the distance between the maxima in the phosphorus density distribution along the membrane normal reported in Figure 2).

* The distance has been calculated considering the inner peaks of the distribution

Model	Area per lipid [nm²]	Global_{P-P} Distance [nm]	Close_{P-P} Distance* [nm]	Far_{P-P} Distance [nm]
DPPC	0.6524 ±0.0013	3.7	-	-
L31	0.6188 ±0.0089	3.9	2.9	4.2
L61	0.6203 ±0.0014	3.9	3.3	4.0
L62	0.6181 ±0.0059	4.1	3.4	4.1
L64	0.6331 ±0.0077	4.1	3.7	4.0

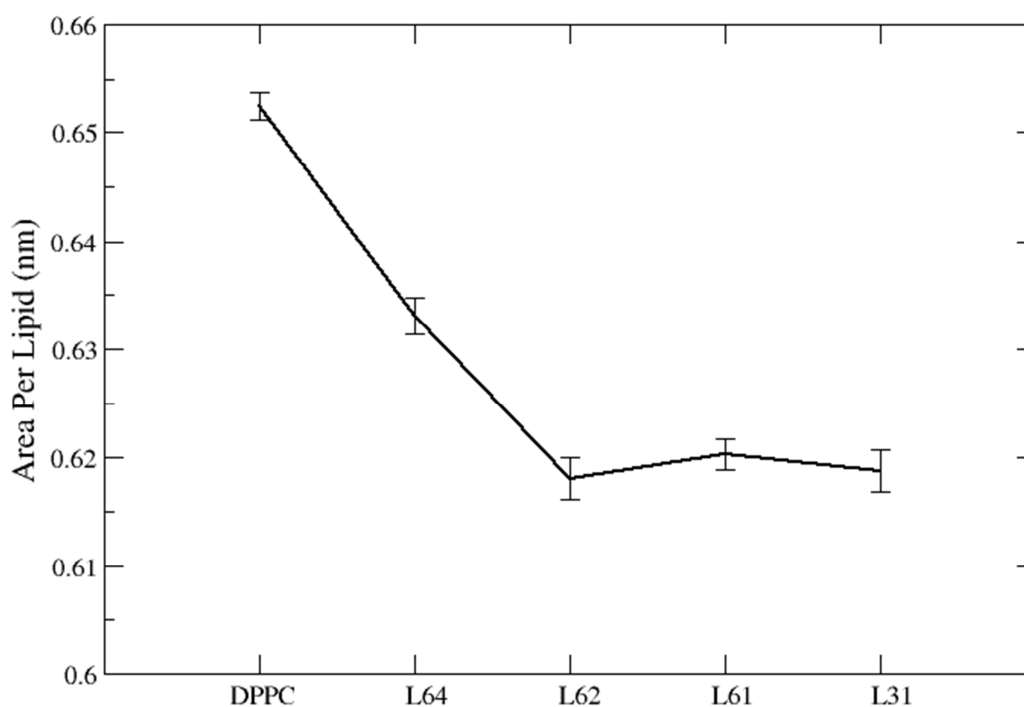


Figure 4.1: The average area per lipid for all the different systems in comparison with the area per lipid in a pure DPPC bilayer membrane. The line connecting the points is drawn only to help the reader to follow the plot.

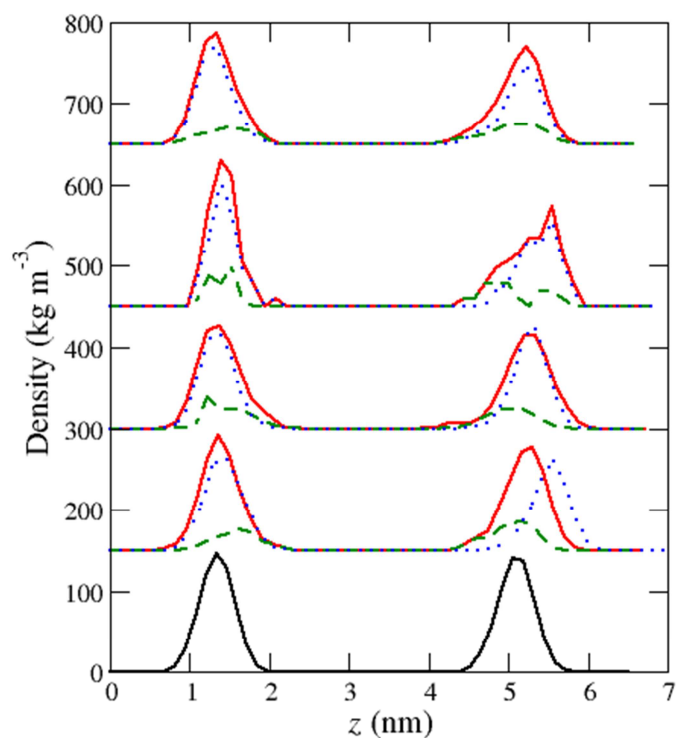


Figure 4.2: P-P density profiles for all the systems averaged over the last 10 ns of the trajectory. From the bottom: pure DPPC, L31, L61, L62, L64. The calculation is carried out for lipids close to the copolymer chain (dashed green line), far from the copolymer chain (pointed blue line) and for all the lipids (solid red line). The plots are shifted for clarity.

The reduced area per lipid and the increased membrane thickness shown by the membrane/polymer systems indicate that the interactions between the oxygen atoms of the PEO monomers and the polar atoms of the lipids favour the interactions between lipids that pack tighter together. This chemical affinity leads to different structural modifications of the membrane depending on the length of the PEO blocks. From the results presented so far we can suggest that the length of the PEO blocks within the copolymer chain has a dual effect: it increases the binding with the membrane (shown by the trend in the values of the experimental K_b with the percentage of PEO content see Table 4.2) and it stabilizes, over a short time scale, the membrane structure. In fact we see from the simulations that Pluronics featuring short PEO blocks (L31 and L61), have a faster disruptive effect on the membrane local mechanical properties compared with copolymers with longer PEO blocks (L62 and L64). Short PEO blocks perturb the local organization of the lipids dragging them toward the centre of the membrane already

after 50 ns (see snapshots extracted from the trajectories of L31 reported in Fig. 4.3). In comparison, long PEO blocks are fully adsorbed into the layer formed by the phosphorus atoms (see the snapshot for L64 in Fig. 4.3).

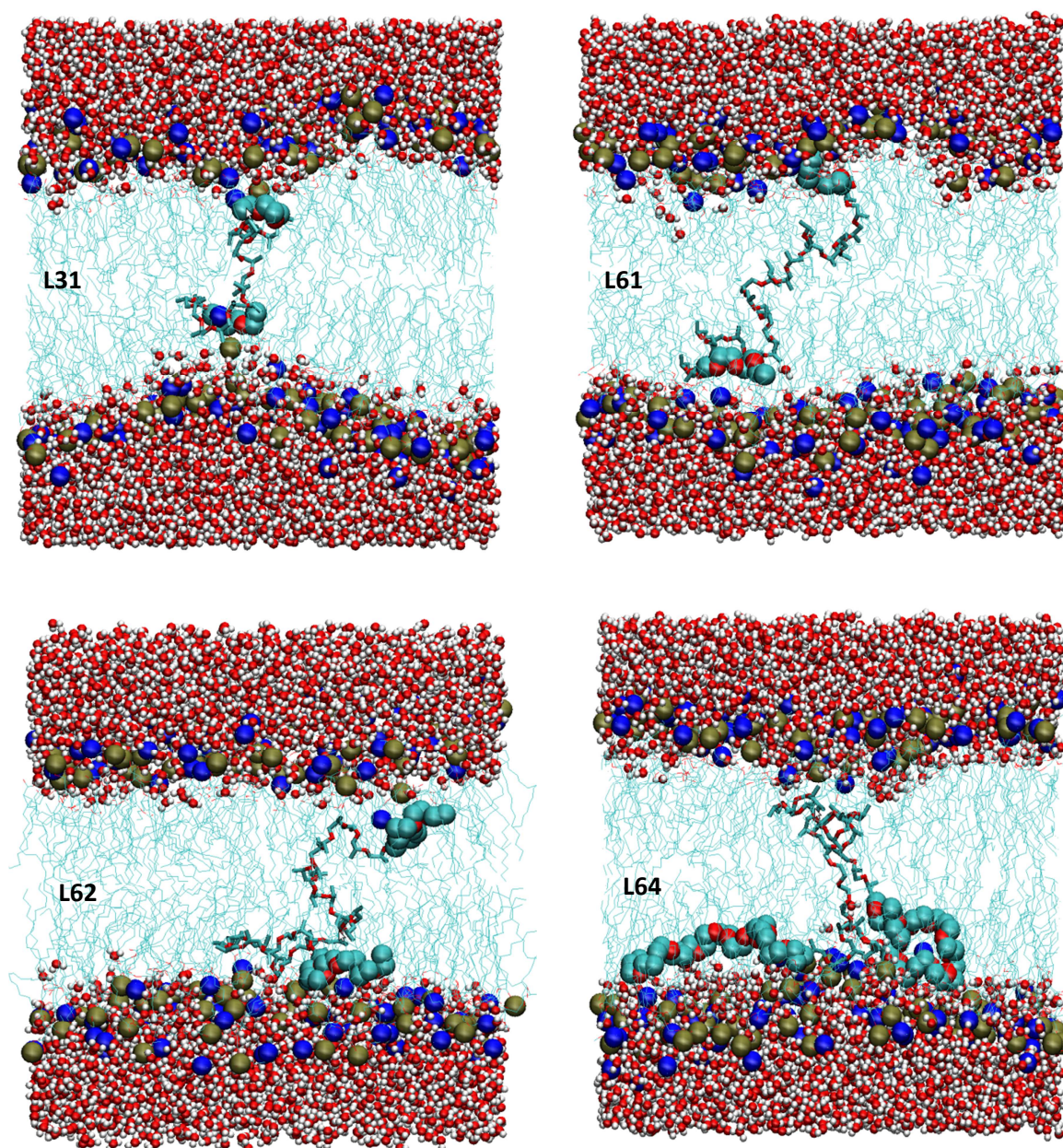


Figure 4.3: Snapshots taken of selected Pluronics at different times (L31 and L61 at 50 ns, L62 at 100 ns, L64 250 ns) absorbed in a DPPC bilayer membrane: The top and bottom layers of red and white beads in each snapshot correspond to water molecules in the system. The gold and blue beads correspond to, respectively, the phosphorus and nitrogen atoms of the DPPC lipid. The large aqua (carbon atoms) and red (oxygen atoms) beads are the PEO blocks of the copolymer chain whereas the smaller ones in the centre correspond to the PPO block (same colour scheme is used for the PPO and PEO blocks). For clarity the hydrophobic carbonyl tails are shown as thin aqua line.

4.5.4 Lipids order parameter and packing properties

The orientation and ordering of the phospholipid tails in the bilayer with respect to the bilayer normal can be measured calculating the lipid tail deuterium order parameter S_{CD} . [49] Fig. 4.4 shows the global order parameter S_{CD} calculated for the different modelled copolymers after 200 ns of simulation. The results obtained using all the lipid chains (labelled in the Figure legend as “ALL”) are displayed alongside the values obtained using the two subsets of lipid chains selected as a function of the distance from the copolymer centre of mass. Overall it can be noticed that in all cases the presence of the copolymer chain increases the order parameter. However, a closer look at the S_{CD} values calculated separately for the lipids adjacent to the copolymer chain and far from it, shows a different picture. For the copolymers with the shortest PEO blocks (L31 and L61), we clearly see that the presence of the Pluronic chain reduces dramatically the local order of the aliphatic chains of the lipid adjacent to it. Moreover, the latter effect is not homogeneously distributed along the tails with an evident stronger effect on the part of the acyl tails close to the head groups, i.e. those that interacts with the PEO blocks, and a milder effect on the S_{CD} calculated for the last five carbon atoms of the tails, i.e. those which only interact with the PPO block. On the contrary, the ordering of the phospholipids that do not interact directly with the Pluronic (indicated as “FAR” in the figure legend) increases upon the insertion of the block copolymer. This increased order is not due to direct chemical interactions but rather to steric reasons.

The two Pluronic characterized by longer PEO blocks (L62 and L64) show a different behaviour. In particular, the model with the highest PEO content (L64) shows only a very small change in the order parameter of the lipid tails adjacent to the copolymer chain compared with the pure DPPC results. This latter fact can be explained observing that the adsorption of the PEO repeating units onto the polar head interface (see Fig. 4.3) produces a tension that is distributed along several lipids and the resulting the local ordering of the lipid tails is only mildly affected as also indicated by the negligible bending of the membrane.

It is interesting to notice that the Pluronic with 6 EO repeating units on each hydrophilic block (L62) shows a behaviour that is halfway between those shown by L31 (and L61) and L64. The averaged value of the S_{CD} calculated for the lipids close to the polymer chain is similar to that of the pure DPPC, however the order parameter of the

carbon atoms decreases notably along the lipid tails. These results are consistent with the double peaked phosphorus density distributions shown by this model (see Figure 2). This result indicates that the relatively long PEO blocks, interacting with the polar head groups, drag towards the membrane centre only the lipid molecules they interact with, increasing the interdigitation of the tails and consequently decreasing their local order. It is important to notice that in this case the bending of the membrane becomes visible after 130 ns ca. (see for example Figure 4 showing that no membrane bending has occurred before 100 ns).

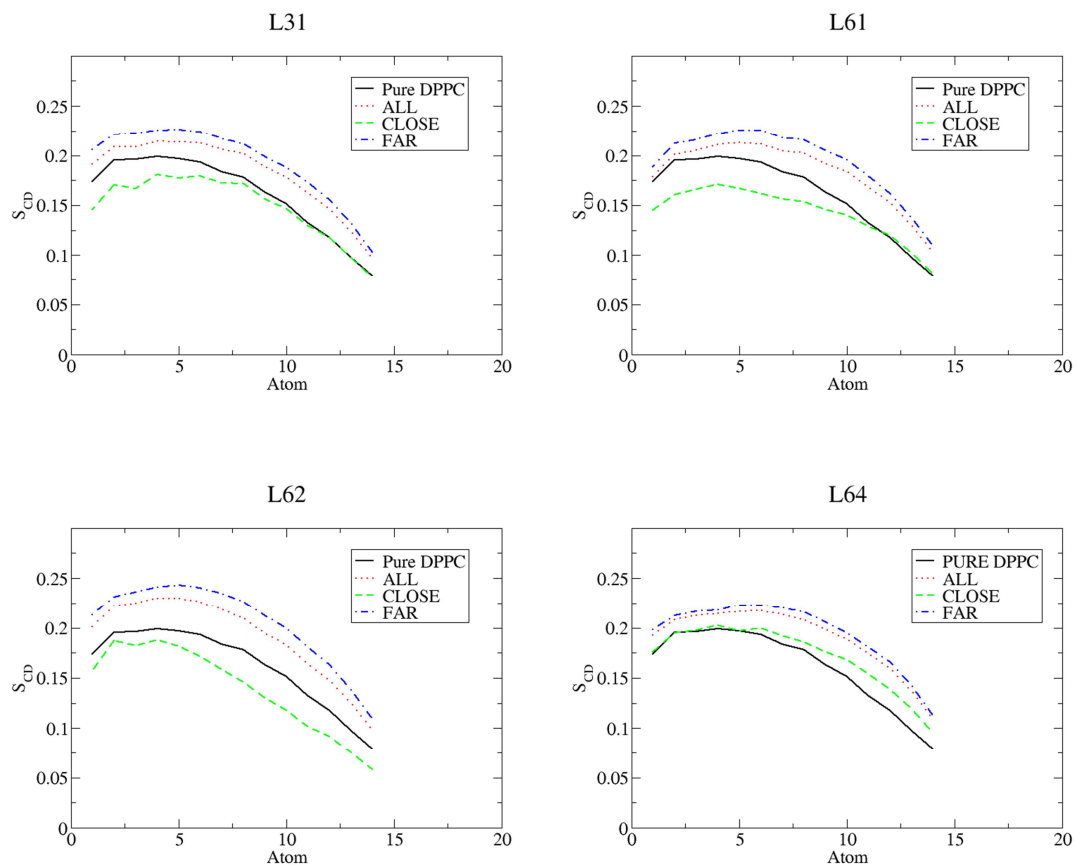


Figure 4.4: Deuterium order parameter (S_{CD}) calculated using the last 10 ns of a simulation of 200 ns.

In order to obtain a better understanding of the molecular mechanism that drives the changes in the ordering of the phospholipid tails, we estimate the free area (A_{free}) properties and the DPPC close-packed area (a_{DPPC}) for each system under investigation following the procedure that Falck et al. [50] used to estimate such properties for phospholipid/cholesterol bilayers and that, more recently, we employed to calculate the

surface contact area of amphiphilic dendrimers at air/water interface [51]. In this procedure the simulation box is sliced along the z axis and the van der Waals area occupied by the atoms belonging to each slice is calculated. The area occupied by the atoms in each slice is calculated by partitioning the slab in a fine 2D grid and summing up the grid points whose positions lie within the van der Waals radius of an atom belonging either to a DPPC molecule or to the polymer chain. The mesh of the grid is tuned until the resulting area converges. Once the occupied area (A_{occ}) is calculated for each slice the corresponding free area (A_{free}) can be easily calculated as the difference between the value of the total area of the slice (corresponding to the area of the box in the x and y directions) and the occupied area. Fig. 4.5 reports the value of the free area calculated for each slice along the z -direction for all the DPPC/polymer systems under investigation and for the polymer free DPPC membrane. The water molecules are excluded from the calculation and the membrane is sliced every 0.2 nm. From Fig. 4.5 we can notice that the distribution of the amount of A_{free} along the z axis is in agreement with the typical partial density profile of the DPPC molecules calculated across the simulation box obtained for DPPC bilayers and reported in Fig. 4.6. In fact, at values of z (~ 2.0 and ~ 4.5 nm) where the maxima of the DPPC mass density profile are located, correspond to the two minima in the A_{free} profile; while at the value of z in the middle of the bilayer where the DPPC density distribution shows a minimum associated with the terminal methyl groups, correspond a maximum in the A_{free} distribution ($z \sim 3.3$ nm). Fig. 4.6 shows also that upon insertion of the Pluronic molecule characterized by the shortest PEO block (L31, L61 and L62) the free area available in proximity of one leaflet is reduced while the presence of the longest polymer chain (L64) does not affect visibly the distribution of A_{free} within the membrane.

These result are in agreement with the large peaks obtained from the phosphorus density profile reported in Fig. 4.2 which shows that a fraction of the lipid molecules (those that interact directly with the polymer) have partially been dragged towards the centre of the membrane. This is further confirmed by looking at the cross sectional mass density distribution obtained for the whole DPPC molecules reported in Fig. 4.6 where the contributions to the total density profile of the lipids close and far from the polymer have been separated. Fig. 4.6, which reports only the results for the L31/DPPC system but very similar results have been obtained for the L61/DPPC and L62/DPPC systems. This shows that the lipids that directly interact with the polymer chain and that are characterized by wide peaks in the P-P mass density distribution in

Fig. 4.2 (green line) are also characterized by a higher interdigitation in the middle of the bilayer than those that are located far from the polymer.

From the knowledge of the free and occupied area, it is possible to calculate the cross-sectional DPPC close-packed area (a_{DPPC}) counting how many DPPC molecules (N) are located in each slice and dividing the total occupied area by this number ($a_{\text{DPPC}}=A_{\text{occ}}/N$) [50]. The calculation was performed separately for the DPPC molecules close and far from the polymer chain. Fig. 4.7 reports the value of a_{DPPC} obtained for all systems under investigation. Due to the fact that the copolymer chain spans the whole bilayer the close-packed area value is relatively constant across the simulation box except for the bilayer centre ($z \sim 3.3$ nm) where a_{DPPC} increases due to a decrease in the number of DPPC molecules as shown by the DPPC density profile reported in Figure 6. The average value of a_{DPPC} is around 0.4 nm in agreement with the calculated for DPPC molecules in the middle of the bilayer [50]. Moreover it can be noticed that upon insertion of the L31, L61 and L62 copolymer chain, the pack area values calculated for the lipids far from the polymer (Fig. 4.7a) are clearly slightly smaller than those calculated for the polymer-free DPPC bilayer while the values of a_{DPPC} calculated for the lipids close to the polymer chain are higher than those obtained for the pure DPPC.

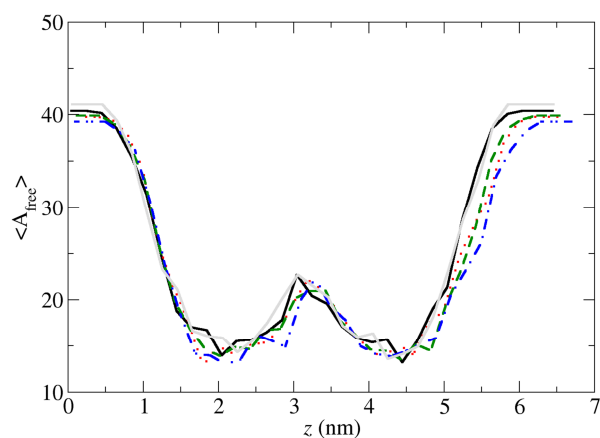


Figure 4.5: Free area (A_{free}) profile calculated for all the systems: L31 (dotted red), L61 (dashed green), L62 (dash-dotted blue), L64 (solid grey) and pure DPPC (solid black).

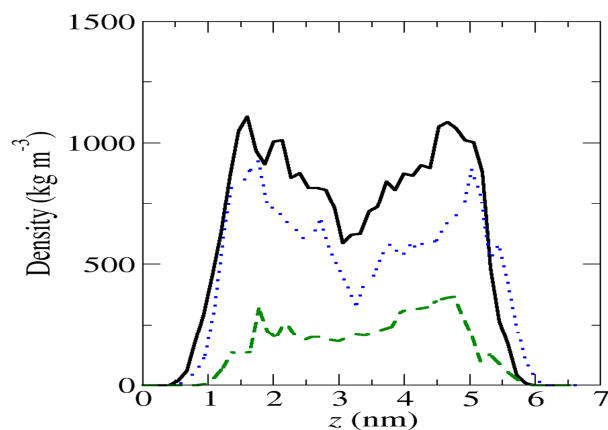


Figure 4.6: DPPC mass density profiles for the polymer-free DPPC (black solid line) and the L31/DPPC (dotted and dashed lines) system. The calculation is carried out for lipids close to the copolymer chain (dashed green line), far from the copolymer chain (pointed blue line).

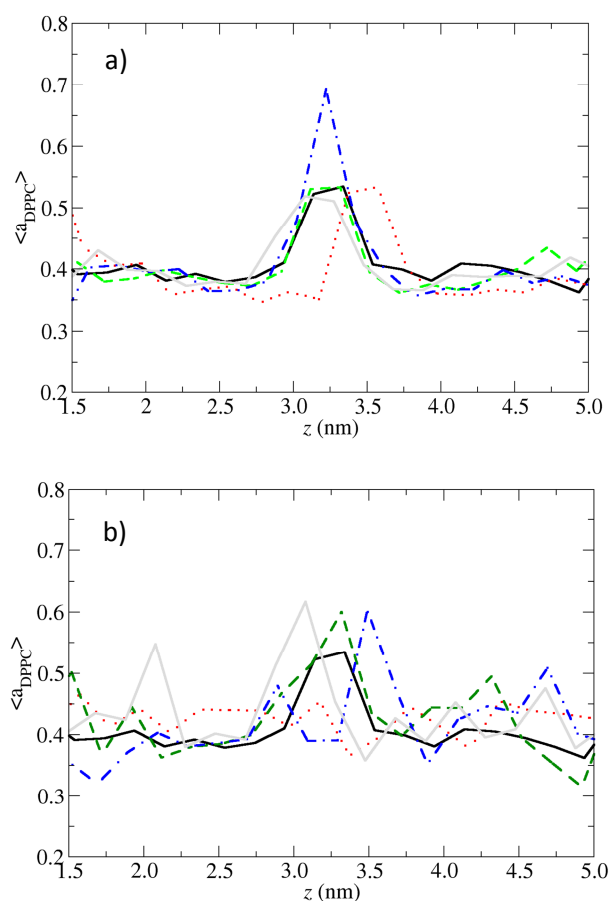


Figure 4.7: Close packed area (a_{DPPC}) calculated for all the systems: L31 (dotted red), L61 (dashed green), L62 (dash-dotted blue), L64 (solid grey) and pure DPPC (solid black) and averaged over the last nanosecond of the trajectory. The calculations are carried out separately for the phospholipids far (a) and close (b) to the polymer chain.

Based on these structural analyses we can therefore conclude that although the copolymer chain occupies a certain amount of space, the lipid molecules adjacent to it do not move away, due to (i) enhanced interactions between the polar heads of the phospholipids favoured by the presence of the PEO blocks and ii) the flexible hydrophobic PPO block of the copolymer favourably interacting with the hydrophobic acyl tails. The reduced free area available increases globally the order parameter S_{CD} , however the values of the close-pack area, a_{DPPC} , calculated separately for the lipids close and far from the polymer chain shows that lipids that are not in direct contact with the polymer exhibit a smaller close-pack area, and therefore higher S_{CD} , compared with that calculated for the polymer-free DPPC and also with that calculated for the DPPC close to the polymer chain that, in agreement with their high S_{CD} , show the lowest a_{DPPC} . The lower order parameter obtained for the latter can be also explained with an increased interdigitation of the acyl chains in the middle of the membrane. It is interesting to notice that the reorganization of the apolar region of the membrane not directly in contact with the polymer has also been observed experimentally [3]. Moreover experimental and computational studies have showed that the addition of amphiphilic macromolecules is indeed responsible for lipid condensation and may trigger a phase transition [52] or even change the phase diagram of the membrane [53].

The latter observations indicate that the presence of the copolymer chain into the DPPC membrane affects its structure and that this is dependent mainly on the length of the PEO blocks. In effect, if the hydrophilic PEO blocks are long enough, they are adsorbed just below the polar heads and, by interacting with several lipid molecules, temporarily stabilize the membrane structure. In contrast, for shorter PEO blocks the hydrophilic interactions are localized in a small region of the membrane and the PEO blocks thus work as anchor points to pull the lipids toward the internal part of the membrane and the bending takes place. The fact that the PEO blocks can penetrate into the lipid core membrane instead of lying entirely outside the membrane in the water phase has also been observed in molecular dynamics simulation of PEGylate membrane [22].

4.5.5 Orientation of the lipid heads

As shown above (Fig. 4.2) upon the addition of the co-polymers to the DPPC bilayer the distribution of the phosphorus atoms across the membrane becomes wider particularly towards the hydrophobic core of the bilayer. The effect that this interaction has on the orientation of the lipid head groups can be quantified by calculating the average angle (θ) between the vector connecting the phosphorus (P) and nitrogen (N) atoms of the lipid molecules and the outward bilayer normal. Angles of 0° or 180° correspond to a vector aligned with the membrane normal pointing toward the aqueous phase or toward the bilayer hydrophobic core respectively.

The P-N distributions obtained at the end of 200 ns of simulation for all the modelled Pluronics are reported in Fig. 4.8 and compared with the results obtained from the pure DPPC bilayer. The calculations are performed separately for the two leaflets considering that they could behave differently and, in order to highlight the effect of the presence of the copolymer chain, only the lipids molecules identified as adjacent to the copolymers are accounted in the calculation. In agreement with previous simulation results of pure DPPC bilayer, θ shows a wide distribution that peaks at $\sim 90^\circ$ (averaged value of the angle is 81.64 ± 0.3888 and 81.32 ± 0.3330 for the two separate leaflets) [54], which indicates that the choline groups are exposed to the aqueous phase.

Fig. 4.5 shows that the angle distribution is slightly affected upon the addition of Pluronics to the membrane. For example L31 shows a P-N angle distribution shifted toward low values of the angle for the leaflet 1 (corresponding to the lower layer in Fig. 4.3) and a symmetrically shifted distribution toward larger value of θ for the opposite leaflet indicating that the PEO blocks pulls the phosphorus atoms toward the internal hydrophobic region of the bilayer. Similarly, L61 shows deviations from the DPPC distribution in both leaflets. However, L62 shows the largest deviation from the pure DPPC distribution for the leaflet that is subjected to the largest bending (leaflet 2) in agreement with the dual distribution obtained from the P distributions showed in Fig. 4.2. It is interesting to notice that the presence of the polymer not only affects the orientation of the head groups belonging to the leaflet which is in direct contact with the PEO blocks. In fact the polymer-free leaflet (leaflet 1) in the L64 system shows a double peaked distribution.

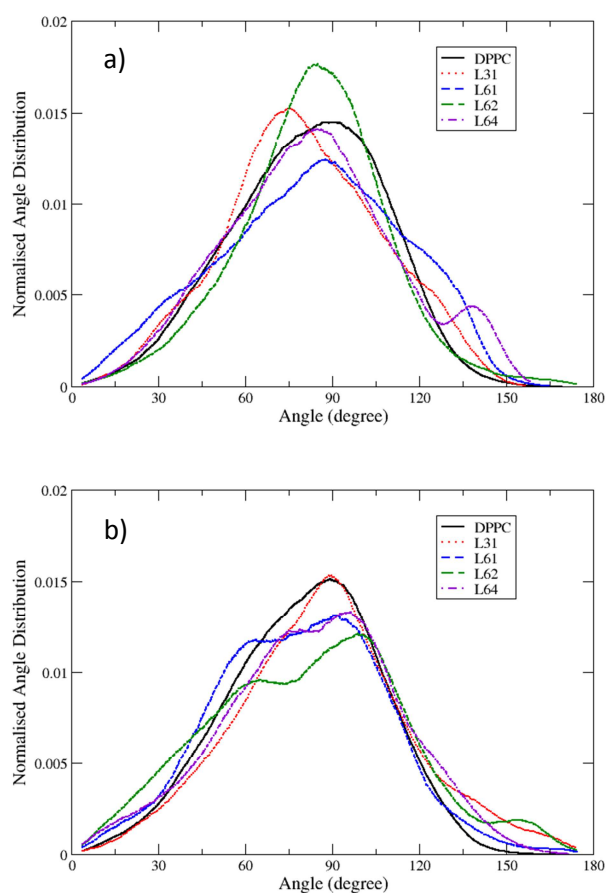


Figure 4.8: Distribution of the angle between the vector joining the P-N vector of DPPC and the upward normal of the bilayer on both lipid layers: a) leaflet 1 (corresponding to the bottom monolayer in Fig. 4.4), b) leaflet 2 (corresponding to the top monolayer in Fig. 4.3)

4.5.6 Comparison between simulation and experimental results

As mentioned above previous experimental results and our recent biological activity assays have shown that all the Pluronic-type copolymers under investigation in this paper affect lipid packing, accelerate the flip-flop activity, facilitate doxorubicin permeation and show a certain degree of toxicity [14, 41, 42, 55]. In agreement with these findings, the simulations show that in all cases investigated, the presence of the copolymer chains highly perturbs the membrane structure and that a certain number of water molecules penetrate deeper (compared with the pure DPPC membrane) into hydrophobic region of the bilayer (see Fig. 4.3). Our computational results suggest also that in membranes that incorporate the copolymer chains with short PEO blocks the structural defects appear earlier than in those that interact with Pluronics of higher PEO content. The latter result agrees well with previous experimental observations showing

that an increased PEO content along the copolymer chain reduces the lipid flip-flops and the membrane permeability [14].

In order to evaluate whether the structural modifications predicted by the atomistic simulations could be qualitatively related with the biological activity experimentally shown by these copolymers, we investigated whether the predicted relationship between the PEO blocks length and the rate at which membrane disruptive effects are displayed, could be verified experimentally. To do so the kinetics of haemoglobin released from erythrocytes exposed to Pluronic copolymers of the same structure as those modelled was monitored (haemoglobin released into the media is a marker of membrane lysis). Figure 9 indicates that the length of the PEO blocks has an effect on the kinetics of lysis when the length of the PPO block is maintained constant: haemolysis occurs quicker when erythrocytes were exposed to Pluronics containing 2 and 3 PEO monomers per block than when they were in contact with polymers with longer PEO blocks. The time needed for 50% of the cells to be lysed (T_{50}) is 44 ± 1 minutes and 41 ± 1 minutes for L31 and L61 respectively, while $T_{50} = 55 \pm 2$ minutes for L62 and $T_{50} = 77 \pm 14$ minutes for L64. The experimental kinetic data therefore seem to indicate that, in agreement with the computational predictions, polymers with long PEO blocks, although eventually cytotoxic, initially maintain membrane integrity. However it is important to notice that in the present discussion we have not considered whether the copolymers diffusion mechanism towards the lipid membrane is affected by their molecular weight and structure, or whether the actual translocation mechanism plays any role in the cytotoxicity effect that the Pluronics under investigation here have shown experimentally.

It is important to note that the trend in structural results presented above are not affected by the initial conformation of the polymer, although we notice that membranes that incorporate the U-shape Pluronics show structural alterations earlier during the simulation than those which embed Pluronics in extended conformations. This result could be explained considering firstly that in the case of a U-shape polymer in addition to the alterations caused by the chemical and steric interactions with the copolymer, the membrane is subjected to an asymmetric tension in the two leaflets. This effect has been proved to be responsible for membrane poration in the case of insertion of short peptides into DPPC model membranes [56]. Secondly, although sterically impaired by the presence of the methyl group, the oxygen of the PPO monomer, that bears a fairly large negative charge can interact with the lipid head groups belonging to the leaflet not

in direct contact with the PEO. This interaction could lead to a bending of the polymer-free leaflet and a consequent increased instability of the membrane. In the supporting information (Fig. 4S and 5S) the deuterium order parameter S_{CD} calculated for the two different global configurations (U-shape and extended configurations) are reported separately for the two leaflets. It can be noticed that globally the order parameter increases in all cases, however the effect that the presence of the polymer has on the packing order of the lipids in its proximity seems to depend on the polymer global configuration. In reality what seems to matter is which leaflets the PEO blocks interact with. In the case of the U-shape polymer, the lipid molecules that belong to the leaflet that interacts with the PEO blocks (leaflet 1 for both L61 and L62 in Fig. 4S and 5S) present reduced order parameters, while the lipids belonging to the leaflet not in direct contact with the polymer chain show an S_{CD} higher than that obtained from the polymer-free DPPC bilayer.

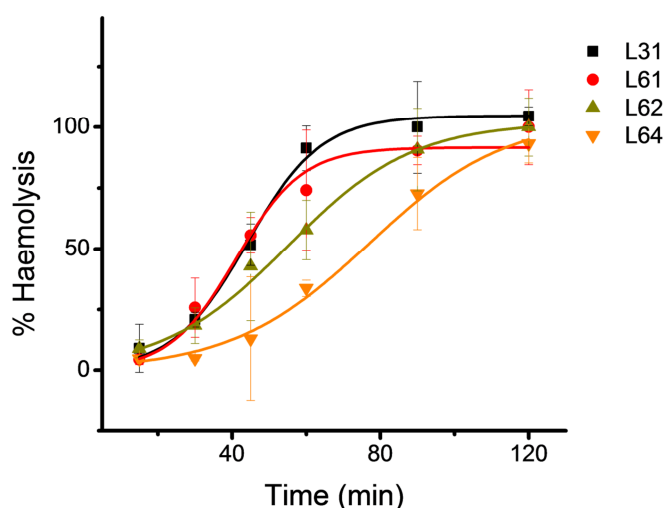


Figure 4.9: Kinetics of haemolysis during exposure to Pluronic at a concentration of 0.5M. Data are presented as mean \pm standard deviation calculated using three different samples.

4.6 Summary and conclusions

By means of molecular dynamics simulations, we investigated the modifications that Pluronic of different molecular weight and hydrophilic/hydrophobic content generate on the structure and stability of model biological membranes. Our simulation results showed that all the Pluronic-type copolymers investigated induce a certain

degree of instability in the membrane which leads to membrane bending, an increased membrane permeability and eventually, experimentally, to concentration dependent haemolytic effects. We observed that upon insertion of Pluronics, the area per lipid slightly decreases and the membrane bends. These structural changes increase the permeability of the membrane and water molecules are allowed to penetrate deep in the hydrophobic region of the bilayer although a hydrophilic pore is not formed within the time span of our longest simulation. We showed that the membrane-disruptive effect of Pluronics is mainly due to the presence of the two hydrophilic blocks that interact with the polar head groups of the lipid molecules. However, the time scale at which membrane destabilization occurs is inversely proportional to the PEO block length: short PEO blocks quickly drag the phosphorus or nitrogen atoms of the lipid head groups toward the internal part of the membrane leading to an early bending and permeabilization of the bilayer. In contrast, Pluronics with long PEO blocks seems to temporarily stabilize the membrane local structure. These computational predictions correlate well with erythrocyte haemolysis assays performed on Pluronic PEO-PPO-PEO block copolymers of the same chemical composition as those simulated. The experimental results demonstrated that the haemoglobin release occurs earlier for those Pluronics characterized by short PEO blocks. The length of the PPO block has instead a double effect: the PPO block mainly stabilizes the membrane structure through its hydrophobic interactions with the acyl chains of the lipids and maintains intact the membrane keeping the two leaflets together. However, due to the random contacts that can occur between the oxygen of the polypropylene-oxide unit and the lipid polar heads, the presence of the PPO block could also be responsible of enhancing the membrane bending.

Our computational results help in understanding the molecular mechanisms underpinning the interactions between amphiphiles and lipid membranes. They suggest relations between polymer microstructure and biological activity data and rationalize previous experimental results. Our findings may guide the design of amphiphilic copolymer structures that display desirable properties in applications such as drug delivery but without undesired cytotoxicities.

4.7 References

1. Blanz, A., S.P. Armes, and A.J. Ryan, *Self-Assembled Block Copolymer Aggregates: From Micelles to Vesicles and their Biological Applications*. Macromolecular Rapid Communications, 2009. **30**(4-5): p. 267-277.
2. Discher, D.E., et al., *Emerging applications of polymersomes in delivery: From molecular dynamics to shrinkage of tumors*. Progress in Polymer Science, 2007. **32**(8-9): p. 838-857.
3. Tribet, C. and F. Vial, *Flexible macromolecules attached to lipid bilayers: impact on fluidity, curvature, permeability and stability of the membranes*. Soft Matter, 2008. **4**(1): p. 68-81.
4. Gaspar, R. and R. Duncan, *Polymeric carriers: Preclinical safety and the regulatory implications for design and development of polymer therapeutics*. Advanced Drug Delivery Reviews, 2009. **61**(13): p. 1220-1231.
5. Discher, D.E. and F. Ahmed, *Polymersomes*. Annual review of biomedical engineering, 2006. **8**: p. 323-41.
6. Adams, M.L., A. Lavasanifar, and G.S. Kwon, *Amphiphilic block copolymers for drug delivery*. Journal of Pharmaceutical Sciences, 2003. **92**(7): p. 1343-1355.
7. Batrakova, E.V., et al., *Effects of pluronic and doxorubicin on drug uptake, cellular metabolism, apoptosis and tumor inhibition in animal models of MDR cancers*. Journal of Controlled Release, 2010. **143**(3): p. 290-301.
8. Sriadibhatla, S., et al., *Transcriptional activation of gene expression by pluronic block copolymers in stably and transiently transfected cells*. Molecular Therapy, 2006. **13**(4): p. 804-813.
9. Wu, G., et al., *Lipid Corralling and Poloxamer Squeeze-Out in Membranes*. Physical Review Letters, 2004. **93**(2): p. 028101.
10. Wu, G., et al., *Interaction between Lipid Monolayers and Poloxamer 188: An X-Ray Reflectivity and Diffraction Study*. Biophysical Journal, 2005. **89**(5): p. 3159-3173.
11. Wu, G. and K.Y.C. Lee, *Effects of poloxamer 188 on phospholipid monolayer morphology: an atomic force microscopy study*. Langmuir, 2009. **25**(4): p. 2133-9.

12. Wang, J.Y., et al., *Effects of PEO-PPO-PEO Triblock Copolymers on Phospholipid Membrane Integrity under Osmotic Stress*. Langmuir, 2010. **26**(15): p. 12953-12961.
13. Lee, B. and M.A. Firestone, *Electron Density Mapping of Triblock Copolymers Associated with Model Biomembranes: Insights into Conformational States and Effect on Bilayer Structure*. Biomacromolecules, 2008. **9**(6): p. 1541-1550.
14. Demina, T., et al., *Relationship between the structure of amphiphilic copolymers and their ability to disturb lipid bilayers*. Biochemistry, 2005. **44**(10): p. 4042-4054.
15. Makarucha, A.J., N. Todorova, and I. Yarovsky, *Nanomaterials in biological environment: a review of computer modelling studies*. European Biophysics Journal with Biophysics Letters, 2010. **40**(2): p. 103-115.
16. Lin, J.Q., et al., *Penetration of Lipid Membranes by Gold Nanoparticles: Insights into Cellular Uptake, Cytotoxicity, and Their Relationship*. ACS Nano, 2010. **4**(9): p. 5421-5429.
17. Wong-Ekkabut, J., et al., *Computer simulation study of fullerene translocation through lipid membranes*. Nat Nano, 2008. **3**(6): p. 363-368.
18. Yang, K. and Y.Q. Ma, *Computer simulation of the translocation of nanoparticles with different shapes across a lipid bilayer*. Nature Nanotechnology, 2010. **5**(8): p. 579-583.
19. Lee, H. and R.W. Pastor, *Coarse-Grained Model for PEGylated Lipids: Effect of PEGylation on the Size and Shape of Self-Assembled Structures*. Journal of Physical Chemistry B, 2011. **115**(24): p. 7830-7837.
20. Pal, S., G. Milano, and D. Roccatano, *Synthetic polymers and biomembranes. How do they interact?: Atomistic molecular dynamics simulation study of PEO in contact with a DMPC lipid bilayer*. Journal of Physical Chemistry B, 2006. **110**(51): p. 26170-26179.
21. Yang, S.C. and R. Faller, *Pressure and Surface Tension Control Self-Assembled Structures in Mixtures of Pegylated and Non-Pegylated Lipids*. Langmuir, 2012. **28**(4): p. 2275-2280.
22. Stepniowski, M., et al., *Study of PEGylated Lipid Layers as a Model for PEGylated Liposome Surfaces: Molecular Dynamics Simulation and Langmuir Monolayer Studies*. Langmuir, 2011. **27**(12): p. 7788-7798.

23. Hatakeyama, M. and R. Faller, *Coarse-grained simulations of ABA amphiphilic triblock copolymer solutions in thin films*. *Physical Chemistry Chemical Physics*, 2007. **9**(33): p. 4662-4672.
24. Groot, R.D. and K.L. Rabone, *Mesoscopic simulation of cell membrane damage, morphology change and rupture by nonionic surfactants*. *Biophysical Journal*, 2001. **81**(2): p. 725-736.
25. Srinivas, G. and M.L. Klein, *Coarse-grain molecular dynamics simulations of diblock copolymer surfactants interacting with a lipid bilayer*. *Molecular Physics*, 2004. **102**(9-10): p. 883-889.
26. Zhang, D., M.A. Carignano, and I. Szleifer, *Cluster Structure and Corraling Effect Driven by Interaction Mismatch in Two Dimensional Mixtures*. *Physical Review Letters*, 2006. **96**(2): p. 028701.
27. Biocomputing, U.o.C. *DPPC pdb and topolgy* 2010; Available from: http://moose.bio.ucalgary.ca/index.php?page=Structures_and_Topologies.
28. Tieleman, D.P. and H.J.C. Berendsen, *Molecular dynamics simulations of a fully hydrated dipalmitoylphosphatidylcholine bilayer with different macroscopic boundary conditions and parameters*. *The Journal of Chemical Physics*, 1996. **105**(11): p. 4871-4880.
29. Berger, O., O. Edholm, and F. Jähnig, *Molecular dynamics simulations of a fluid bilayer of dipalmitoylphosphatidylcholine at full hydration, constant pressure, and constant temperature*. *Biophysical journal*, 1997. **72**(5): p. 2002-2013.
30. Glattli, A., X. Daura, and W.F.v. Gunsteren, *Derivation of an improved simple point charge model for liquid water: SPC/A and SPC/L*. *The Journal of Chemical Physics*, 2002. **116**(22): p. 9811-9828.
31. M. J. Frisch, et al., *Gaussian 09*. , 2009.
32. Breneman, C.M. and K.B. Wiberg, *Determining atom-centered monopoles from molecular electrostatic potentials- the need for high sampling density in formamide conformational analysis*. *Journal of Computational Chemistry*, 1990. **11**(3): p. 361-373.
33. Hezaveh, S., et al., *Structure and dynamics of 1,2-dimethoxyethane and 1,2-dimethoxypropane in aqueous and non-aqueous solutions: A molecular dynamics study*. *Journal of Chemical Physics*, 2011. **135**(16): p. 11.

34. D. van der Spoel, E.L., B. Hess, A. R. van Buuren, E. Apol, P. J. Meulenhoff, D. P. Tieleman, A. L. T. M. Sijbers, K. A. Feenstra, R. van Drunen and H. J. C. Berendsen, *Gromacs User Manual* version 4.5, 2011.
35. Hess, B., et al., *LINCS: A linear constraint solver for molecular simulations*. *Journal of Computational Chemistry*, 1997. **18**(12): p. 1463-1472.
36. Darden, T., D. York, and L. Pedersen, *Particle mesh Ewald: An N [center-dot] $\log(N)$ method for Ewald sums in large systems*. *The Journal of Chemical Physics*, 1993. **98**(12): p. 10089-10092.
37. Essmann, U., et al., *A smooth particle mesh Ewald method*. *The Journal of Chemical Physics*, 1995. **103**(19): p. 8577-8593.
38. Grillo, D., M. Olvera de la Cruz, and I. Szleifer, *Theoretical studies of the phase behavior of DPPC bilayers in the presence of macroions*. *Soft Matter*, 2011. **7**(10): p. 4672-4679.
39. Berendsen, H.J.C., et al., *Molecular dynamics with coupling to an external bath*. *The Journal of Chemical Physics*, 1984. **81**(8): p. 3684-3690.
40. Lichtenberg, D., *Characterization of the solubilization of lipid bilayers by surfactants*. *Biophysica Acta*, 1985(821): p. 470-478.
41. Redhead, M., et al. *PE-PPO-PEO Block Co-Polymers and Bio-Membrane 12* *Chemistry B*, 2000. **104**(25): p. 6059-6064.
44. Shang, B.Z., Z. Wang, and R.G. Larson, *Molecular Dynamics Simulation of Interactions between a Sodium Dodecyl Sulfate Micelle and a Poly(Ethylene Oxide) Polymer*. *The Journal of Physical Chemistry B*, 2008. **112**(10): p. 2888-2900.
45. Ahlstrom, P., et al., *Molecular-dynamics simulation of structural and conformational properties of poly(propylene oxide)*. *Journal of Chemical Physics*, 2000. **112**(23): p. 10669-10679.
46. Rzepiela, A.J., et al., *Membrane poration by antimicrobial peptides combining atomistic and coarse-grained descriptions*. *Faraday Discussions*, 2010. **144**(3): p. 431-443.
47. Gurtovenko, A.A., J. Anwar, and I. Vattulainen, *Defect-Mediated Trafficking across Cell Membranes: Insights from in Silico Modeling*. *Chemical Reviews*, 2010. **110**(10): p. 6077-6103.
48. Patra, M., et al., *Molecular Dynamics Simulations of Lipid Bilayers: Major Artifacts Due to Truncating Electrostatic Interactions*. *Biophysical Journal*, 2003. **84**(6): p. 3636-3645.

49. Tieleman, D.P., S.J. Marrink, and H.J.C. Berendsen, *A Computer Perspective of Membranes: Molecular Dynamics Studies of Lipid Bilayer Systems*, in *Biochimica et biophysica acta. Reviews on biomembranes* 1997. p. 36.
50. Falck, E., et al., *Lessons of slicing membranes: Interplay of packing, free area, and lateral diffusion in phospholipid/cholesterol bilayers*. *Biophysical Journal*, 2004. **87**(2): p. 1076-1091.
51. Nawaz, S. and P. Carbone, *Stability of Amphiphilic Dendrimers at the Water/Air Interface*. *Journal of Physical Chemistry B*, 2011. **115**(42): p. 12019-12027.
52. Hung, W.C., et al., *The condensing effect of cholesterol in lipid bilayers*. *Biophysical Journal*, 2007. **92**(11): p. 3960-3967.
53. De Meyer, F. and B. Smit, *Effect of cholesterol on the structure of a phospholipid bilayer*. *Proceedings of the National Academy of Sciences*, 2009. **106**(10): p. 3654-3658.
54. Lopez Cascales, J.J., et al., *Model of an Asymmetric DPPC/DPPS Membrane: Effect of Asymmetry on the Lipid Properties. A Molecular Dynamics Simulation Study*. *The Journal of Physical Chemistry B*, 2006. **110**(5): p. 2358-2363.
55. Frey, S.L. and K.Y.C. Lee, *Temperature dependence of poloxamer insertion into and squeeze-out from lipid monolayers*. *Langmuir*, 2007. **23**(5): p. 2631-2637.
56. Leontiadou, H., A.E. Mark, and S.J. Marrink, *Antimicrobial peptides in action*. *Journal of the American Chemical Society*, 2006. **128**(37): p. 12156-12161.

4.8 Supporting Information

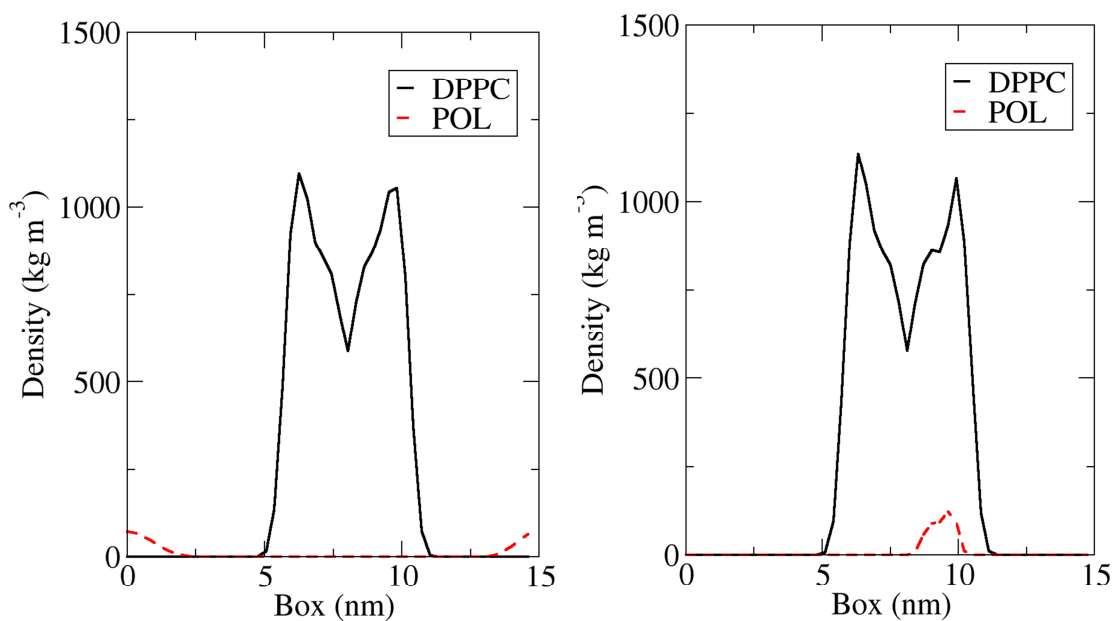


Figure 1S: Mass density profile for Pluronic L64 and DPPC atoms. Left: initial configuration with the polymer in the water phase. Right: final configuration after 300 ns after the polymer has translocated inside the DPPC membrane. The distributions have been averaged over 10 ns.

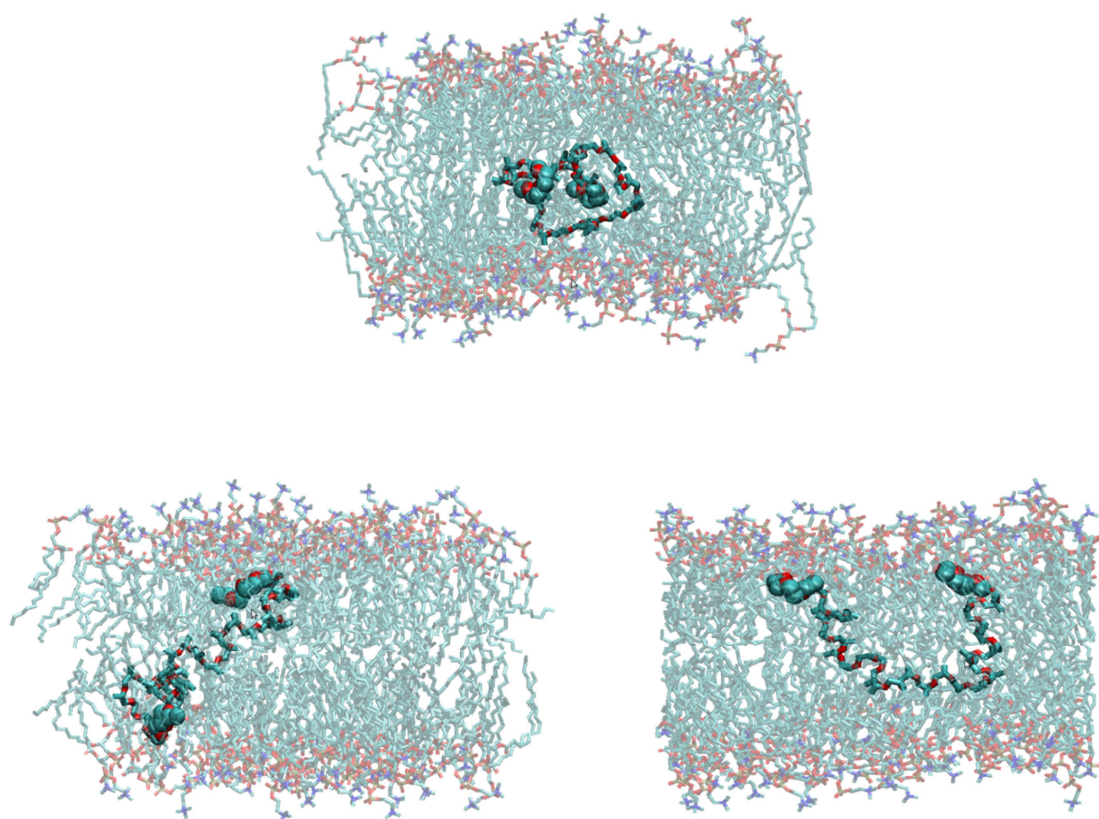


Figure 2S: Two different conformations of the Pluronic L61($\text{EO}_3\text{-PO}_{31}\text{-EO}_3$) adopted after 200ns starting from the same initial configuration. Top: initial arrangement of L61 immersed in a coiled configuration placed centrally in the membranes hydrophobic region. Large beads represent the PEO blocks connected either side of a central PPO block. Bottom left: the Pluronic is spread across the bilayer spanning both monolayers with the PEO block interacting with adjacent monolayers of the bilayer membrane. Bottom right: the Pluronic adopts a U-shaped configuration where both PEO block interact with the same monolayer.

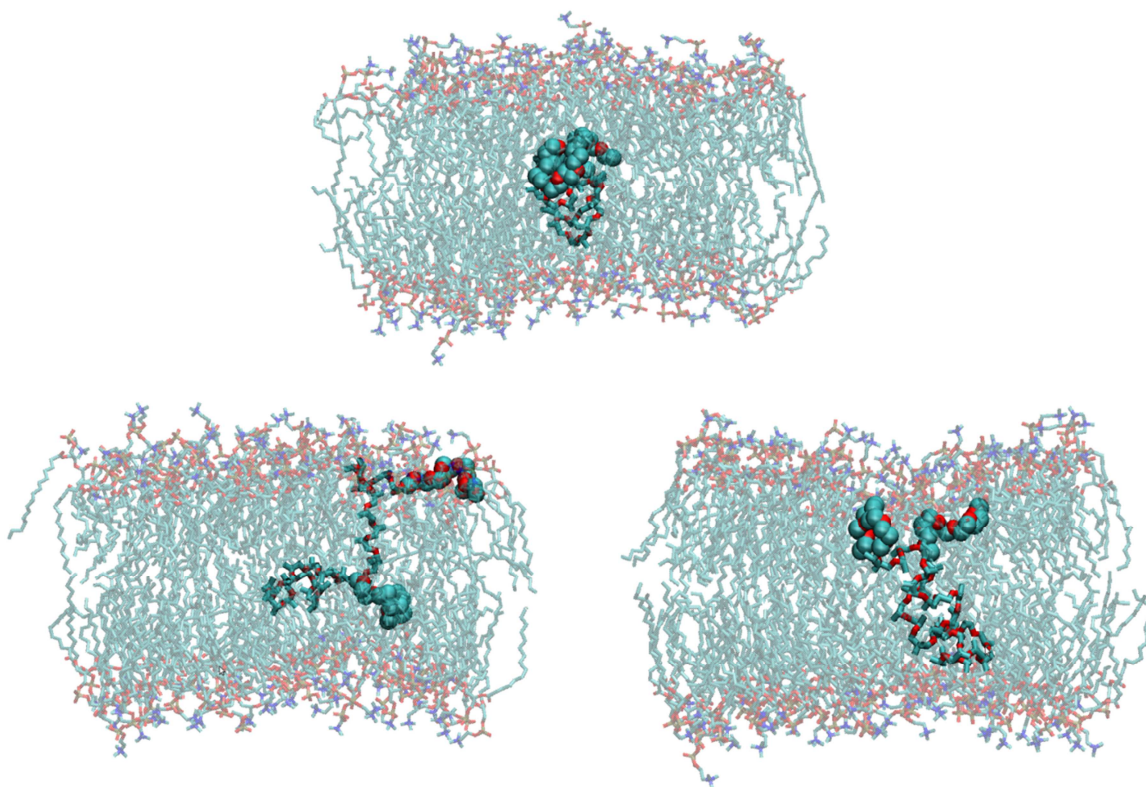


Figure 3S: Two different conformations of the Pluronic L62($\text{EO}_6\text{-PO}_{31}\text{-EO}_6$) adopted after 200ns starting from the same initial configuration. Top: initial arrangement of L62 immersed in a coiled configuration placed centrally in the membranes hydrophobic region. Large beads represent the PEO blocks connected either side of a central PPO block. Bottom left: the Pluronic is spread across the bilayer spanning both monolayers with the PEO block interacting with adjacent monolayers of the bilayer membrane. Bottom right: the Pluronic adopts a U-shaped configuration where both PEO block interact with the same monolayer.

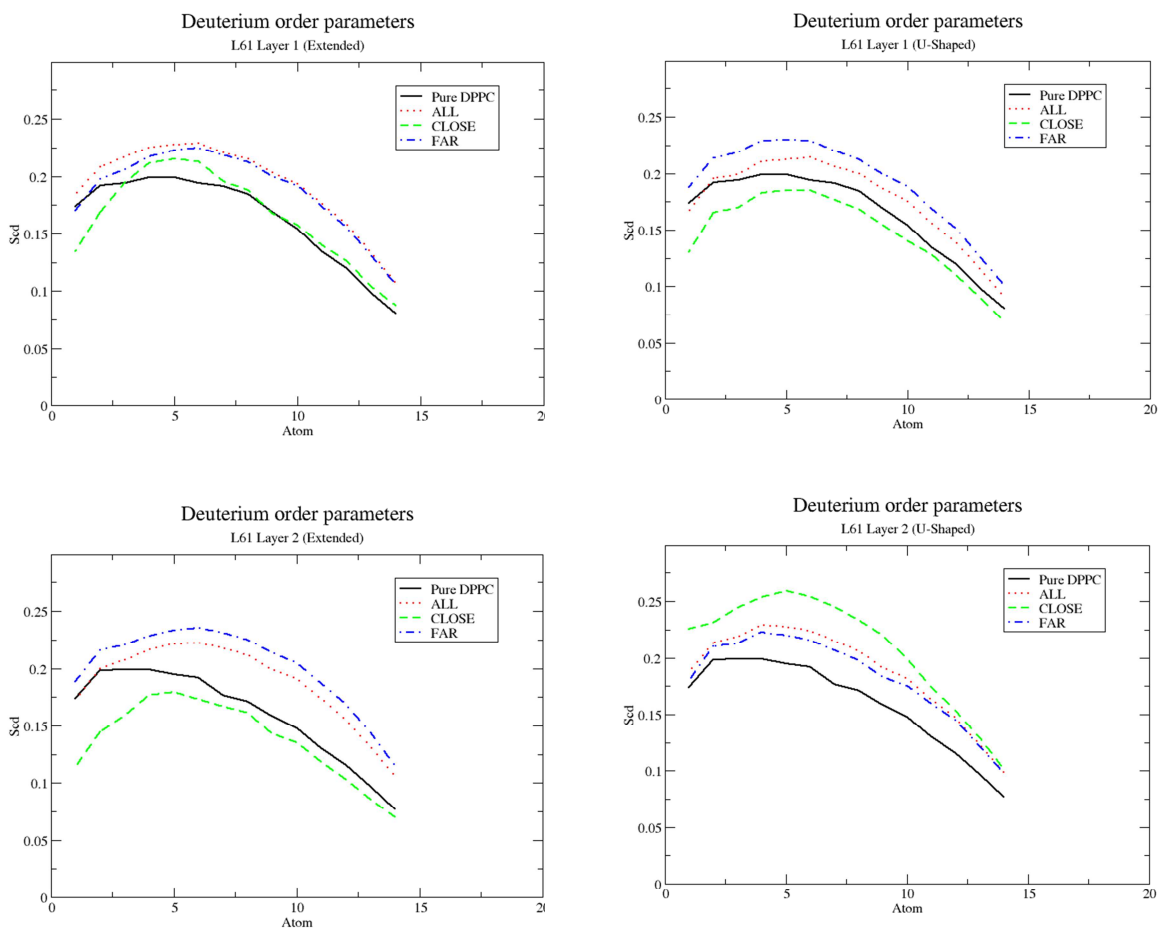


Figure 4S: Deuterium order parameter calculated per monolayer using the last 10ns of a 200ns simulation for the Pluronic L61($\text{EO}_3\text{-PO}_{31}\text{-EO}_3$) adopting both the U-shaped and spanned configuration. Layer 1 corresponds to the top layer of the membrane from figure 2S and layer 2 corresponds to the bottom layer.

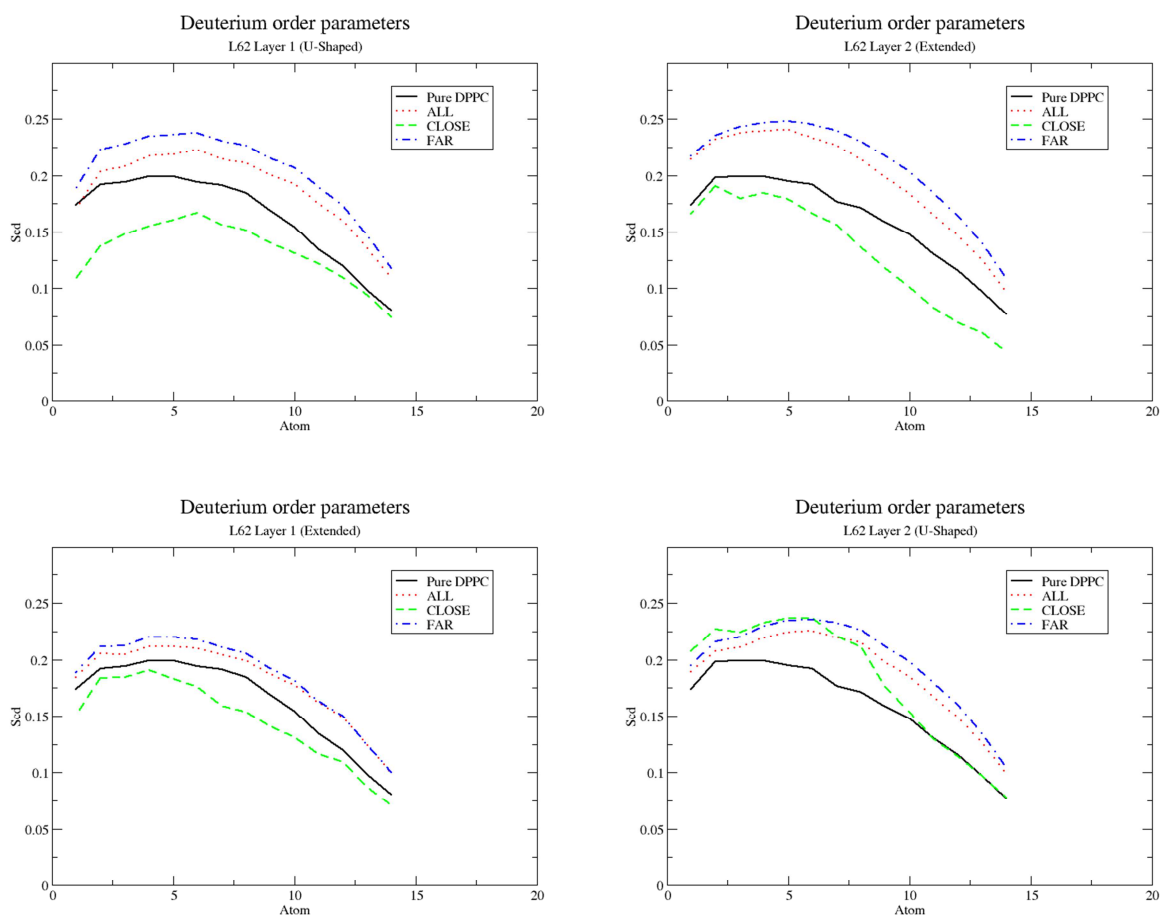


Figure 5S: Deuterium order parameter calculated per monolayer using the last 10ns of a 200ns simulation for the Pluronic L62($EO_6-PO_{31}-EO_6$) adopting both the U-shaped and spanned configuration. Layer 1 corresponds to the top layer of the membrane from figure 3S and layer 2 corresponds to the bottom layer.

Biological Effects of PEO-PPO-PEO Block Copolymers: Relationship between Polymer Composition and their Interactions with Biological Membranes

This chapter has been published in Pharmaceutical Research (see Appendix C)

Authors: Martin Redhead, Guiseppe Mantovani, Selina Nawaz, Paola Carbone, Dariusz C. Gorecki. Cameron Alexander and Cynthia Bosquillon

This Chapter focuses on the experimental work carried out by Martin Redhead from the University of Nottingham based on the simulations carried out in the previous chapter. The molecular modelling in this work was carried out by S. Nawaz. Thorough discussions were communicated between S. Nawaz, M. Redhead and all other supervisory authors for this collaboration study.

5.1 Introduction

PEO-PPO-PEO block copolymers (synonyms: Pluronics®, Synperonics®, Poloxamers) are ABA triblock copolymers, with a central hydrophobic poly(propylene oxide) (PPO) block flanked by two hydrophilic poly(ethylene oxide) (PEO) blocks. In solution, PEO-PPO-PEO block copolymers can assemble into micelles, with the PPO blocks forming a hydrophobic core and the PEO blocks the surrounding hydrophilic corona [1]. The hydrophobic core of these micelles can be used to incorporate poorly water soluble drugs, and thus improve their pharmacokinetics and biodistribution [2, 3].

Although PEO-PPO-PEO block copolymers are widely used and many are essentially inert to biological substrates, materials within the overall class have recently been reported to elicit marked biological responses, both *in vitro* and *in vivo*. Copolymers of differing chemical composition have shown varying cytotoxicity profiles, as well as therapeutically desirable effects [4, 5]. For instance, they have the capacity to circumvent multi drug resistance in cells overexpressing the antiapoptotic protein Bcl-2 [6], or to inhibit the P-glycoprotein pump (P-gp) which, when overexpressed leads to the rapid efflux of cytotoxic drugs out of tumoral cells [7]. Formulations of Pluronics and doxorubicin have reached clinical trials in cancer therapy

and have shown to be more efficacious than the drug alone [8, 9]. Other reported biological effects of PEO-PPO-PEO block co-polymers include the depletion of glutathione and ATP, NF κ B activation and enhanced expression of transfected genes [4, 10, 11], although this latter effect may be promoter dependent [12].

It has been shown both the PEO and PPO blocks of the copolymer impact on the intensity of the biological effects measured, with moderately lipophilic copolymers being the most potent [4, 5]. Nevertheless, detailed relationships between polymer composition and biological effects remain to be defined. Similarly, it is unclear whether cellular responses to amphiphilic co-polymer exposure result from their interactions with biological membranes. For example, P-gp inhibition has been ascribed to their effect on membrane fluidity [7, 13]. In contrast, the mechanism by which they induce NF κ B activation remains speculative, although it has been suggested this may involve a previously undisclosed signalling pathway [14].

One of the possible mechanisms by which amphiphilic polymers such as PEO-PPO-PEO block copolymers cause cytotoxicity might be via cell membrane solubilisation. Indeed, a high hydrophobic content in PEO-PPO-PEO block copolymers has been shown to increase their surfactant activity in dipalmitoylphosphatidylcholine (DPPC) monolayers and to reduce the surface pressure required to penetrate the lipid layers [15]. For polymers with long PEO blocks, penetration into monolayers was enhanced by the presence of cholesterol, reportedly due to hydrogen bonding between PEO chains and cholesterol [16].

While several studies have explored the mechanisms of PEO-PPO-PEO block copolymer insertion into artificial membranes [15-18], their interactions with cellular membranes have not been extensively investigated, which has, so far, prevented polymer adverse effects on cells to be related to their affinity for biomembranes. Accordingly, a systematic investigation of Pluronic cytotoxic potential is required to assist in the selection of safe and efficient carriers for specific biomedical applications.

In this study, a combination of cytotoxicity and haemolysis assays were employed to probe relationships between the structural features of PEO-PPO-PEO block copolymers and their interaction with biomembranes. Cytotoxic end-points in the intestinal epithelial Caco-2 cell line and in Human Microvascular Endothelial Cells HMEC-1 were compared to copolymer membrane binding constant. Correlations between the polymer chemical constituents and biological responses measured were investigated to gain a better understanding of the mechanism behind the cellular effects of PEO-PPO-PEO block copolymers.

5.2 Materials and Methods

5.2.1 Materials

Caco-2 and HMEC-1 cells were obtained from the European Collection of Cell Cultures (ECACC, Salisbury, UK). PEO-PPO-PEO block copolymers L31, F38, P85, L62 and L122 were purchased from BASF (Cheadle, UK), the MTS Reagent and CytotoxONE™ LDH assay kit were obtained from Promega (Southampton, UK) and the cell culture medium RPMI 1640 from Lonza (Slough, UK). 96 well plates were obtained from Corning, (Birmingham, UK). All other reagents were purchased from Sigma-Aldrich (Poole, UK) and used as received. The PPO vs. PEO content of the PEO-PPO-PEO block copolymers was determined by ¹H NMR by comparing the integral of the methyl group of the propylene oxide repeating unit (3H) at 1.2 ppm to those of the CH and CH₂ of the PPO (3H) and PEO (4H) units, respectively, at 3.3-3.8 ppm.

5.2.2 Cell Culture

Caco-2 cells (passage 55-70) were cultured in Dulbecco's Modified Eagle Medium supplemented with 2 mM L-glutamine, 1000 IU/mL penicillin, 10 µg/mL streptomycin and 10% FBS. HMEC-1 cells (passage 1) were cultured in RPMI 1640 supplemented with 2 mM L-glutamine, 1000 IU/mL penicillin, 10 µg/mL streptomycin and 10% FBS. Cells were maintained at 37 °C and 5% CO₂ in a humidified atmosphere.

5.2.3 MTS Metabolism Assay

Caco-2 cells were plated at a density of 15,000 cells per well in 96 well plates and allowed to attach overnight. They were treated with a series of PEO-PPO-PEO block copolymers (Table 5.1) over a concentration range of 0.0005-1% w/v for 5 hours. Untreated cells (100% MTS metabolism) and cells treated with 2% SDS (0% MTS metabolism) were included as controls. The cells were then washed with PBS, and fresh media containing the MTS reagent was added. After two hours of incubation, the absorbance was read at 490 nm using a colorimetric plate reader (TECAN, Männedorf, Switzerland). The assay was performed on two separate occasions (n= 6 replicates per plate)

Dose response curves were generated for each polymer, showing MTS metabolism relative to the controls versus polymer concentration. Integrals were

calculated for each dose response curve in order to compare cytotoxic effects in lieu of LD50 values. LD50 values were not obtained for all polymers due to concerns that cytotoxicity would be caused at higher polymer concentrations by mechanisms other than membrane disruption, e.g. hypertonicity.

The integrals were fitted to a matrix against M_n PPO and %PEO using the Renka-Kline algorithm, and a 3D surface plot was overlaid on the data points using the Origin Pro 8.0 software (OriginLab, Northampton, UK).

Table 5.1: Polymer composition and measured cytotoxicity Endpoints. (- indicates the Pluronic was not tested in the assay; * values set at 0 as polymer did not induce haemolysis)

Polymer Name	M_n PPO	% PEO		Integrated MTS score (Caco-2)	Integrated LDH score		Haemolysis			jC-1 Green:Red Fluorescence ratio
		Quoted	1H NMR		Caco-2	HMEC-1	R_c (μM)	D_w (μM)	K_b (M^{-3})	
L31	900	10	14	0.3039	0.06597	0.20532	955.	7639	0.13	2.44
F38	900	80	86	1.10646	-	0.08561	-	-	-	-
L61	1800	10	13	-0.00829	0.4366	0.61353	77.9	1018	0.97	-
L62	1800	20	29	-0.04603	0.28918	-	-	-	-	1.48
L64	1800	40	39	0.20236	-	0.31583	336.	599.5	1.66	-
F68	1800	80	81	0.86001	-0.13604	-0.03245	0*	0*	0*	3.32
L81	2400	10	11	-	0.55	0.77279	-	-	-	-
P85	2400	50	50	0.85686	0.03591	-	-	-	-	0.98
P105	3000	50	51	0.70631	-	-	-	-	-	1.08
L121	3600	10	15	0.97248	0.017958	-0.01397	0*	0*	0*	-
L122	3600	20	25	1.11403	-	-	-	-	-	-
F127	3600	70	73	1.00599	0.04207	-0.11096	0*	0*	0*	-

5.2.4 LDH Release Assay

Throughout the lactate dehydrogenase (LDH) assay, cells were incubated with serum in which any endogenous LDH present had been inactivated by incubation at 70 °C in a water bath for 40 minutes. HMEC-1 and Caco2 cells were plated at a density of 15,000 cells per well and allowed to attach overnight. They were treated with a series of PEO-PPO-PEO block co-polymers (Table 5.1) over a concentration range of 0.0005-1% w/v for 5 hours. Untreated cells (spontaneous LDH release), cells treated with 4% Triton X-100 (100% LDH release) and culture media containing heat inactivated serum without cells (endogenous background LDH activity) were included as controls. Following incubation, the plates were centrifuged at 250 g, 4°C for 4 minutes and 100

μL of media was added to each well. 100 μL of media was removed from each well, placed in a fresh plate and incubated with an equal volume of CytotoxONETM -reagent, containing pyruvate, NAD⁺, ATP, rezazurin and diaphorase, for 15 minutes. 50 μL stop solution (Promega) was added to each well. The fluorescence was then read in a fluorometric plate reader with an excitation wavelength of 560 nm and emission wavelength of 590 nm. The assay was performed on 2 sets of 6 replicates. Dose response curves showing LDH activity normalised against controls versus polymer concentration were generated for each polymer. Integrals of each dose response curve were calculated and plotted against M_n PPO and % PEO. A surface was fitted to the data points using Origin Pro 8.0 and surfaces generated for the two cell lines were directly compared.

5.2.5 Determination of Polymer Membrane Binding Constants

Ethical approval was obtained from the University of Nottingham Medical School Ethics Committee to collect blood samples from healthy adult male volunteers. The erythrocytes were separated by centrifugation and suspensions containing erythrocytes at hematocrits ranging from 0.03%-0.3% were prepared. These were added to 96 well plates containing various PEO-PPO-PEO block co- polymers of increasing concentrations over the range 0.0005-0.1 M. Untreated erythrocytes (spontaneous lysis), erythrocytes treated with 4% Triton X-100 (100% lysis) and solutions of each polymer without erythrocytes (background absorbance) were run simultaneously as controls. After four hours of incubation, the plates were centrifuged, the supernatant containing released haemoglobin was extracted and placed in a fresh plate. The absorbance was read at 410nm in a TECAN colorimetric plate reader (2 sets of 6 replicates). Dose response curves showing percentage haemolysis normalised against controls versus polymer concentration were drawn.

In order to determine membrane binding constant values (K_b) from the haemolysis assay, the analysis of Litchenberg *et al.* [19] was employed. The concentration at which the membrane is saturated with surfactant (C^{sat}) was obtained from the sigmoidal haemolysis dose response curves as the point where the exponential increase in haemolysis ended and further increases were linear (around 10% haemolysis). These C^{sat} values were then plotted against the molar concentration of lipid (calculated according to Malheiros *et al.* [20]) resulting in a straight line predicted by Eq. 5.1.

$$D_t = R_e \left[\frac{L+1}{K_b(R_e+1)} \right] \quad (5.1)$$

where D_t is the total surfactant, R_e is the molar ratio of lipid to surfactant and K_b is the membrane binding constant. The gradient of this line can be used to derive R_e and the intercept gives D_w , the free surfactant in water. This can be used to derive K_b values via Eq. 5.2.

$$R_e = \frac{K_b \cdot D_w}{(1 - K_b \cdot D_w)} \quad (5.2)$$

K_b values were then fitted to a matrix against M_n PPO and %PEO using Origin Pro 8.0.

5.2.6 Erythrocyte Protection Assay

Erythrocytes collected as previously described were adjusted to a haematocrit of 0.5% in PBS. The erythrocytes were added to Pluronic solutions in PBS so that the final polymer concentration was 50 mM and the haematocrit was 0.25%. Solutions containing 4% w/v Triton X-100 (100% lysis), PBS (spontaneous lysis) and PBS containing polymer without erythrocytes (background absorbance) were used as controls. The polymer/erythrocyte preparations were incubated at 37°C for 5 minutes to allow the polymers to bind to the membrane and 150 μ L were then added to an equal volume of dH₂O. After 10 minutes of incubation, samples were centrifuged for 4 min at 600g and the supernatant was transferred into a fresh 96 well plate. The absorbance was measured at 410nm (3 replicates). The absorbance values were normalised against the controls and expressed as % haemolysis.

5.2.7 JC-1 Mitochondrial Membrane Potential Assay

JC-1 is a lipophilic cationic dye which forms J-aggregates that fluoresce in the red at high mitochondrial membrane potential ($\Delta\psi_m$) and switches to a monomeric form which fluoresces in the green at low $\Delta\psi_m$ [21].

Caco-2 cells were plated at a density of 25,000 cells per well. After 48 hours, cells were treated with a range of PEO-PPO-PEO block copolymers (Table 5.1) at a concentration of 0.3 mM, which was the highest concentration that did not cause complete cytotoxicity in the MTS and LDH assays for any of the polymers. Untreated cells and cells incubated with 0.01 mg/mL valinomycin for 1 hour were used as controls. The plates were then incubated for 3 hours. The media was aspirated and cells were incubated for 15 minutes with the JC-1/bisbenzimidazole staining solution (Sigma-Aldrich). The JC-1/bisbenzimidazole staining solution contained 9.2 μ M JC-1, 11.2 μ M

bisbenzimidazole in 5 mL JC-1 staining buffer and was made up to 10 mL with 5 mL Caco-2 culture media. JC-1 staining buffer contained 137 mM NaCl, 3.6 mM KCl, 0.5 mM, MgCl₂, 1.8 mM CaCl₂, 0.8 mM HEPES, 1 mg/mL D-glucose, 1% non-essential amino acids and was adjusted to pH 7.2 with NaOH. The plates were washed twice with the JC-1 staining buffer. The plates containing JC-1 staining buffer were placed on ice, and the wells were imaged with a Leica DM IRB microscope with a QICAM FAST1394 camera (QImaging, Surrey, Canada) on the red, green and blue fluorescence channels.

The images obtained from the red (JC-1 aggregates) and green (JC-1 monomers) fluorescence channels were each independently merged with the images from the blue channel (bisbenzimidazole nuclear stain) using paint.net (obtained from dotPDN llc). The images were then analysed using Origin Pro 8.0, and histograms were generated to show the relative levels of fluorescence per pixel in the red and blue channels, and green and blue channels, respectively (Fig. S1). These histograms were used to calculate the total fluorescence for each channel, and the red and green fluorescence were normalised to the blue fluorescence in each image. The pair of images for each well was then used to generate green to red fluorescence ratios. An increase in green to red fluorescence ratio was interpreted as a decrease in mitochondrial membrane potential.

5.2.8 Molecular modelling

Atomistic molecular dynamics simulations were used to investigate the molecular structure of a model biological membrane composed of a 128 molecules of DPPC and hydrated with 3655 water molecules upon insertion on one PEO-PPO-PEO copolymer chain. The simulations were carried out at 325 K for 300 ns and at constant lateral pressure (1 atm) in order to simulate a tensionless bilayer. The software used was the GROMACS package version 4.3.2.

5.2.9 Statistical Analysis

Data sets were compared by performing a 2 sample *F*-test for variance using Origin Pro 8.0.

5.3 Results

5.3.1 MTS Metabolism Assay

The MTS assay was employed to determine the effects of the structural

components of the polymers, namely the size of the PPO central block (M_n PPO) and the weight percentage of hydrophilic PEO side blocks, on Caco-2 cell metabolism. Within the group of Pluronics tested (Table 5.1), both cytotoxic and non cytotoxic polymers were identified. Concentration-dependent effects were observed for the polymers that caused a decrease in MTS metabolism but with varying cytotoxic potency (Fig. 5.1A). It is noteworthy that no alteration in the trend of the dose response curve was observed above the critical micelle concentration (CMC) for any of the copolymers tested.

As it was not possible to generate LD50 values for the polymers which did not display cytotoxic effects, the integrals of the dose response curves were compared. For polymers containing 10% PEO (w/w), a relationship was found between the M_n PPO and the integrated MTS metabolism values which fitted the general form of a quadratic (parabolic) function (Fig. 5.1B). Polymers with a M_n PPO of around 1.8 kDa caused the greatest reduction in MTS metabolism, whereas polymers with a M_n PPO of 3.6 kDa had no impact on MTS biotransformation. For polymers with a M_n PPO of 1.8 kDa, increasing the percentage of PEO content linearly decreased the polymer ability to affect MTS metabolism. Polymers with 10% PEO were the most cytotoxic in the MTS assay, whereas polymers with 80% PEO did not affect the dye conversion (Fig. 5.1C). These two dimensional relationships were fitted into a matrix with M_n PPO and % PEO against the integrals of the dose response curves for each polymer (Fig. 5.1D). It was found that a polymer consisting of M_n PPO 1.8 kDa and 10% PEO, i.e., polymer L61, caused maximum reduction in MTS metabolism.

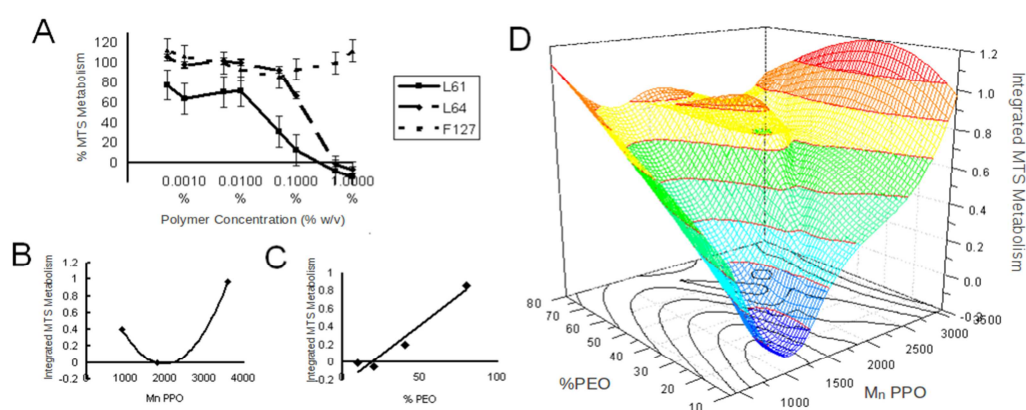


Figure 5.1: Effect of PEO-PPO-PEO block co-polymers on MTS metabolism in Caco-2 cells. A: examples of dose response curves for a non cytotoxic polymer (F127), a polymer with moderate cytotoxicity (L64) and a very cytotoxic polymer (L61); data are

mean \pm SEM. B: parabolic relationship between M_n PPO and MTS metabolism for polymers of equal % PEO (10%). C: linear relationship between % PEO and MTS metabolism for polymers of equal M_n PPO (1800 Da). D: 2D surface plot generated using the Renka-Kline Algorithm detailing the effects of both M_n PPO and % PEO on integrated MTS metabolism.

5.3.2 LDH Release Assay

The LDH assay was performed in the cancerous cell line Caco-2 and in the immortalized HMEC-1 cells to evaluate polymer cytotoxicity via membrane disruption/solubilisation. As in the MTS assay, polymers which caused LDH release as well as polymers which did not display cytotoxic effects were highlighted. Again, the integrals of each dose response curve were compared in lieu of LD50 values.

In both the Caco-2 and HMEC-1 cell lines, for polymers exhibiting a PEO content of 10% (w/w), the molar mass (M_n) of PPO again fitted with LDH release in terms of a parabolic function, with polymers of a M_n PPO around 2.2 kDa causing the greatest increase in LDH release, and polymers with a M_n PPO of 3.6 kDa having no effect on membrane integrity (Fig. 5.2 A and D). For polymers with a similar M_n PPO of 1.8 kDa, an inverse relationship was found between the percentage PEO and LDH release, with polymers composed of 80% PEO (w/w) being non membrane disruptive (Fig. 5.2B and E).

Two dimensional surfaces were fitted to the data sets against both M_n PPO and percentage PEO. The resulting matrix was found to obey a 2D parabolic relationship (Fig. 5.2 C and F). This empirical relationship can be described by Eq. 5.3.

$$LDH \text{ release} = A \cdot \exp \left[\frac{1}{2} \left(\frac{M_n PPO - 2200}{750} \right)^2 - \frac{1}{2} \left(\frac{\% PEO - 10}{20} \right)^2 \right] \quad (5.3)$$

where A is the maximum LDH release under the system, i.e. LDH release caused by a polymer which, according to our model, is predicted to have a M_n PPO of 2.2 kDa and to contain 10% PEO (w/w). The chemical composition of this polymer is intermediate between that of Pluronics L61 and L81.

No significant difference was found when the data sets derived from each cell line were compared ($p=0.7$), indicating these were neither affected by the cancerous nature nor the tissue origin of the cells.

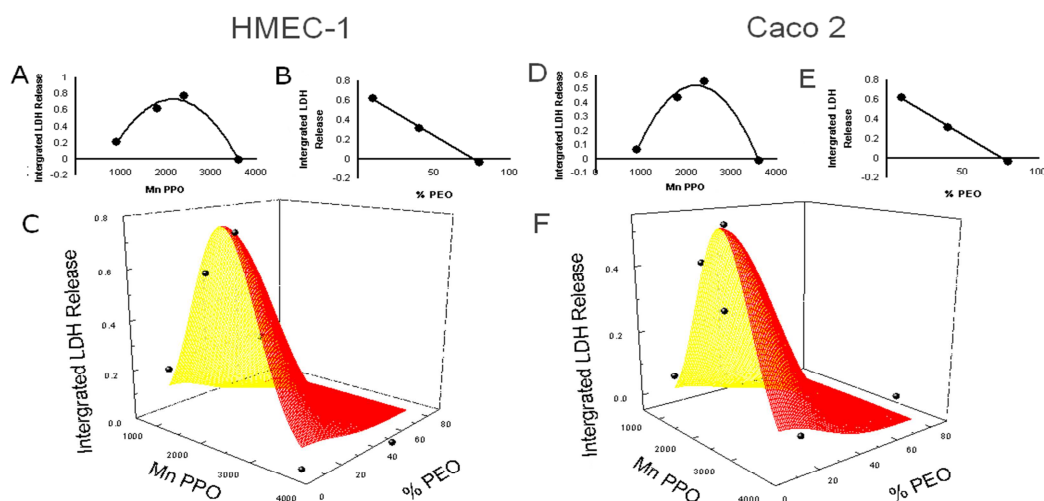


Figure 5.2: Effect of PEO-PPO-PEO block co-polymers on LDH release in HMEC-1 and Caco-2 cells. A and D: parabolic relationship between polymer M_n PPO and LDH release for polymers of equal % PEO (10%) in HMEC-1 and Caco-2 cells respectively. B and E: linear relationship between LDH release and % PEO for polymers of equal M_n PPO (1800 Da) in HMEC-1 and Caco-2 cells respectively. C and F: surface fit models showing LDH release against M_n PPO and % PEO in HMEC-1 and Caco-2 cells respectively.

5.3.3 Haemolysis Assay

Haemolysis assays were performed to assess the affinity of the polymers for erythrocyte membranes, and consequently their ability to solubilise biological membranes.

Similarly to observations in the two cytotoxicity assays, different polymers had variable haemolysis capacity (Table 5.1). Haemolysis dose response curves were generated for each polymer in order to evaluate their effect on membrane solubilisation (Fig. 5.3 A). The polymer concentration at which the membrane was saturated (C^{sat}) was used for determination of K_b values instead of the concentration at which complete lysis occurred (C^{sol}). This is due to the presence of mixed micelles of lipid and polymer, rather than intact erythrocytes at concentrations above C^{sat} . As predicted by Eq. 5.1, a linear relationship between the C^{sat} and lipid concentration was observed for the haemolytic polymers (Fig. 5.3B). These plots allowed the calculation of the ratio of lipid to surfactant (R_e) from the gradient, and the free surfactant in water (D_w). From this K_b values could be generated using Eq. 5.2.

By analogy with the LDH assay, K_b values were compared to both M_n PPO and percentage PEO and a 2D surface was fitted to the data (Fig 5.3. C). Since not all polymers displayed haemolytic properties, the K_b values was set as 0 for non lytic polymers. The 2D parabolic relationship observed can be described by Eq. 5.4.

$$K_b = 1.5 \cdot \exp \left[\frac{1}{2} \left(\frac{M_n PPO - 2200}{750} \right)^2 - \frac{1}{2} \left(\frac{\% - 40}{20} \right)^2 \right] \quad (5.4)$$

wherein a polymer with a M_n PPO of 2.2 kDa and 40% PEO (w/w) is predicted to have the greatest affinity for erythrocyte membranes with a K_b of 1.5 M^{-3} .

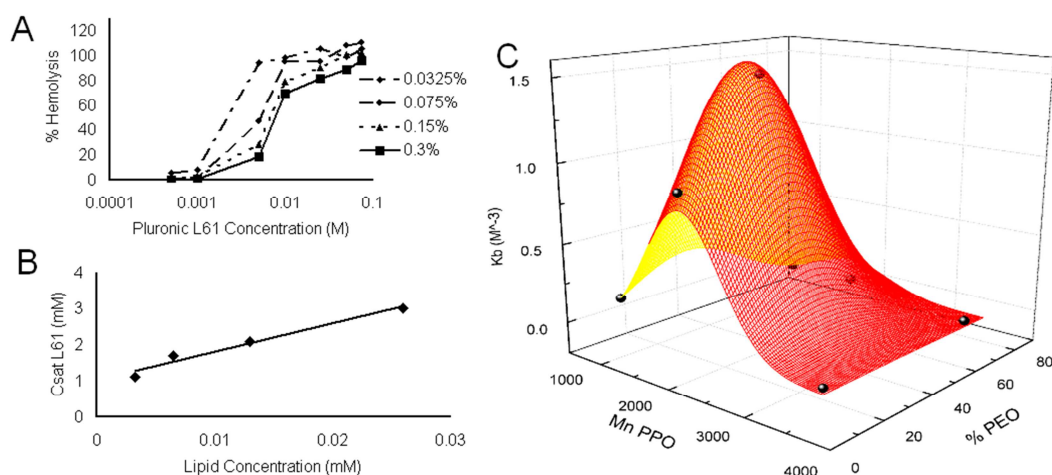


Figure 5.3: Affinity of PEO-PPO-PEO block co-polymers for erythrocyte membranes. A: example of haemolysis dose response curves over a range of haematocrits. B: example of linear relationship between C_{sat} values derived from A, as predicted by eq1. C: surface fit model showing K_b values against polymer M_n PPO and % PEO.

5.3.4 Erythrocyte Protection Assay

In the erythrocyte protection assay, polymers capable of forming ion traversable pores within the cell membrane protect erythrocytes from lysis induced by hypotonic stress.

A reduction in the level of haemolysis was observed when erythrocytes were pre-treated with Pluronic L61, L64 and L81; i.e., polymers that were highly cytotoxic in the LDH assay or showed a high K_b (Fig. 5.4). In contrast, polymers P85, F38 and L121 that do not seem to interact with cell membrane based on LDH data and K_b values were unable to protect erythrocytes against hypotonic stress (Fig.5. 4).

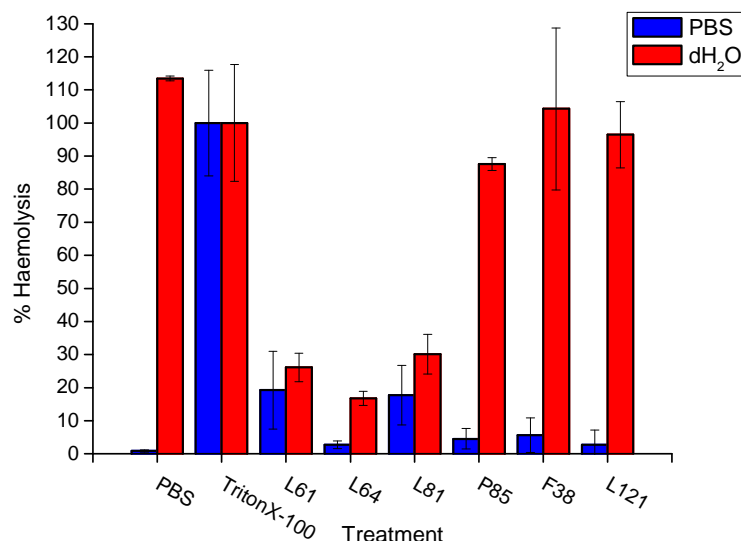


Figure 5.4: Effect of PEO-PPO-PEO block co-polymer on erythrocyte lysis induced by hypotonic stress. Data are presented as mean \pm standard deviation (n = 3 replicates)

5.3.5 JC-1 Mitochondrial Membrane Potential Assay

The JC-1 assay detects any reduction in mitochondrial membrane potential ($\Delta \Psi_m$) via an increase in the ratio of green to red fluorescence of the JC-1 dye, relative to the blue fluorescent *bisbenzimidazole* nuclear stain (Fig. 5.5A).

Polymers with a M_n PPO of 3.6 kDa, which had shown no activity in the MTS, LDH or haemolytic assays (Table 5.1) did not affect $\Delta \Psi_m$ in Caco-2 cells (Fig. 5.5B). All other polymers tested were able to lower $\Delta \Psi_m$ to some extent, although the intensity of the effect appeared independent of the polymer composition (Fig. 5.5B).

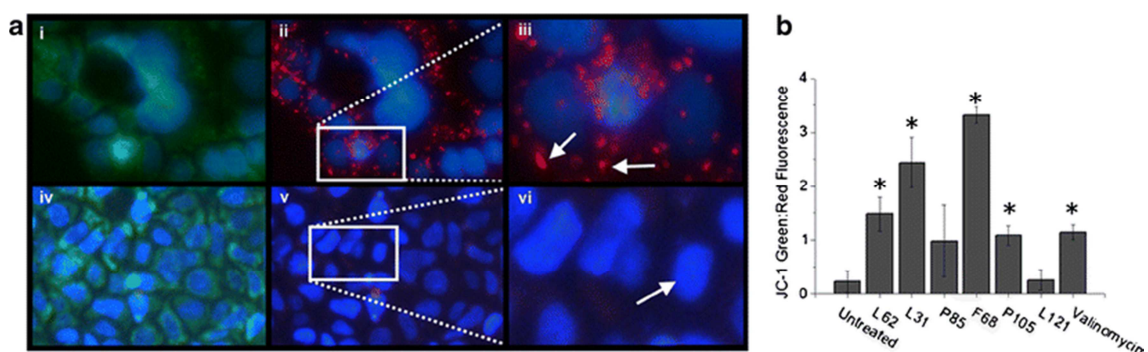


Figure 5.5: Effect of PEO-PPO-PEO block co-polymer treatment on mitochondrial membrane potential in Caco-2 cells. A: fluorescent microscopy images obtained from the JC-1 assay multiplexed with a blue bisbenzimidazole nuclear stain. Images i&ii show cells following treatment with polymer L31, and images iii&iv untreated cells. Images

i&iii show green JC-1 fluorescence merged with blue fluorescence from the nuclear stain and indicative of monomeric JC-1 found in the cytoplasm and images ii & iv show red JC-1 fluorescence merged with the blue nuclear stain, indicative of healthy mitochondria with high $\Delta\psi_m$. B: ratio of green to red JC-1 fluorescence normalised against blue bisbenzimidazole fluorescence after various treatments. Data are presented as mean \pm standard deviation (n = 3 replicates)

5.4 Discussion

The interest in PEO-PPO-PEO block copolymers as active biomaterials rather than inert excipients arose from the discovery that, when included in drug delivery systems, certain of these polymers were able to increase the efficacy of their therapeutic cargo. Their use has been shown to be advantageous in a number of different applications, including cancer therapy where circumvention of multi drug resistance (MDR) via P-gp inhibition [7] and ATP/glutathione depletion have been demonstrated [11]. As, to date, studies have principally described their interactions with artificial membranes [15-18], the link between the cellular effects of the polymers and their affinity for biological membranes that has been previously suggested [5] has not yet been experimentally confirmed. Moreover, a more wide-ranging determination of the relationship between polymer structure and biological responses is required to assist in the selection of the most promising drug carriers.

In the present study, we followed a systematic approach based on a combination of cytotoxicity, haemolysis and apoptosis assays to investigate the interactions of PEO-PPO-PEO block copolymers with biomembranes and their consequences on key cellular processes. We showed the chemical constituents of the copolymers are determinants of both their affinity for biological membranes and intensity of their cytotoxic effects. Our data strongly suggests a correlation between the two phenomena and highlights the importance of the polymer composition on their ability to trigger biological responses.

The acute cytotoxicity of a defined series of PEO-PPO-PEO block copolymers was evaluated in Caco-2 and HMEC-1 cells after 5 h of exposure. This was to capture cellular events that might have occurred as a result of membrane disruption by the polymers, independently of mechanisms of delayed toxicity. Concordant results were obtained in both the MTS and LDH assays with a general trend being that, when the same mass of each polymer was tested, the more hydrophobic the polymer, the higher

its cytotoxicity, with polymers containing 10% PEO causing the greatest cytotoxic effect. Based on the empirical model obtained by interpolation of our experimental data, polymers with a Mn PPO around 2 kDa were predicted to be the most cytotoxic. The haemolysis assays supported this finding as polymers with a Mn PPO of around 2 kDa were predicted to give the highest membrane binding constant and hence, to be the most efficient at solubilising erythrocyte membranes. They also suggested that a polymer containing around 40% PEO would solubilise cell membranes most efficiently as a consequence of its high affinity for lipid bilayers. This polymer displays a 30% increase in PEO content as compared to the most cytotoxic polymer identified in the two cytotoxicity assays. This apparent discrepancy could be explained by considering that dose response curves were obtained in the MTS and LDH assays utilising equal mass of each polymer, whereas an equal number of macromolecular chains (derived from concentrations expressed in moles) was employed in the haemolysis assays. The polymer with the highest Kb values, i.e., L64, has a total Mn of 3.0 kDa whereas the most cytotoxic polymer in the MTS and LDH assays, i.e., L61, has a total Mn of 2.0 kDa (Table 5.1). This results in a 50% increase in the number of polymer chains available for interaction with cell membranes at any given concentration based on polymer mass. It must be noted that when a plot similar to Fig. 5.2c was built using integrated LDH release values based on Pluronic molar concentrations, a polymer with a Mn PPO of 2.0 kDa and 40% PEO was predicted to be the most membrane disruptive (Fig. S2). Although it has been reported that the toxicity of Pluronics was reduced at concentrations higher than their CMC due to the formation of micelles [1], this phenomenon was not observed in our study. Likewise, exposure of calcein-loaded liposomes to Pluronic L64 resulted in the leakage of the dye following membrane permeabilisation both below and above its CMC, suggesting a transfer of polymer molecules from the micelles to the lipid bilayer [22].

Both PPO and PEO blocks were shown to modulate polymer affinity for biological membranes and their cytotoxic effects. Similarly, the extent of P-gp inhibition by the Pluronics was affected by the length of the PPO block and their overall hydrophilicity [5]. Moderately lipophilic copolymers with an intermediate number of PPO units were the most potent due to their ability to increase the fluidity of the cell membrane [5]. It has been reported that the central hydrophobic PPO block of the polymers is able to anchor into the hydrophobic subspace of artificial biomembranes [17]. However, polymers with a PPO block shorter than the bilayer thickness incorporated poorly and had limited effects on the fluidity of the biomembrane mimics

[18]. In our study, polymers with a large PPO central block (Mn PPO of 3.6 kDa) were consistently found to be biologically inactive, which may be due to their hydrophobic section being too bulky to allow penetration within the cell membrane. For polymers that can insert into the membranes, the hydrophilic PEO blocks were shown to interact with the polar head groups of the phospholipids within the same leaflet or in the two opposite leaflets depending on the length of the PPO block [18]. Our preliminary computational dynamic simulations of the interactions between Pluronic molecules and model DPPC membranes reveal that, in the latter case, the PEO blocks drag the polar head groups toward the centre of the bilayers, providing a potential mechanism underlying the formation of aqueous pores observed in the experimental erythrocyte protection assay (Fig. 5.6). Similarly, the ability of Pluronic L64 to create pores in artificial lipid bilayers has been described [23]. Detailed simulations are ongoing to dissect the molecular interactions between the PEO blocks and membrane lipids with the aim to better understand the influence of chain length on membrane disruption. It has nevertheless been reported previously that very long PEO chains are able to project outside artificial membranes [18]. In our study, Pluronics with a very high hydrophilic content were generally found to be non cytotoxic (Table 5.1). This could be due to limited interaction sites between long PEO chains and phospholipid head groups within the membrane, which possibly minimises the disruptive potential of highly hydrophilic polymers.

The JC-1 assay revealed that exposure to certain polymers caused a drop in the mitochondrial membrane potential of Caco-2 cells, which is one of the defining steps in the apoptotic process [24]. This might possibly be via formation of ion traversable pores within the mitochondria membranes as demonstrated in the external cell membrane (Fig. 5.4). PEO-PPO-PEO block copolymers are capable of circumventing anti-apoptotic strategies in Bcl-2 overexpressing MDR cancer cells when co-delivered with doxorubicin [6]. Bcl-2 overexpression protects MDR cells through prevention of MAC (mitochondrial apoptosis induced channels) formation. The MAC allow the influx of Ca²⁺ ions to the mitochondria, which lowers the mitochondrial membrane potential [24]. It is therefore possible that Pluronics reverse MDR strategies due to creation of pores in the mitochondrial membrane independently of the MAC. Polymers with lower Kb values showed a greater effect on the mitochondrial membrane potential than polymers with a high affinity for the erythrocyte membrane (Fig. 5.5). This may be ascribed to the tendency of polymers with a high Kb value to remain in the outer cell membrane due to the strength of their lipophilic interactions. The ability of the PEO-

PPO-PEO block co-polymer L31 to interact with the mitochondrial membrane preferentially to the external cell membrane can be illustrated by comparing its dose response curves in the MTS and LDH assays. Although this polymer appeared non destructive in the LDH assay, causing little LDH release above the baseline, it showed much greater efficacy in inhibiting MTS metabolism (Table 5.1, Fig. S3). This ability of non-ionic surfactants to cause changes in the micro-fluidity of mitochondrial membranes and hence, disturb the cytochrome P450 family of enzymes has been previously described and suggested as a possible strategy for reducing drug metabolism in the intestinal barrier [25].

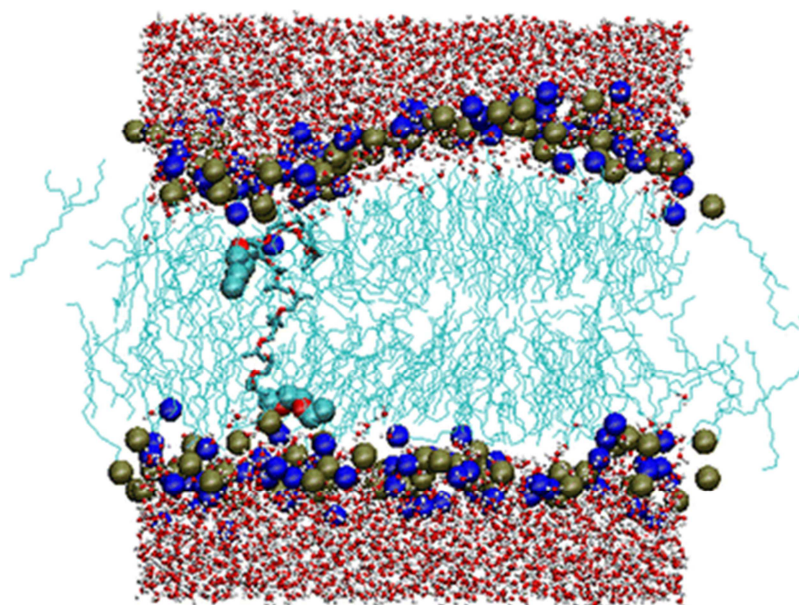


Figure 5.6: Snapshot of L31 absorbed in a dipalmitoyl phosphatidycholine (DPPC) bilayer membrane taken 200ns after the initiation of the computational simulation. The top and bottom layers of red and white beads represent water molecules in the system. The gold and blue bead correspond to, the phosphor and nitrogen atoms of the DPPC polar heads. The large aqua and red beads are the PEO blocks of the copolymer chain whereas the PPO block is represented by thick lines. For clarity the hydrophobic carbonyl tails of the lipids are shown as thin aqua line.

5.5 Conclusions

A combination of cytotoxicity and haemolysis assays performed on a defined series of PEO-PPO-PEO block copolymers revealed similar 2D-parabolic relationships between the chemical constituents of the copolymers and their affinity for biological

membranes or between polymer structure and their cytotoxicity potential, suggesting the biological effects of the copolymers are linked to their interactions with cell membranes. The chemical composition of the polymers was equally shown to affect their ability to reduce the mitochondrial membrane potential. We believe these findings may help to elucidate the mechanisms behind the biological effects of PEO-PPO-PEO block copolymers, as well as contribute to the design of safe drug formulations with optimal efficacy.

5.6 References

1. Batrakova, E.V. and A.V. Kabanov, *Pluronic block copolymers: Evolution of drug delivery concept from inert nanocarriers to biological response modifiers*. Journal of Controlled Release, 2008. **130**(2): p. 98-106.
2. Kozlov, M.Y., et al., *Relationship between pluronic block copolymer structure, critical micellization concentration and partitioning coefficients of low molecular mass solutes*. Macromolecules, 2000. **33**(9): p. 3305-3313.
3. Kabanov, A.V., E.V. Batrakova, and D.W. Miller, *Pluronic block copolymers as modulators of drug efflux transporter activity in the blood–brain barrier*. Advanced drug delivery reviews, 2003. **55**(1): p. 151-164.
4. Sriadibhatla, S., et al., *Transcriptional activation of gene expression by pluronic block copolymers in stably and transiently transfected cells*. Molecular Therapy, 2006. **13**(4): p. 804-813.
5. Batrakova, E.V., et al., *Optimal structure requirements for pluronic block copolymers in modifying P-glycoprotein drug efflux transporter activity in bovine brain microvessel endothelial cells*. Journal of Pharmacology and Experimental Therapeutics, 2003. **304**(2): p. 845-854.
6. Minko, T., et al., *Pluronic block copolymers alter apoptotic signal transduction of doxorubicin in drug-resistant cancer cells*. Journal of Controlled Release, 2005. **105**(3): p. 269-278.
7. Batrakova, E.V., et al., *Effect of pluronic P85 on ATPase activity of drug efflux transporters*. Pharmaceutical Research, 2004. **21**(12): p. 2226-2233.
8. Danson, S., et al., *Phase I dose escalation and pharmacokinetic study of pluronic polymer-bound doxorubicin (SP1049C) in patients with advanced cancer*. British journal of cancer, 2004. **90**(11): p. 2085-2091.
9. Valle, J.W., et al., *A phase 2 study of SP1049C, doxorubicin in P-glycoprotein-*

- targeting pluronics, in patients with advanced adenocarcinoma of the esophagus and gastroesophageal junction*. Investigational new drugs, 2011. **29**(5): p. 1029-1037.
10. Lemieux, P., et al., *A combination of poloxamers increases gene expression of plasmid DNA in skeletal muscle*. Gene therapy, 2000. **7**(11): p. 986.
 11. Alakhova, D.Y., et al., *Differential metabolic responses to pluronic in MDR and non-MDR cells: a novel pathway for chemosensitization of drug resistant cancers*. Journal of Controlled Release, 2010. **142**(1): p. 89-100.
 12. Lavigne, M.D., et al., *Promoter Dependence of Plasmid-Pluronics Targeted α Galactosidase A Expression in Skeletal Muscle of Fabry Mice*. Molecular Therapy, 2005. **12**(5): p. 985-990.
 13. Batrakova, E.V., et al., *Mechanism of pluronic effect on P-glycoprotein efflux system in blood-brain barrier: contributions of energy depletion and membrane fluidization*. Journal of Pharmacology and Experimental Therapeutics, 2001. **299**(2): p. 483-493.
 14. Yates, L.L. and D.C. Górecki, *The nuclear factor-kappaB (NF-kappaB): from a versatile transcription factor to a ubiquitous therapeutic target*. Acta Biochimica Polonica English edition, 2006. **53**(4): p. 651.
 15. Chang, L.C., et al., *Interactions of Pluronics with phospholipid monolayers at the air-water interface*. Journal of Colloid and Interface Science, 2005. **285**(2): p. 640-652.
 16. Chang, L.C., Y.Y. Chang, and C.S. Gau, *Interfacial properties of Pluronics and the interactions between Pluronics and cholesterol/DPPC mixed monolayers*. Journal of Colloid and Interface Science, 2008. **322**(1): p. 263-273.
 17. Firestone, M.A., A.C. Wolf, and S. Seifert, *Small-angle X-ray scattering study of the interaction of poly (ethylene oxide)-b-poly (propylene oxide)-b-poly (ethylene oxide) triblock copolymers with lipid bilayers*. Biomacromolecules, 2003. **4**(6): p. 1539-1549.
 18. Lee, B. and M.A. Firestone, *Electron density mapping of triblock copolymers associated with model biomembranes: Insights into conformational states and effect on bilayer structure*. Biomacromolecules, 2008. **9**(6): p. 1541-1550.
 19. Lichtenberg, D., *Characterization of the solubilization of lipid bilayers by surfactants*. Biochimica et Biophysica Acta (BBA)-Biomembranes, 1985. **821**(3): p. 470-478.
 20. Malheiros, S.V.P., N.C. Meirelles, and E. de Paula, *Pathways involved in trifluoperazine-, dibucaine-and praziquantel-induced hemolysis*. Biophysical chemistry, 2000. **83**(2): p. 89-100.

21. Reers, M., T.W. Smith, and L.B. Chen, *J-aggregate formation of a carbocyanine as a quantitative fluorescent indicator of membrane potential*. *Biochemistry*, 1991. **30**(18): p. 4480-4486.
22. Pembouong, G., et al., *A comprehensive study in triblock copolymer membrane interaction*. *Journal of Controlled Release*, 2011. **151**(1): p. 57-64.
23. Gau-Racine, J., et al., *PEO-PPO block copolymer vectors do not interact directly with DNA but with lipid membranes*. *The Journal of Physical Chemistry B*, 2007. **111**(33): p. 9900-9907.
24. Ryu, S.Y., et al., *Role of mitochondrial ion channels in cell death*. *Biofactors*, 2010. **36**(4): p. 255-263.
25. Christiansen, A., et al., *Effects of non-ionic surfactants on cytochrome P450-mediated metabolism in vitro*. *European Journal of Pharmaceutics and Biopharmaceutics*, 2011. **78**(1): p. 166-172.

5.6 Supplementary Material

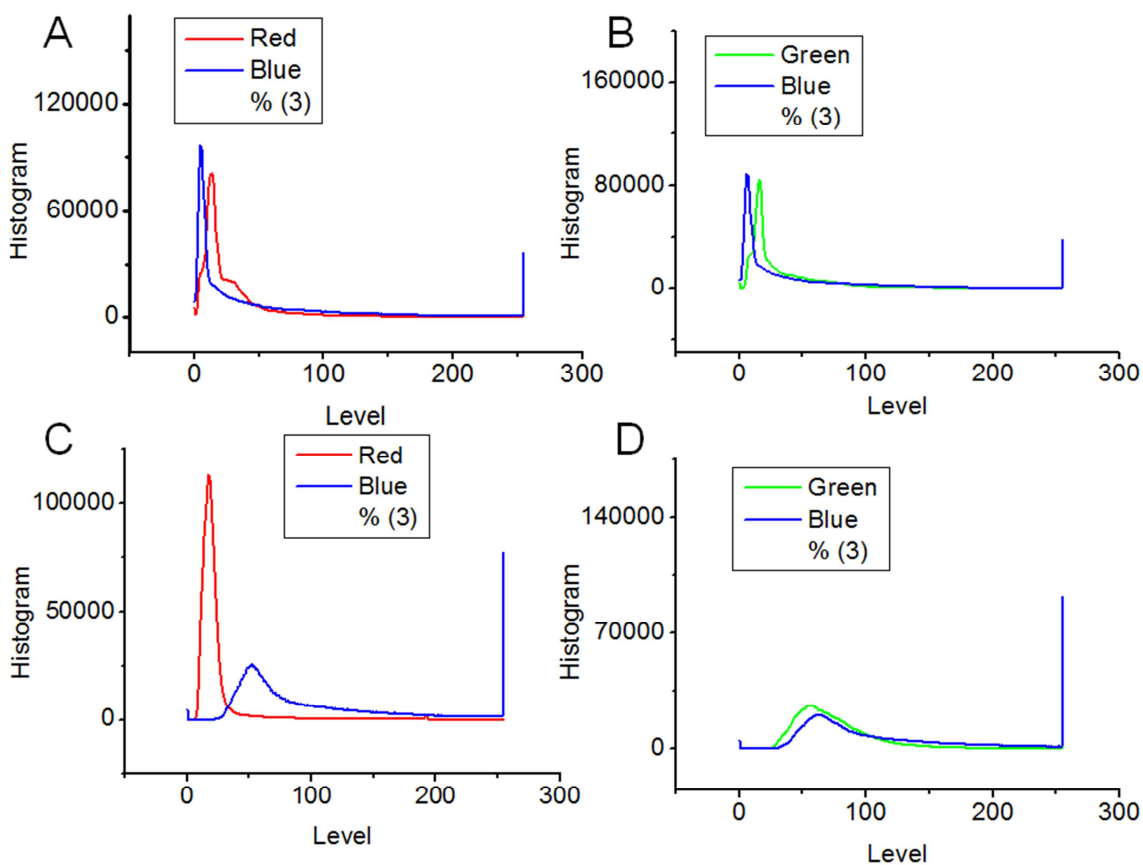


Fig. S1 (Supplementary information): Examples of histograms generated by Origin Pro 8.0 from fluorescent images obtained in the JC-1 assay. Relative levels of fluorescence per pixel in the red and blue channels (A&C) or green and blue channels (B&D) for untreated cells (A &B) or cells treated with polymer L31 (C&D).

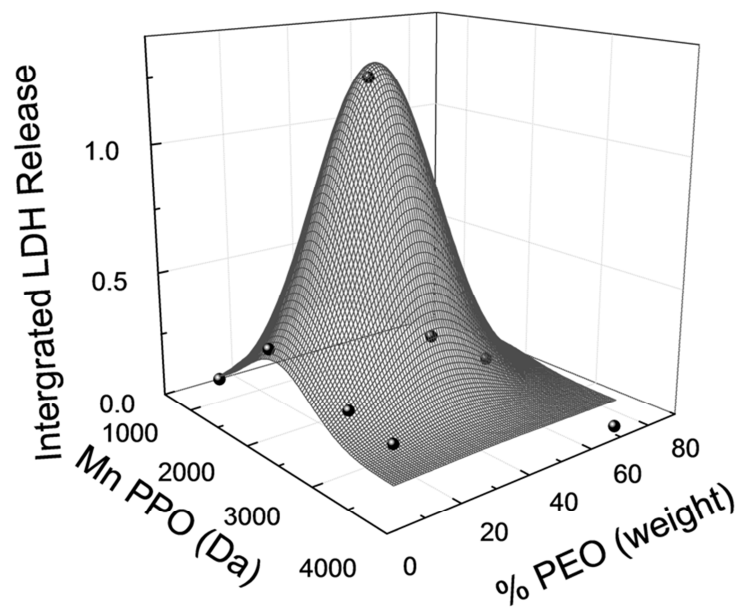


Fig. S2 (Supplementary information): 2D plot showing LDH release against M_n PPO and % PEO in HMEC-1 cells when polymer concentration is expressed in moles/l.

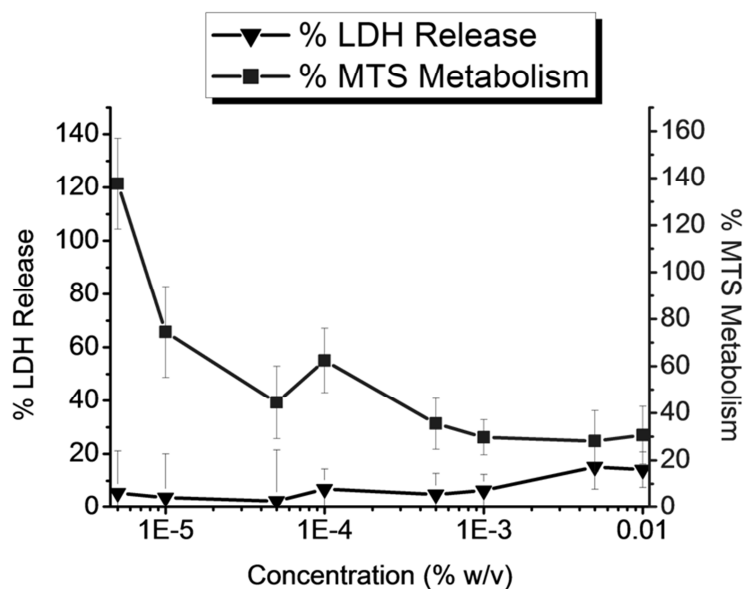


Fig. S3 (Supplementary information): Cytotoxicity of polymer L31 as measured in the LDH or MTS assay. Data are mean \pm SEM (n = 2 plates; 6 replicates per plate) and are expressed as percentage of control.

Coarse Graining Poly-ethylene-oxide-Poly-propylene-oxide-Poly-ethylene-oxide (PEO-PPO-PEO) Block Copolymers using the MARTINI Force Field

This chapter is in preparation for submission

Authors: S. Nawaz, P. Carbone

6.1 Introduction

Pluronics is the trade mark for a class of amphiphilic linear triblock copolymers consisting of two hydrophilic polyethylene oxide (PEO) blocks connected to a central hydrophobic polypropylene oxide (PPO) block. These copolymers have a wide range of important uses in a widespread of industrial sectors ranging from cosmetic and more recently medical and pharmaceutical. They can be used on nanoparticles as a surface coating [1] and even as drug/gene nano carriers exploiting their ability to self-assemble in polar solvents [2, 3]. Recently some Pluronic class copolymers have shown to enhance gene transcription [4] and to have elicit biological responses in vitro and vivo showing an increased susceptibility of multi drug resistant cancer cells to chemotherapeutic agents such as doxorubicin [5]. Experimentally Mortensen et al. have extensively studied the structural features of Pluronics characterizing their micellar aggregates and mesophases using techniques such as SANS (Small Angle Neutron scattering) and Cryo-TEM (Cryogenic transmission electron microscopy) over the last two decades [6-9]. Alexandridis et al. studied the effect of temperature on the micelles structural properties formed from two different Pluronics where the hydrophobic (PPO) core content remained the same but the size hydrophilic (PEO) blocks was varied [10]. Pedersen et al. showed the structure of a specific Pluronic polymer, namely P85, micelles using SANS experiments focusing again on the temperature effect and analysing the obtained data with a model based on Monte Carlo simulations [11, 12]. More recently the effect of different Pluronics on biological materials has also been studied [13].

Computer simulations have helped in clarifying several aspects of the self-assembly properties of amphiphilic block copolymers [14], however so far most of the simulations on amphiphilic molecules have been performed using generic coarse grained models which are only able to retain few chemical features [15, 16]. The self-consistent mean field theory is also largely used to model the self-assembly of block copolymers. For example Sevink and Zvelindovsky have simulated polymeric amphiphiles in solvent observing the entire fusion process into the formation of complex vesicles using the self-consistent field theory [17]. Per Linse specifically used the mean field lattice theory to study the micellization of PEO-PPO-PEO triblock copolymers [18]. More recently the only computational study on Pluronics have only used a generic coarse grain model showing the effect of Pluronic solutions under confinement [19].

Although these models have been proved to be able to provide interesting insights into the behaviour of these materials, the chemical specificities of the copolymers should be ideally retained into the models when properties-structure relationships are sought. For instance, in the specific case of biological applications, a detailed description of the interactions between the copolymers and the biological material is necessary in order to model properly the system. To clarify the actual mechanism underpinning interactions between amphiphiles and model membranes, atomistic studies have been used although are affected by the well-known limitations of length and timescale [20].

Several procedures have been devised in the last decade to develop coarse-grained models that retain specific chemical features of the underlying atomistic structure [21]. Coarse-grained models developed in these ways overcome the time and length scale limitations typical of the atomistic simulations by grouping a cluster of atoms into a single particle or bead, reducing the overall number of particles in the system and also, when employed in molecular dynamics simulations, allowing an increase in the value of the timestep. In order to retain the chemical specificities of the system in the model, the procedure to develop the potential interactions acting between the beads may use information coming both from experimental and detailed atomistic simulations data.

There are a number of methodologies used for developing CG models for polymers with specific chemical properties. The structure-based CG models [21-23] are

quite often used to coarse-grain polymeric systems, however they have their limitations. For example Carbone et al. have shown that while the CG potentials developed targeting structural data (i.e. distance, angle distributions and radial distribution functions) obtained from detailed atomistic simulations are able to reproduce several system properties, their transferability over thermodynamic states different than those used to perform the atomistic simulations has an erratic behaviour [21]. These force fields are transferable over different molecular weights in all the cases studied but they can reproduce the correct glass transition temperature and thermal expansion coefficient only for specific CG models.

While structural-based models are very popular when isotropic systems are coarse-grained, very few examples of this type of models are present in the literature for case of amphiphilic molecules which show self-assembly properties. This method has been followed by Bedrov et al. to develop a solvent free coarse grain model for Pluronics where they utilized a multiscale approach. The latter was initiated from quantum chemistry (QC) calculations used to parameterize an atomistic explicit solvent (AES) model which in turn was used in the building of coarse grain implicit solvent (CGIS) model to investigate the properties for the self-assembly of Pluronics [24]. Although the structural-based CG model might be used to coarse-grain polymers in solutions or polymer blends their use is very limited as ultimately either an additional parameterisation of the cross term (solvent-polymer or polymer-polymer) is required or a specific mixing rule has to be sought [25-27].

Another CG techniques which might represent a better alternative in coarse-graining polymer solution is the one where thermodynamic data properties such as density or surface tension [28] are used as target properties to develop the force field parameters acting between the beads. In this case, the parameterization of the potential is done on a trial and error basis and usually include very few (if not none) structural properties. The modelling of biological environments and amphiphilic molecules have often been coarse grained using thermodynamics approaches [29] and using this approach Srinivas et al. have developed a CG force field able to predict the self-assembly of diblock copolymers [30].

The CG force field known as MARTINI force field is also a thermodynamic based coarse grain model, originally developed specifically for the phospholipids forming the biological membranes [31, 32], was later extended to model other chemical

systems such as proteins [33], carbohydrates [34] and fullerene molecules [35]. The parameterisation in the MARTINI approach is determined by the reproduction of densities and free energies of partitioning between polar and apolar phases. An advantage of the MARTINI approach is that in multicomponent systems (such as solutions or a protein/lipid bilayer mixture) the parameterisation of the cross term (solvent/solute or protein/lipids) non-bonded interactions is a relatively easy task as they only consist of a simple Lennard Jones and Coulomb functions. Therefore the parameters developed for new building blocks can be made compatible with existing MARTINI ones. Recently Rossi et al [36] and Lee et al. [37] have used the MARTINI approach to develop CG models for polymer melts and solution. However since the structural properties are quite important in modelling polymers, they included in their parameterization procedure some properties targeting mainly the polymer radius of gyration.

In the present work, the development of a MARTINI-compatible CG force field for Pluronics is reported. The force field development, that uses both thermodynamic and few structural data, has been optimized to work with the MARTINI water model [31]. The paper is organized as follows: initially the details of the atomistic simulations used to develop the CG force field and the CG molecular dynamics simulations are reported. Then CG force field optimization procedure and the results follow. The conclusions close the paper.

6.2 Computational Details

In order to develop the CG force field, atomistic simulations of a single chain of PEO and atactic PPO homopolymer with varying the number of monomers were performed in SPC type water [38]. In addition simulations of a copolymer test chain composed by 10 monomers of PEO on either side and 10 monomers of PPO in the centre (PEO₁₀PPO₁₀PEO₁₀) capped with methyl groups were performed in SPC type water [38]. Furthermore atomistic simulations were also performed on some popular Pluronic copolymers reported in Table 6.1. The parameterization was performed using coarse grain beads in standard MARTINI water [31]. A single polymer or copolymer chain was initially placed in vacuum to allow a slight coiling up before being placed in a box size double the approximated radius of gyration full of water molecules. The

atomistic simulations were equilibrated for 50 nanoseconds and the coarse grained simulations were run for 1-3 microsecond depending on the length of the polymer/copolymer chain. The conditions used to run atomistic and coarse grain simulations are described in the following sections.

Table 6.1: Characteristics of Pluronics investigated. N_n represents the number of PEO units on each side and N_m is the number of PPO units in the central block of triblock copolymer.

Pluronics	N_n PEO	N_m PPO
L31	2	16
L61	3	31
L62	6	31
L64	14	31

6.2.1 Atomistic Simulations

Molecular dynamics simulations on the all atom models used parameters from the OPLS-AA force field [39] and performed using the Gromacs (version 4.5.4) software package [40]. A time step of 2fs was employed and bonds were constrained using the SHAKE algorithm [41]. Long range electrostatics were calculated using the particle mesh Ewald summation (PME) [42, 43] with Fourier spacing of 0.12nm and a fourth order interpolation. The van der Waals and coulomb cut-off was set to 1.1nm and 0.9nm respectively. The neighbour list was updated every 10 steps using a grid with a 0.9nm cut-off distance. An isothermal-isobaric (NPT) ensemble was used to equilibrate all systems maintaining the temperature at 300K with a Berendsen thermostat and a coupling time of 0.1ps [44]. Isotropic pressure coupling was used for all the systems under investigations using a Berendsen barostat with a reference pressure of 1bar, coupling time of 1.0 ps and compressibility of $4.5 \times 10^{-5} \text{ bar}^{-1}$ [44].

6.2.2 Coarse-grained Simulations

Coarse grained simulations were performed using again the Gromacs (version 4.5.4) software package [40]. A time step of 20 fs was used and the neighbour list for the non-bonded interactions was updated every 200 fs. The shift function for dispersion

interactions starting from 0.9 nm was used with a cut-off of 1.2 nm. An isothermal-isobaric (NPT) ensemble was used to equilibrate all systems maintaining the temperature at 300K with a Berendsen thermostat and a coupling time of 0.5 ps [44]. Isotropic pressure coupling was used for all the systems under investigations using a Berendsen barostat with a reference pressure of 1.0 bar, coupling time of 4.0 ps and compressibility of $5.0 \times 10^{-6} \text{ bar}^{-1}$ [44].

6.3 Development of the CG Model

Coarse graining development requires the need of two fundamental choices, the mapping procedure for the coarse grain particles and structural or thermodynamic properties to target in order to validate the model. The mapping procedure involves the selection of interaction sites that are often chosen arbitrarily. A few attempts have recently been made to automate the mapping procedure [45-49]. For the purpose of this study, each EO and PO monomers have been mapped as a single coarse grained particles. The parameterisation of the bonded interactions connecting the coarse grained beads is based on the corresponding pseudo interactions from all-atom simulations. To validate the model, structural and thermodynamic properties i.e. the radius of gyration and free energy of partitioning of the monomers and dimers between polar and apolar phases data respectively are targeted from available experimental data and atomistic simulations. We begin with illustrating a description of the mapping scheme followed by the parameterization process of the bonded and non-bonded interactions. The bonded potential is described by bond, angle and dihedral functions whereas the non-bonded potential is described by Lennard Jones (LJ) interactions. The energy function was designed to be consistent with MARTINI force field.

6.3.1 Mapping Scheme

The mapping scheme for the Pluronics considers the EO and PO monomers as a single particle. MARTINI coarse beads typically consist of four heavy atoms [31] with a Lennard Jones parameter σ as 0.47 nm, more recently smaller beads have been introduced for cyclic/aromatic structures representing three heavy atoms per bead with σ as 0.43 nm [32]. For our Pluronic model, the 3 to 1 mapping scheme is chosen for the

mapping procedure. The EO monomer includes three heavy atoms, which include two CH₂ groups and an oxygen atom per bead. The PPO monomers are formed by four heavy atoms, CH₂, CH, O and a CH₃ pendant group. Although here there are four heavy atoms in each bead only three of them are incorporated in the backbone and so therefore again a smaller bead type is selected. The chosen mapping scheme is reported in Fig. 6.1.

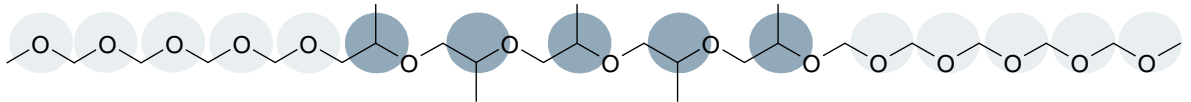


Figure 6.1: Superposed description of an atomistic and coarse grain sample of a Pluronic molecule. The lighter outer CG beads represent the PEO segments and the darker central CG beads represent the PPO segments.

6.3.2 Parameterisation of the Bonded Part of the CG Potential

The bonded interactions in the MARTINI force field is generally described using distributions of bonds, angels and dihedrals obtained from atomistic simulations. The distribution of the bonds is calculated using a harmonic potential:

$$V_{bond}(b) = \frac{1}{2}K_b(b - b_0)^2 \quad (6.3.1)$$

where K_b is the bond force constant, b and b_0 are the instantaneous bond length and bond length at lowest energy respectively.

The angle distributions are also calculated using a harmonic potential:

$$V_{angle}(\theta) = \frac{1}{2}K_\theta(\cos(\theta) - \cos(\theta_0))^2 \quad (6.3.2)$$

where K_θ is the angle force constant, θ and θ_0 are the defined angle and angle at minimum energy respectively.

Finally the dihedral distributions are calculated as follows:

$$V_{dihedral}(\phi) = \sum_{i=1}^m K_\phi (1 + \cos(n_i\phi - \phi_i)) \quad (6.3.3)$$

where n_i and ϕ_i are the multiplicity offsets respectively. In the present parameterisation $m=4$ for the individual dihedral terms.

In the parameterisation of the bonded interactions for the CG Pluronics, we used the bond distance, angle and dihedral distributions from atomistic simulations. Atomistic simulation trajectories of a single chain of PEO30 and PPO30 in a box of water and the corresponding CG trajectories using the MARTINI force field were initially generated. These trajectories were used in the parameterisation process and carried out separately for pure PEO and pure PPO homopolymer chains. The centre of mass corresponding to the mapping scheme shown in Fig. 6.1 were used to calculate the bond distance, angle and dihedral distributions (Fig 6.2). Harmonic potentials were used in the coarse grain with the appropriate bond distance, angles and dihedrals from the atomistic simulations. We tuned the force constant to reproduce the width of the distributions obtained from atomistic simulations (Table 6.2). We then run a simulation of dummy Pluronic chain consisting of PEO₁₀PPO₁₀PEO₁₀ using both again atomistic and coarse simulations. The bond distance and angle distribution for the interconnecting beads between the PEO and PPO part of the Pluronics were matched using the same procedure described above (Fig. 6.3).

Table 6.2: Bonded interactions for CG Pluronics

	Bond		Angle		Dihedral		
	b_0 (Å)	K_b (kJ mol ⁻¹ nm ⁻²)	Θ_0 (deg)	K_θ (kJ mol ⁻¹)	Φ_0 (deg)	K_ϕ (kJ mol ⁻¹)	N
PEO-PEO	0.265	17000	115	50	180	1.96	1
					0	0.18	2
					0	0.33	3
					0	0.12	4
PPO-PPO	0.355	17000	120	50	180	1.96	1
					0	5.00	2
					0	0.33	3
					0	0.12	4
PEO-PPO	0.355	17000	120	50			

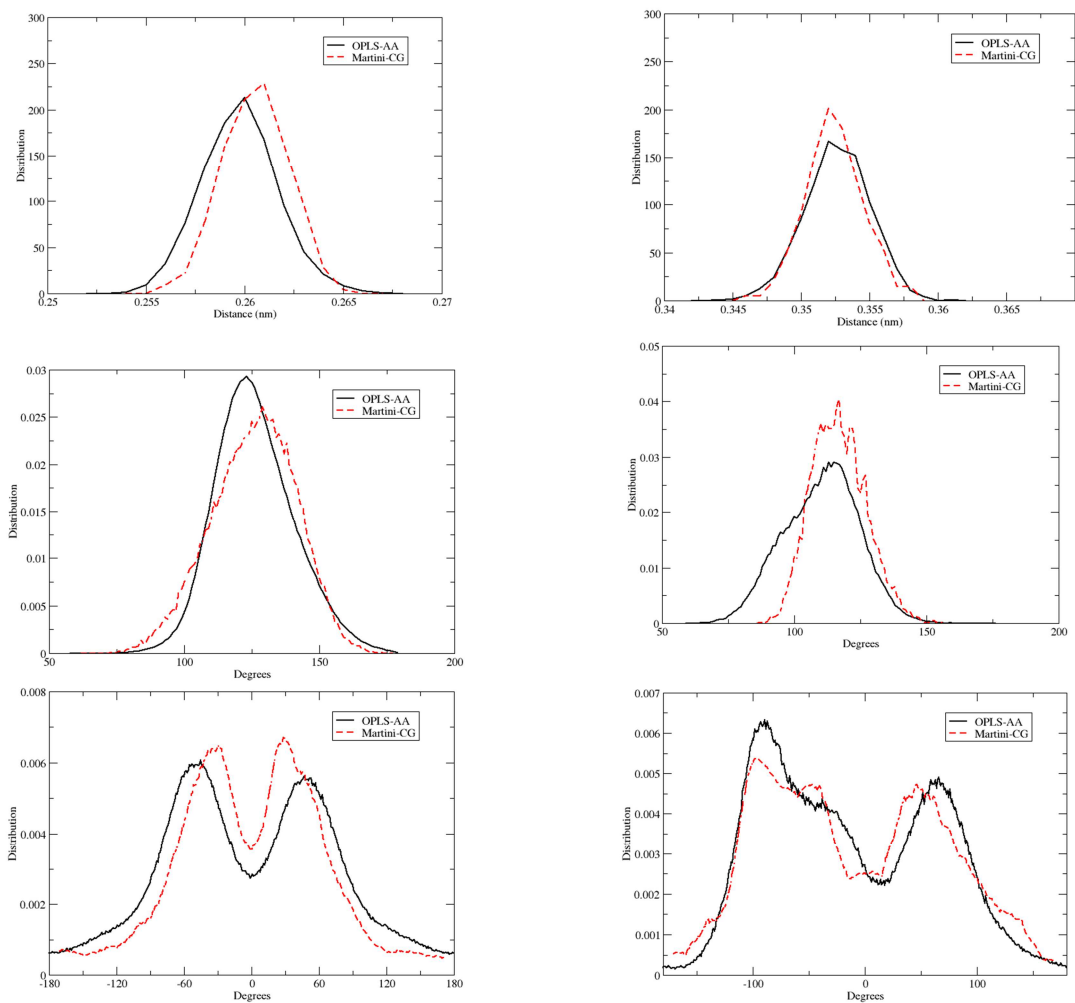


Figure 6.2: PEO bond distance distribution (top left), PEO angle distribution (middle left), PEO dihedral distribution (bottom left), and PPO bond distance distribution (top right), PPO angle distribution (middle right), PPO dihedral distribution (bottom right).

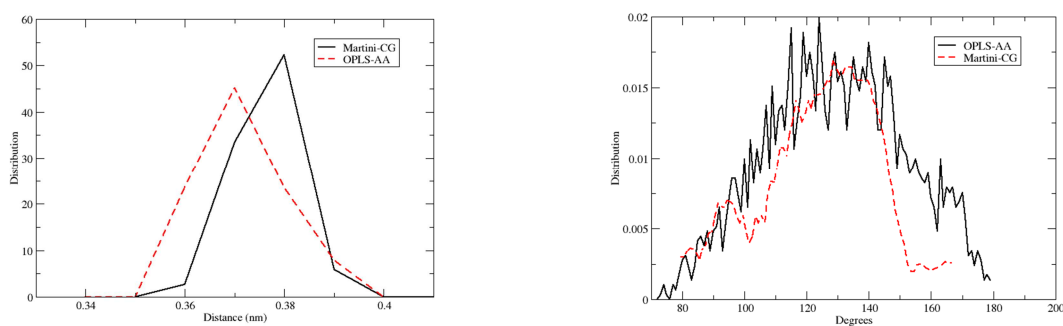


Figure 6.3: PEO₁₀PPO₁₀PEO₁₀ bond distance distribution (left), PEO₁₀PPO₁₀PEO₁₀ angle distribution (right).

6.3.3 Parameterisation of the Non-bonded Part of the CG Potential

The MARTINI force field non-bonded interactions between particles are primarily based on the Lennard Jones (LJ) potential:

$$U_{LJ} = 4\varepsilon_{ij} \left[\left(\frac{\sigma_{ij}}{r} \right)^{12} - \left(\frac{\sigma_{ij}}{r} \right)^6 \right] \quad (6.3.4)$$

where ε and σ are constants representing the strengths and range of the potential respectively while r is the distance between the particles.

To parameterise the Pluronics for the non-bonded interactions, the partition coefficient between octanol and water for the homopolymers are first targeted to match with experimental values. The experimental partition coefficient, $\log P_{OW}$, between octanol and water for dimers of PEO 1,2-dimethoxyethane (DME) and PPO 1,2-dimethoxypropane (DMP) are 0.21 and 1.78 respectively [30, 50, 51]. The partition coefficient between octanol and water is obtained from equilibrium densities of the molecules in both phases and can be denoted as follows:

$$\log P_{OW} = \log \frac{[\text{solute}]_{\text{octanol}}}{[\text{solute}]_{\text{water}}} \quad (6.3.5)$$

where $[\text{solute}]_{\text{octanol}}$ and $[\text{solute}]_{\text{water}}$ corresponds to the concentration of molecules in octanol and water respectively. From these partition coefficient values the free energy of transfer between octanol and water ($\Delta G_{\text{trans}/OW}$) can be calculated from the following equation:

$$\Delta G_{\text{trans}/OW} = kT \log P_{OW} \quad (6.3.6)$$

where k is the Boltzmann constant (1.38 J/K) and T is the temperature in kelvin.

The free energy of transfer for the PEO and PPO dimers at 300 K from atomistic simulations turns out to be -3.9kJ/mol and 4.4 kJ/mol respectively [30, 50, 51]. In order to identify a coarse grained MARTINI type bead, it is essential to match these values of free energy of transfer to the corresponding coarse grain beads. The first step followed in the parameterization is to verify if there is any existing bead in the MARTINI force field library whose free energy of transfer value match the experimental one for the corresponding dimers. In a recent study, Rossi et.al. [52] have proposed a new set of parameters for PEO monomers in the MARTINI force field and have named this bead as PO. They validated the non-bonded parameters using the thermodynamic integration

method to calculate the free energy of transfer between octanol and water reproducing experimental thermodynamics data efficiently. For the PO bead we chose the MARTINI type bead is N₀ which has a ΔG_{OW} value of 5 kJ/mol. The Lennard-Jones parameters for the corresponding beads to PPO and PEO are reported in table 6.3.

Table 6.3: Non-bonded interactions for CG Pluronic beads

	σ (Å)	ϵ (kJ mol ⁻¹)
PEO-PEO	4.3	3.375
PPO-PPO	4.3	2.625
PEO-PPO	4.3	3.75
PEO-W	4.7	3.19
PPO-W	4.7	2.625

6.4 Results and Discussions

In order to validate our model for the Pluronic molecules, structural properties such as the radius of gyration (R_g) and the corresponding Flory exponent were compared with the values obtained from atomistic simulations. The persistent length (l_p) for the homopolymers is also calculated from end to end values of the polymer chains in solution and compared to experimental values. The transferability of the force field parameters in a different chemical environment (polar and apolar) and temperatures is also checked by comparing the R_g values to atomistic simulations. Finally some Pluronic models are validated against Mortensen's structural small-angle neutron scattering studies of aqueous solutions of PEO-PPO-PEO triblock copolymers [6]. The model is also tested over a wide range of temperature values.

6.4.1 Homopolymer Validation

Validation of the coarse-grained model

To begin with the validation of the homopolymers PEO and PPO coarse-grained model, various lengths of the homopolymer chains were simulated. The corresponding values of the radius of gyration (R_g) were favourably compared to atomistic results obtained for the same polymer lengths (see Table 6.4).

Table 6.4: Radius of gyration data for PEO and PPO homopolymers at 300K.

Number of PEO/PPO Monomers	Radius of gyration R_g (nm)	
	OPLS	MARTINI
30 (PEO)	0.927±0.170	0.831±0.111
60 (PEO)	1.43±0.203	1.34±0.206
90 (PEO)	1.99±0.242	1.71±0.285
30 (PPO)	0.979±0.159	0.922±0.141
60 (PPO)	1.24±0.148	1.40±0.165
90 (PPO)	1.32±0.056	1.56±0.198

The radius of gyrations (R_g) of many more molecular weight homopolymers of PEO and PPO (see Appendix D) were calculated and plotted (Fig. 6.4-6.5) against the polymer molecular weights (specifically the number of monomers). The resulting plot was then fitted by an exponential function:

$$Rg = a M_W^\nu, \quad (6.4.1)$$

where M_W is the molecular weight in number of monomers and ν is the Flory exponent.

The fitting parameters for PEO, a and ν turns out to be $a=0.0879$ and $\nu= 0.65$. These values clearly indicate that the polymer chain is in a good solvent. Previous atomistic simulations of PEO simulations of polymer chains ranging from 18-43 monomers [53] have resulted in a power law as:

$$Rg = 0.017 M_W^{0.59}, \quad (6.4.2)$$

Experimental light scattering data for larger molecular weight PEO in water have shown $\nu = 0.67$ [54] agreeing very well with $\nu = 0.65$ from our coarse grained simulations.

The fitting parameters for PPO, a and ν were calculated to be $a=0.1767$ and $\nu=0.49$. These values indicate that water is a bad solvent for PPO at this temperature and M_w . Atomistic simulations of PPO simulations of polymer chains ranging from 18-43 monomers by Hezaveh et al. have resulted in a power law as:

$$Rg = 0.019 M_W^{0.55}, \quad (6.4.3)$$

Hezaveh et al. have also claimed that the solubility of the PPO is affected by chain length in different solvents and as a consequence of the polymer hydrophobicity change, hence being more hydrophobic as the chain length increases [53].

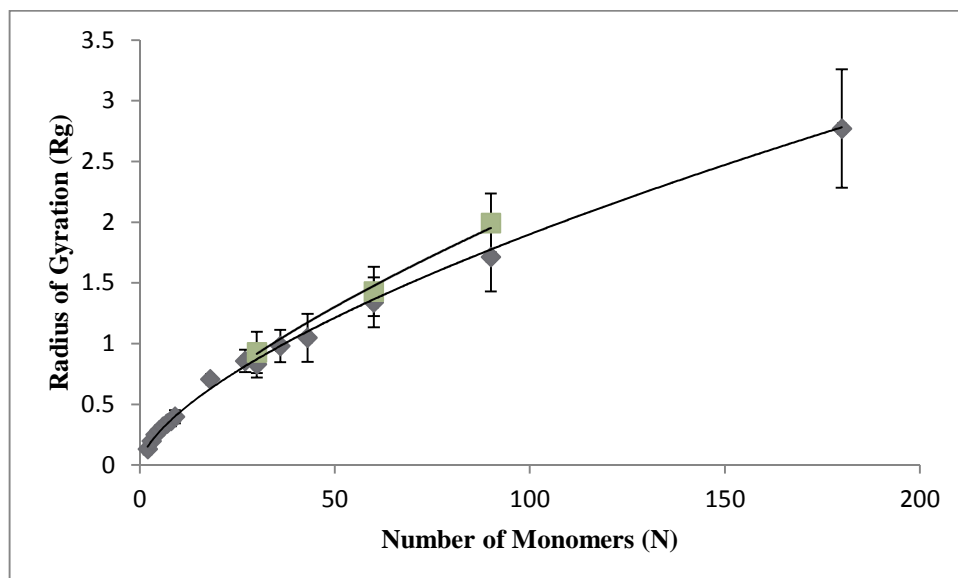


Figure 6.4: Radius of gyration plot versus the number of PEO monomers for all-atom simulations (squares) and MARTINI coarse grain simulations (diamonds) fitted using power exponential. Solid black line corresponds to the fitting curve (see text).

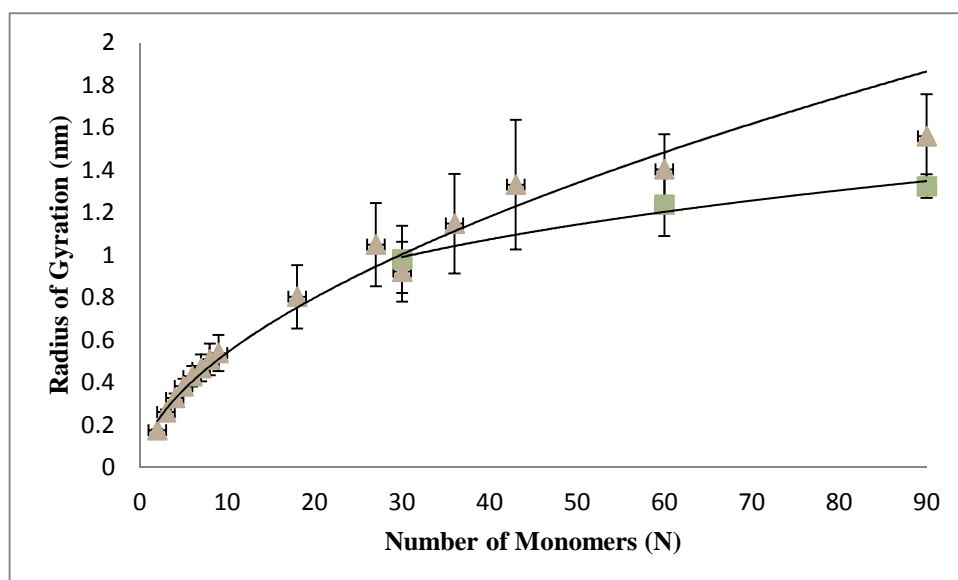


Figure 6.5: Radius of gyration plot versus the number of PPO monomers for all-atom simulations (squares) and MARTINI coarse grain simulations (diamonds) fitted using power exponential.

The Flory characteristic ratio C_n for a polymer is defined as:

$$C_n = \frac{Ree^2}{Nl_b^2} \quad (6.4.4)$$

where Ree is the end to end distance, N is the number of bonds and l_b is the bond length. The Flory characteristic ratio saturates a finite value C_∞ when the polymer chain is separated by many bonds in the polymer chain. The value of C_n calculated for the PEO homopolymer is reported in Fig. 6.6.

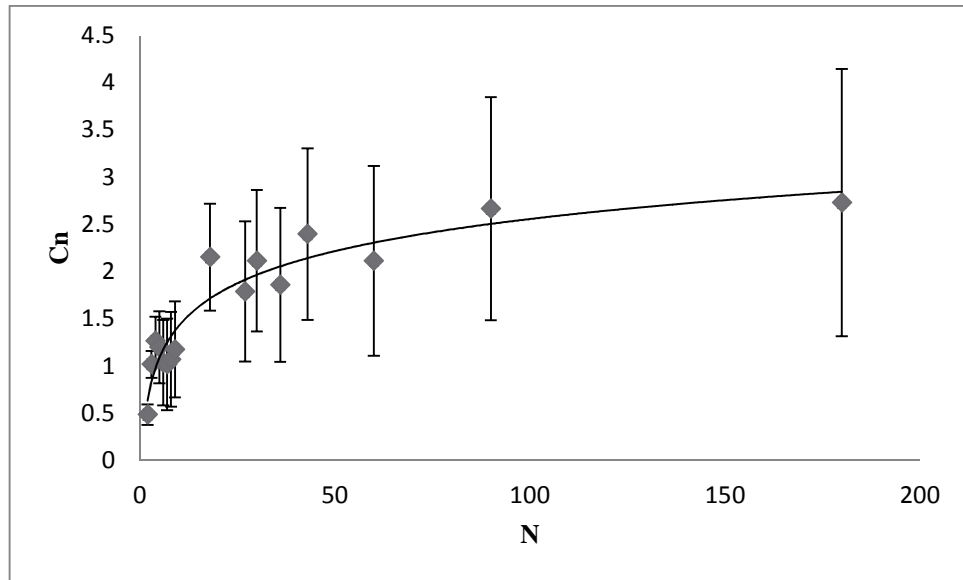


Figure 6.6: Flory characteristic ratio calculated from end to end distances versus the number of monomer for the MARTINI force field for PEO monomers.

Using the Flory characteristic ratio C_∞ , the persistent length for PEO can be calculated using:

$$C_\infty = \frac{2l_p}{l_b} \quad (6.4.5)$$

where l_p is the persistent length and l_b is the bond length.

From this a persistent length of 3.7\AA is calculated from a C_∞ value of 2.7 and l_b of 2.7\AA . This persistent length correlates perfectly with the experimental value of 3.7\AA for PEO by Flory and co-workers [55]. The persistent length for PPO homopolymers calculated from the characteristic ratio (Fig. 6.7) is 0.4nm . For PPO the atomistic model by Hezaveh et al. [53] gives a value of 0.375nm . The indication demonstrates that our

PPO homopolymer chain is stiffer hence more hydrophobic in water. However from experimental studies by Mortensen [6] it is said that the increase in molecular in PPO increases there is an increase in hydrophobicity for the PPO.

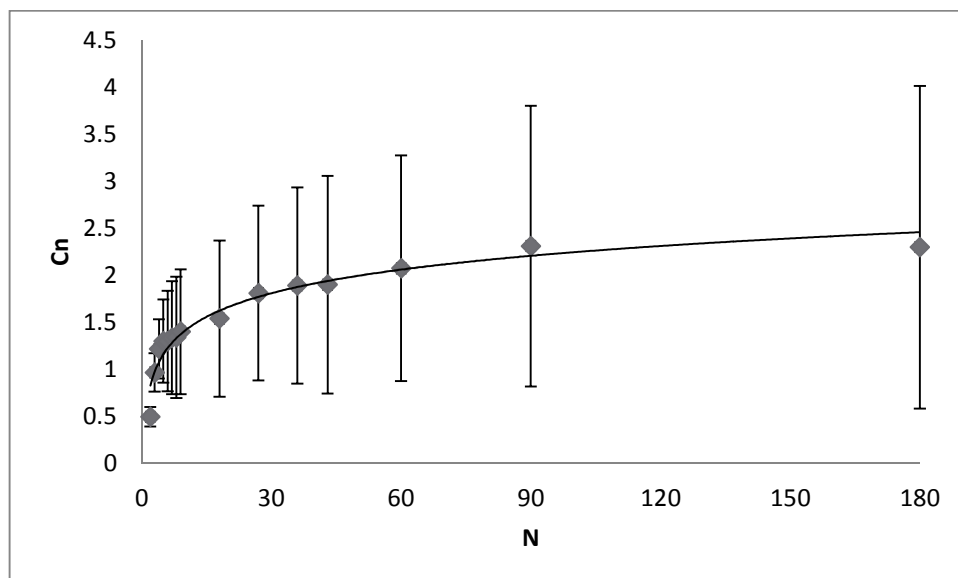


Figure 6.7: Flory characteristic ratio calculated from end to end distances versus the number of monomer of PPO using the MARTINI force field.

To further validate the model we tested the density of dimers of polyethylene oxide (PEO2) which we compared to all-atom simulations and experimental studies (Table 6.5). We saw excellent agreement between the MARTINI coarse grain model and the all atom model. Both the all-atom and coarse grain models agree reasonably within 10% agreement to experimental data [53].

Table 6.5: Bulk density data for PEO2

Bulk Density (kg m^{-3})	Experimental	OPLS-AA	Martini
PEO2	94.5 ± 5.3 [53]	84.88 ± 0.28	84.67 ± 0.58

Temperature transferability of the MARTINI model

The parameterisation process was carried out at 300K; so to test whether the force field parameters are transferable over a range of temperatures, the structure properties of the polymer i.e. the R_g was calculated in a wide temperature range.

Experimentally there are indications that both PEO and PPO are hydrophilic at low temperatures for example Mortensen has shown that at 278K both PEO and PPO exist as single polymer chains known as unimers, however at higher temperatures PPO becomes more hydrophobic [6]. So the first test we did was to check whether the temperature has any effects on our atomistic model and then compared the results with the CG ones assuming that the change in hydrophobic character of the homopolymers can be detected by a change in R_g value.

Table 6.6 and Fig. 6.8 compare the R_g values obtained from the atomistic and CG simulations over wide temperature range (10-60°C). The values obtained from the atomistic model (first column) shows that the average size of the chain increases slightly with the temperature at least up to $T=50$ C. The CG model, on the contrary, does not show any changes in R_g when varying the temperature and R_g oscillates around the same value.

Table 6.6: The radius of gyration (R_g) of PEO30 in all-atom simulations and MARTINI coarse grain simulations over a range of temperatures.

Temperature (°C)	Radius of gyration R_g (nm) OPLS-AA	Radius of gyration R_g (nm) MARTINI
10	0.860±0.163	0.919±0.174
20	0.863±0.177	0.900±0.146
30	0.870±0.162	0.923±0.152
40	0.939±0.170	0.919±0.150
50	0.940±0.182	0.922±0.164
60	0.929±0.173	0.918±0.153

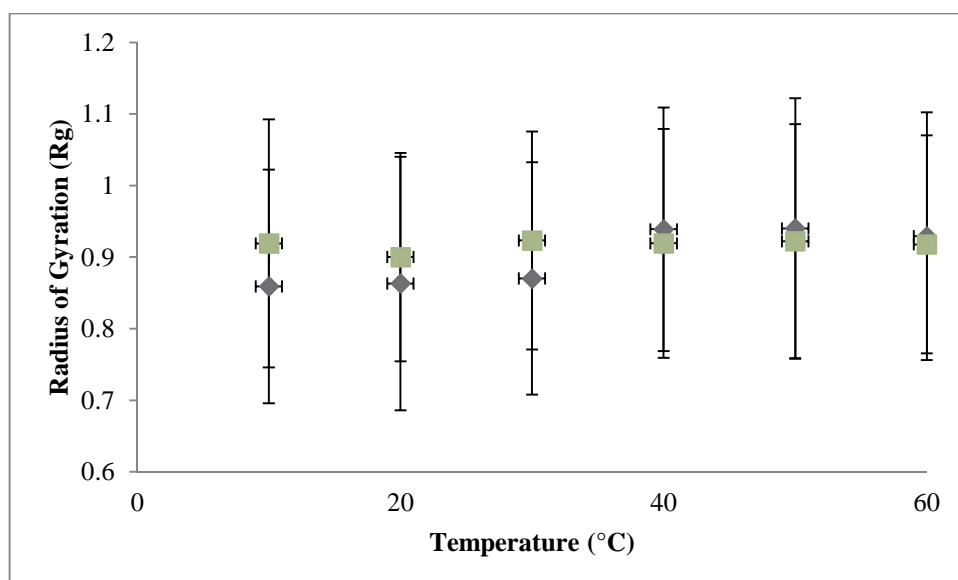


Figure 6.8: Temperature versus the radius of gyration (R_g) of PEO30 in all-atom simulations (diamonds) and MARTINI coarse grain simulations (squares).

The homopolymer PPO consisting of 30 monomers was also tested over a wide range of temperatures to observe the effect on the polymer chain (Fig. 6.9 and Table 6.7).

Table 6.7: The radius of gyration (R_g) of PPO30 in all-atom simulations and MARTINI coarse grain simulations over a range of temperatures.

Temperature (°C)	Radius of gyration R_g (nm)	
	OPLS-AA	MARTINI
10	0.980±0.159	0.968±0.174
20	0.972±0.163	0.979±0.186
30	0.980±0.143	1.01±0.179
40	0.974±0.155	1.03±0.173
50	0.981±0.150	0.998±0.183
60	0.993±0.143	1.02±0.178

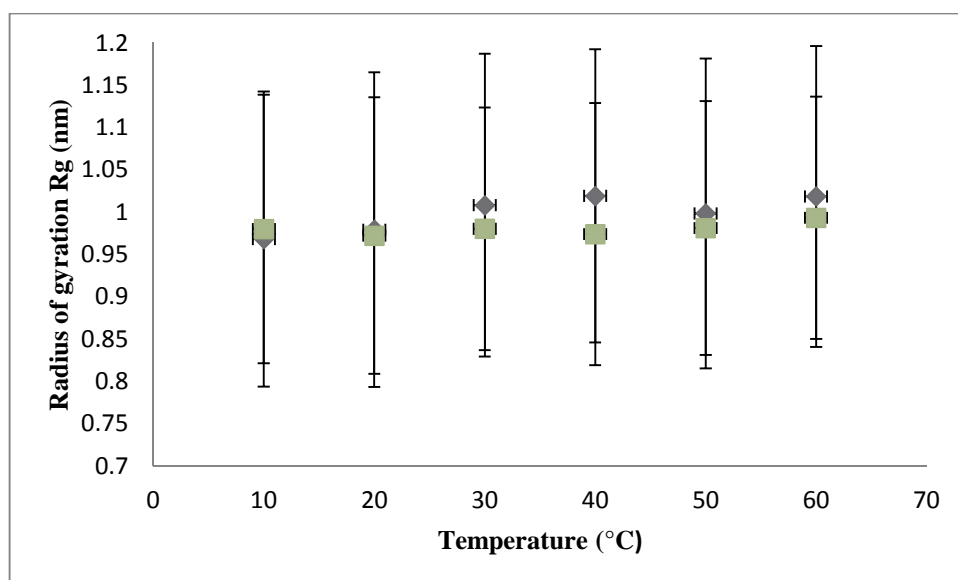


Figure 6.9: Temperature versus the radius of gyration (R_g) of PPO30 in all-atom simulations (squares) and MARTINI coarse grain simulations (diamonds).

As observed for the PEO MARTINI model, there is no significant changes in the polymer radius of gyration (R_g) value over the temperature range for the PPO MARTINI model. However in this case also the values obtained from atomistic model remain almost constant with increasing the temperature. These results might indicate that for the hydrophobic PPO polymer, the coarse grained force field can be used at temperature different than that used to develop it.

Transferability between different chemical environments

In the polymerisation process, the effect of solvents can play a major role. Depending on the chemical nature of the solvent, polymer chains can either collapse to a globule state or swell in an extended conformation depending on the quality of the solvent which is classified as a bad or good respectively. A theta solvent is when a polymer chain acts as an ideal chain, where effect of excluded volume expansion is cancelled out by the effect of the solvent.

The parameterization with the MARTINI force field has the advantage that several beads which might be used to represent solvents are already available. Although the parameterisation of our polymers is performed in water, we tested the transferability of the PPO homopolymer in hexane modelled by SC1 bead types from the original MARTINI parameterisation [32] and compared against all atom simulation data on

corresponding polymer chains (Table 6.8). The agreement between the MARTINI and all-atom model is very good and show that the force field is clearly transferable between different solvents.

Table 6.8: Radius of gyration (R_g) values for three different lengths of PPO in hexane for the all-atom and MARTINI coarse grain simulations.

R_g for PPO	OPLS-AA	MARTINI
30	0.957 ± 0.159	0.960 ± 0.159
60	1.10 ± 0.0366	1.14 ± 0.039
90	1.33 ± 0.049	1.30 ± 0.078

6.4.2 Pluronics

Structural properties

To validate the coarse grain force field, the parameters were tested on a number of low molecular weight Pluronics (L31, L61, L62 and L64) in water. The radius of gyration of a single chain of the copolymers simulated in water was calculated from both all-atom and coarse grain simulations (Table 6.9). Here it could clearly be seen that the radius of gyration obtained from the coarse grained Pluronics models compare very well with the corresponding an all-atom ones.

Table 6.9: Radius of gyration data for Pluronics at 300K.

R_g	OPLS-AA	MARTINI
L31	0.791 ± 0.088	0.905 ± 0.251
L61	1.16 ± 0.169	1.30 ± 0.251
L62	1.27 ± 0.169	1.33 ± 0.257
L64	1.37 ± 0.068	1.32 ± 0.198

Mortensen predicted that Pluronics unimers dissolved in water behave as a Gaussian chain at low temperatures [6]. To test this finding, the radius of gyration for the Pluronics was calculated using:

$$R_g = \sqrt{Nlb/6} \quad (6.4.8)$$

where N is the number of monomers in the Pluronics, l is the monomer length and b is the Kuhn length for the Pluronics, which corresponds to double the mean value from the PEO and PPO persistent length (7.6nm from our MARTINI models).

The radius of gyration values obtained from the calculations above (Eq. 6.4.8) were compared to radius of gyration values from all-atom simulations and the coarse grain force field developed (Fig. 6.10). It could be clearly seen that the Gaussian behaviour is in fact followed by the Pluronics as predicated Mortensen at low temperatures from experimental scattering data [6].

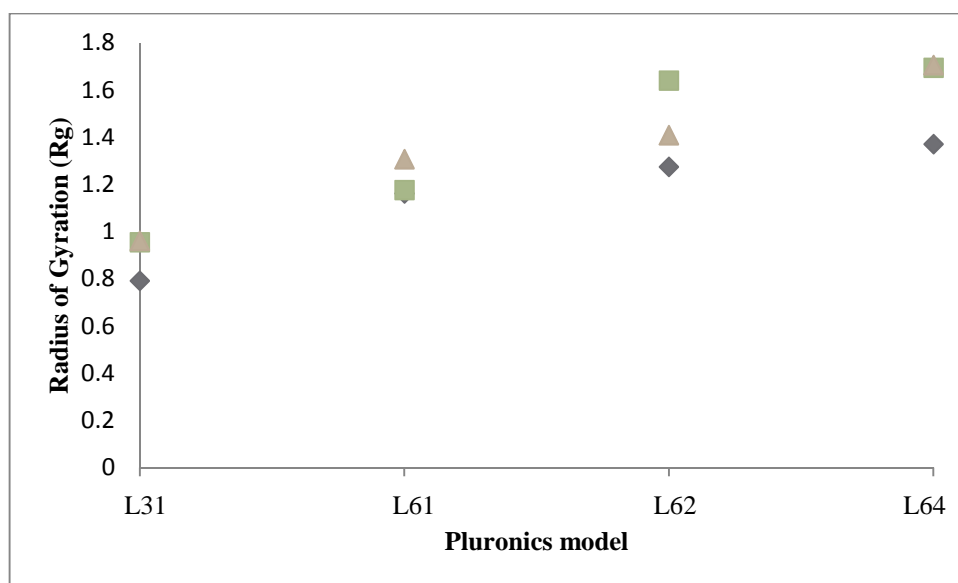


Figure 6.10: The radius of gyration (R_g) for four different Pluronics in solution (water) from atomistic simulations (diamonds), coarse grain simulations (squares) and Gaussian calculations (triangles).

Temperature Transferability

The temperature dependence of Pluronic copolymers can be sensitive at certain temperature affecting its structural properties and dependence on the type of micellar aggregates it will form [6]. The temperature transferability of the force field of the Pluronic CG model was tested over a wide range of temperatures and compared to corresponding atomistic simulations. It could be seen that there were some fluctuations in the R_g value for the larger Pluronic (L62 and L64); however the radius of gyration did not really change much for the smaller Pluronic (L31 and L61) over the range of temperatures tested. From the atomistic simulations (Fig. 6.11) it could be seen that the two largest Pluronic L62 and L64 show a slight decrease in radius of gyration at higher temperatures maybe indicating that the chain is collapsing. Whereas the Pluronic chains are not really affected in the MARTINI force field simulations as much (Fig. 6.12).

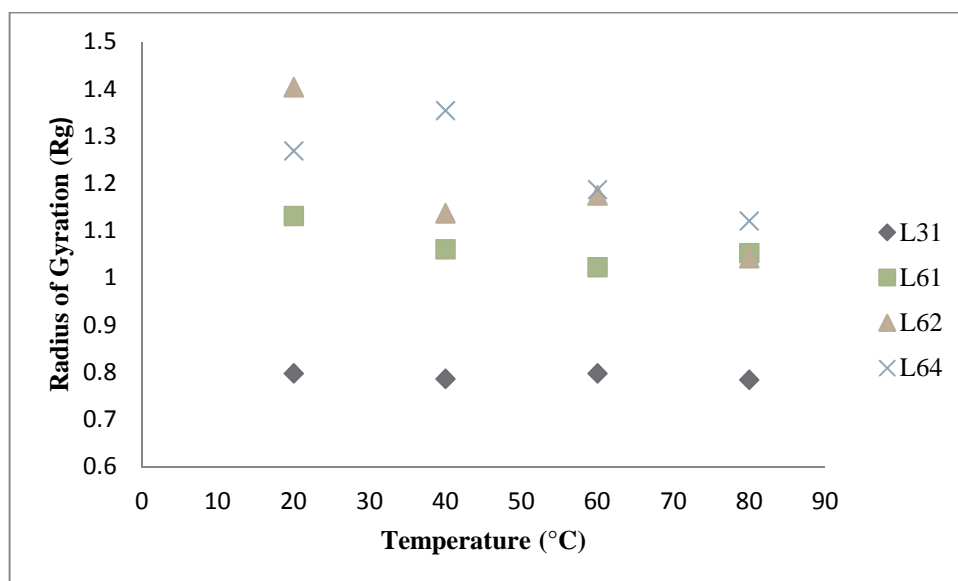


Figure 6.11: Temperature versus the radius of gyration (R_g) of four different Pluronic from all-atom simulations.

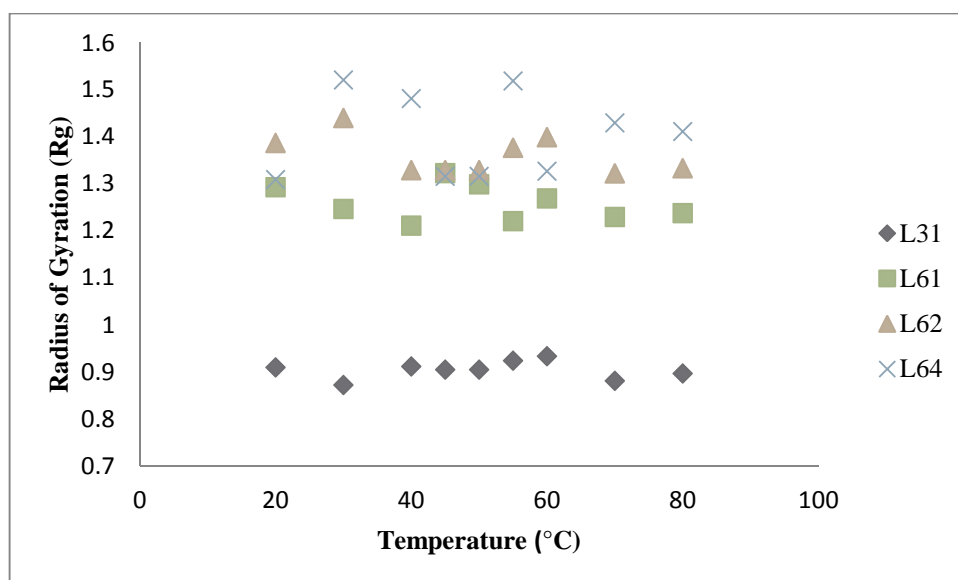


Figure 6.12: Temperature versus the radius of gyration (R_g) of four different Pluronic in the MARTINI coarse grain simulations.

6.5 Conclusion

In this work we have used the MARTINI force field to parameterize triblock copolymer Poly(ethylene oxide) (PEO) and poly(propylene oxide) (PPO) block copolymers (PEO–PPO–PEO) known as Pluronic. The strategy for the parameterization process has been proven to be a benchmark case for Pluronic of all sizes and conformations in solution. We validated the Pluronic model initially separately for the hydrophilic and hydrophobic PEO and PPO components comparing to experimental and all-atom simulation data. The PEO blocks have already been validated in a previous study by Rossi et al. [52], however further structural parameterisation has been performed to validate properties such as radius of gyration (R_g) scaling with the structure size factor to determine the Flory exponent, end to end distance to determine the persistent length. The transferability of the force field over a wide range of temperatures was also tested for the homopolymers showing no significant structural changes.

The PPO parameterisation involved targeting structural properties after suitably selecting a MARTINI bead type that correlates to the experimental free energy of transfer between octanol and water. The PPO structural validation included the matching the R_g of various lengths of homopolymer chains to reliable all-atom

simulations and enabled to calculate again the scaling structure size factor. The PPO homopolymer was tested in more than one chemical environment hence hexane as well as water showing that the R_g value also agreeing reasonably with corresponding all-atom simulations in hexane which proves that this polymer is transferable in solvents of different polarity.

The homopolymer parameters have then been used to build the MARTINI model for the Pluronics. The missing cross term for the PEO-PPO has been targeted to match atomistic bonded parameters. The procedure has shown to be robust as structural properties of different Pluronics match well with corresponding all-atom models. The temperature transferability for all the models including the homopolymer chains and Pluronics varying the temperature over a wide range has shown no effect on the structural results. The procedure to parameterize the Pluronics model in this study can be used to aid in parameterising many other possible polymer cases one may be interested in. The development of the Pluronics using the MARTINI force field shows extremely promising prospects as it is already very well developed for a range of biological macromolecules including lipid membranes. This can open to view future applications of the Pluronics with other matter of interest including biological membranes.

6.6 References

1. Gaspar, R. and R. Duncan, *Polymeric carriers: Preclinical safety and the regulatory implications for design and development of polymer therapeutics*. *Advanced Drug Delivery Reviews*, 2009. **61**(13): p. 1220-1231.
2. Discher, D.E. and F. Ahmed, *Polymersomes*. *Annual review of biomedical engineering*, 2006. **8**: p. 323-41.
3. Adams, M.L., A. Lavasanifar, and G.S. Kwon, *Amphiphilic block copolymers for drug delivery*. *Journal of Pharmaceutical Sciences*, 2003. **92**(7): p. 1343-1355.
4. Sriadibhatla, S., et al., *Transcriptional Activation of Gene Expression by Pluronic Block Copolymers in Stably and Transiently Transfected Cells*. *Mol Ther*, 2006. **13**(4): p. 804-813.

5. Batrakova, E.V., et al., *Effects of pluronic and doxorubicin on drug uptake, cellular metabolism, apoptosis and tumor inhibition in animal models of MDR cancers*. Journal of Controlled Release, 2010. **143**(3): p. 290-301.
6. Mortensen, K., *Structural studies of aqueous solutions of PEO - PPO - PEO triblock copolymers, their micellar aggregates and mesophases; a small-angle neutron scattering study*. Journal of Physics: Condensed Matter, 1996. **8**(25A): p. A103.
7. Mortensen, K., *Cubic Phase in a Connected Micellar Network of Poly(propylene oxide)–Poly(ethylene oxide)–Poly(propylene oxide) Triblock Copolymers in Water*. Macromolecules, 1997. **30**(3): p. 503-507.
8. Mortensen, K., W. Batsberg, and S. Hvidt, *Effects of PEO–PPO Diblock Impurities on the Cubic Structure of Aqueous PEO–PPO–PEO Pluronic Micelles: fcc and bcc Ordered Structures in F127*. Macromolecules, 2008. **41**(5): p. 1720-1727.
9. Mortensen, K. and Y. Talmon, *Cryo-TEM and SANS Microstructural Study of Pluronic Polymer Solutions*. Macromolecules, 1995. **28**(26): p. 8829-8834.
10. Alexandridis, P., T. Nivaggioli, and T.A. Hatton, *Temperature Effects on Structural Properties of Pluronic P104 and F108 PEO-PPO-PEO Block Copolymer Solutions*. Langmuir, 1995. **11**(5): p. 1468-1476.
11. Pedersen, J.S. and M.C. Gerstenberg, *The structure of P85 Pluronic block copolymer micelles determined by small-angle neutron scattering*. Colloids and Surfaces A: Physicochemical and Engineering Aspects, 2003. **213**(2–3): p. 175-187.
12. Svaneborg, C. and J.S. Pedersen, *Form Factors of Block Copolymer Micelles with Excluded-Volume Interactions of the Corona Chains Determined by Monte Carlo Simulations*. Macromolecules, 2001. **35**(3): p. 1028-1037.
13. Redhead, M., et al., *Relationship between the Affinity of PEO-PPO-PEO Block Copolymers for Biological Membranes and Their Cellular Effects*. Pharmaceutical Research: p. 1-11.
14. Srinivas, G., D.E. Discher, and M.L. Klein, Nat. Mater., 2004. **3**: p. 638.
15. Schmid, F., *Toy amphiphiles on the computer: What can we learn from generic models?* Macromolecular Rapid Communications, 2009. **30**(9-10): p. 741-751.
16. Daoulas, K. and M. Müller, *Comparison of Simulations of Lipid Membranes with Membranes of Block Copolymers Polymer Membranes/Biomembranes*, W.P. Meier and W. Knoll, Editors. 2010, Springer Berlin / Heidelberg. p. 43-85.

17. Sevink, G.J.A. and A.V. Zvelindovsky, *Self-Assembly of Complex Vesicles*. *Macromolecules*, 2005. **38**(17): p. 7502-7513.
18. Linse, P., *Adsorption and phase behaviour of Pluronic block copolymers in aqueous solution*. *Colloids and Surfaces A: Physicochemical and Engineering Aspects*, 1994. **86**(0): p. 137-142.
19. Hatakeyama, M. and R. Faller, *Coarse-grained simulations of ABA amphiphilic triblock copolymer solutions in thin films*. *Physical Chemistry Chemical Physics*, 2007. **9**(33): p. 4662-4672.
20. Nawaz, S., et al., *Interactions of PEO-PPO-PEO block copolymers with lipid membranes: a computational and experimental study linking membrane lysis with polymer structure*. *Soft Matter*, 2012.
21. Carbone, P., et al., *Transferability of coarse-grained force fields: The polymer case*. *The Journal of Chemical Physics*, 2008. **128**(6): p. 064904.
22. Milano, G. and F. Müller-Plathe, *Mapping Atomistic Simulations to Mesoscopic Models: A Systematic Coarse-Graining Procedure for Vinyl Polymer Chains*. *The Journal of Physical Chemistry B*, 2005. **109**(39): p. 18609-18619.
23. Sun, Q. and R. Faller, *Systematic coarse-graining of atomistic models for simulation of polymeric systems*. *Computers & Chemical Engineering*, 2005. **29**(11–12): p. 2380-2385.
24. Bedrov, D., C. Ayyagari, and G.D. Smith, *Multiscale Modeling of Poly(ethylene oxide)–Poly(propylene oxide)–Poly(ethylene oxide) Triblock Copolymer Micelles in Aqueous Solution*. *Journal of Chemical Theory and Computation*, 2006. **2**(3): p. 598-606.
25. Qian, H.-J., et al., *Temperature-Transferable Coarse-Grained Potentials for Ethylbenzene, Polystyrene, and Their Mixtures*. *Macromolecules*, 2008. **41**(24): p. 9919-9929.
26. Sun, Q., F.R. Pon, and R. Faller, *Multiscale modeling of polystyrene in various environments*. *Fluid Phase Equilibria*, 2007. **261**(1–2): p. 35-40.
27. Reith, D., et al., *How does the chain extension of poly (acrylic acid) scale in aqueous solution? A combined study with light scattering and computer simulation*. *The Journal of Chemical Physics*, 2002. **116**(20): p. 9100-9106.
28. Nielsen, S.O., et al., *A coarse grain model for n-alkanes parameterized from surface tension data*. *The Journal of Chemical Physics*, 2003. **119**(14): p. 7043-7049.

29. Shelley, J.C., et al., *A Coarse Grain Model for Phospholipid Simulations*. The Journal of Physical Chemistry B, 2001. **105**(19): p. 4464-4470.
30. Funasaki, N., et al., *Intramolecular hydrophobic association of two alkyl chains of oligoethylene glycol diethers and diesters in water*. The Journal of Physical Chemistry, 1984. **88**(24): p. 5786-5790.
31. Marrink, S.J., A.H. de Vries, and A.E. Mark, *Coarse Grained Model for Semiquantitative Lipid Simulations*. The Journal of Physical Chemistry B, 2003. **108**(2): p. 750-760.
32. Marrink, S.J., et al., *The MARTINI Force Field: Coarse Grained Model for Biomolecular Simulations*. The Journal of Physical Chemistry B, 2007. **111**(27): p. 7812-7824.
33. Monticelli, L., et al., *The MARTINI Coarse-Grained Force Field: Extension to Proteins*. Journal of Chemical Theory and Computation, 2008. **4**(5): p. 819-834.
34. López, C.A., et al., *Martini Coarse-Grained Force Field: Extension to Carbohydrates*. Journal of Chemical Theory and Computation, 2009. **5**(12): p. 3195-3210.
35. Wong-Ekkabut, J., et al., *Computer simulation study of fullerene translocation through lipid membranes*. Nat Nano, 2008. **3**(6): p. 363-368.
36. Rossi, G., et al., *Coarse-graining polymers with the MARTINI force-field: polystyrene as a benchmark case*. Soft Matter, 2011. **7**(2): p. 698-708.
37. Lee, H., et al., *A Coarse-Grained Model for Polyethylene Oxide and Polyethylene Glycol: Conformation and Hydrodynamics*. The Journal of Physical Chemistry B, 2009. **113**(40): p. 13186-13194.
38. Glattli, A., X. Daura, and W.F.v. Gunsteren, *Derivation of an improved simple point charge model for liquid water: SPC/A and SPC/L*. The Journal of Chemical Physics, 2002. **116**(22): p. 9811-9828.
39. Jorgensen, W.L. and D.L. Severance, *Aromatic-aromatic interactions: free energy profiles for the benzene dimer in water, chloroform, and liquid benzene*. Journal of the American Chemical Society, 1990. **112**(12): p. 4768-4774.
40. D. van der Spoel, E.L., B. Hess, A. R. van Buuren, E. Apol, P. J. Meulenhoff,, A.L.T.M.S. D. P. Tieleman, K. A. Feenstra, R. van Drunen and H. J. C., and Berendsen, *Gromacs User Manual version 4.5.4*, 2010.
41. Hess, B., et al., *LINCS: A linear constraint solver for molecular simulations*. Journal of Computational Chemistry, 1997. **18**(12): p. 1463-1472.

42. Darden, T., D. York, and L. Pedersen, *Particle mesh Ewald: An N [center-dot] $\log(N)$ method for Ewald sums in large systems*. The Journal of Chemical Physics, 1993. **98**(12): p. 10089-10092.
43. Essmann, U., et al., *A smooth particle mesh Ewald method*. The Journal of Chemical Physics, 1995. **103**(19): p. 8577-8593.
44. Berendsen, H.J.C., et al., *Molecular dynamics with coupling to an external bath*. The Journal of Chemical Physics, 1984. **81**(8): p. 3684-3690.
45. Murtola, T., et al., *Conformational analysis of lipid molecules by self-organizing maps*. The Journal of Chemical Physics, 2007. **126**(5): p. 054707.
46. Zhang, Z., et al., *A Systematic Methodology for Defining Coarse-Grained Sites in Large Biomolecules*. Biophysical Journal, 2008. **95**(11): p. 5073-5083.
47. Zhang, Z., et al., *Defining Coarse-Grained Representations of Large Biomolecules and Biomolecular Complexes from Elastic Network Models*. Biophysical Journal, 2009. **97**(8): p. 2327-2337.
48. Fraccalvieri, D., *Comparison of protein dynamics: a new methodology based on self-organizing maps*, 2011.
49. Fraccalvieri, D., et al., *Conformational and functional analysis of molecular dynamics trajectories by Self-Organising Maps*. BMC Bioinformatics, 2011. **12**(1): p. 158.
50. Sangster, J., *Octanol-Water Partition Coefficients: Fundamentals and Physical Chemistry*, ed. Wiley. 1997, Chichester, U.K./New York.
51. Chemicalland21. www.chemicalland21.com. 2012.
52. Rossi, G., et al., *A Coarse-Grained Martini Model of Polyethylene Glycol and of Polyoxyethylene Alkyl Ether Surfactants*. The Journal of Physical Chemistry B, 2012.
53. Hezaveh, S., et al., *Molecular dynamics simulation study of solvent effects on conformation and dynamics of polyethylene oxide and polypropylene oxide chains in water and in common organic solvents*. The Journal of Chemical Physics, 2012. **136**(12): p. 124901.
54. Srinivas, G., D.E. Discher, and M.L. Klein, *Self-assembly and properties of diblock copolymers by coarse-grain molecular dynamics*. Nat Mater, 2004. **3**(9): p. 638-644.
55. Mark, J.E. and P.J. Flory, *The Configuration of the Polyoxyethylene Chain*. Journal of the American Chemical Society, 1965. **87**(7): p. 1415-1423.

Conclusions and Future Work

This chapter is split into two main sections: the first part summarizes the conclusions drawn from the atomistic MD simulations, highlights their limitations and reviews the validation of a newly coarse grained model for a particular family of polymers namely Pluronics. The second part of this chapter suggests some promising future research directions that the work presented in this thesis has opened.

7.1 Conclusions

This thesis focuses on the importance of using MD simulation methods to investigate the structural and dynamical behaviour of technological and biological relevant polymeric materials at soft (water/air, lipid membrane/water) interfaces. Due to the complexity of the systems simulated, a multiscale approach has been developed where the limitations and advantages of using atomistic or coarser models are highlighted. Depending on the system properties under scrutiny, all-atom, united-atom and coarse-grained models have been utilized throughout this thesis.

All-atom molecular dynamics simulations are used in chapter 3 in order to evaluate the stability of alkyl modified polyamino-amide dendrimers (PAMAM) of various topological structures at the air/water interface. The stability of the molecule at the interface was interpreted in terms of particle wettability and energy components. The agreement with theoretical predictions on the particle orientation and particle shape was also established. For this project the need of using molecular dynamics simulations at an all-atom level was clear, as it provided the detailed information (formation and breakage of hydrogen bonds) about the energy gain which drives the migration of the particle to the interface. From the simulation results it could be anticipated that fully functionalised molecules might show increased stability in comparison to semi-functionalised molecules when they self-assemble into monolayer at the air/water interface.

The importance of molecular dynamics simulations used for studying biological matter has become more apparent in last decade. The advances in computational power enable simulations to aid in the determination and reasoning of complex issues

occurring within these systems. Biological membranes are a fundamental component in living matter whose behaviour needs to be understood at a molecular level in order to design biocompatible materials. Molecular simulations can provide information about the dynamics and structure of the system which cannot be seen with any experimental techniques. Chapter 4 and 5 study the structure of a popular class of block copolymers known as Pluronics and their interactions with biological membranes. A mild level of coarse-graining, united atom model is used in this case due to the complexity of the system under investigation. Although the hydrogen bonds in the united atom force field might be slightly compromised, the reality of molecular interactions between the Pluronics and model membranes are still very much visible. The effect of molecular weight and ratio of hydrophobic to hydrophilic content on the stability of biological membranes is compared to experimental data showing the cytotoxic effects on cell membranes. Molecular dynamics simulations validate experimental claims on Pluronics rupturing cell membranes depending on their microstructure. The findings from this study will aid in the design of amphiphilic block copolymers with reduced cytotoxicity effects, which can then be used as drug delivery nanodevices.

The experimental study of Pluronics with biological membranes in chapter 5 shows the nature of the interaction of these triblock copolymers with cell membranes and the mechanisms behind their cellular response varying the copolymers chemical composition. This experimental study correlates perfectly with the atomistic molecular dynamics study in chapter 4, suggesting the link between the affinity of certain Pluronics and biological membranes and their cellular adverse effects. A clear mechanism behind the biological effects of Pluronic copolymers and possible contribution towards safety in drug design has been elucidated. Here, however the limitation of the use of an atomistic model appeared clear. The polymer concentration that can be modelled with such high resolution model is in fact unrealistically slow and the resort of a coarser model will be necessary for a reliable comparison with the experimental conditions.

Therefore, although atomistic molecular dynamics simulations have the advantage of gaining insight into a molecular system in relatively high resolution, a reduction in the models complexity has to be compromised. In chapter 6, the development of a coarse grain model for Pluronics using the MARTINI force field approach [1] is validated. The MARTINI coarse grain model developed is able to reproduce structural properties of copolymers of any size polymer regardless of the amphiphilicity. The model is validated against experimental and atomistic structural and

thermodynamic data. This model holds extremely promising prospects for future work described in the next section.

7.2 Future Work

The possible avenues for future work are immense; therefore the possible ideas discussed here are by no means exhaustive. Molecular dynamics simulations at an atomistic level itself can yet explore many more aspects of detail. Some routes of the possible research are already in practice by the author and other authors interested in this field. The development of the coarse grain model for Pluronics has also opened many doors in which a range of mechanisms and issues can be addressed. In this section, a few of the possible proposals that can be made from the outcome of the research in this thesis are outlined.

7.2.1 Atomistic Studies

The atomistic simulations of the amphiphilic dendrimers at the air/water interface have clearly identified the possible outcomes from their stability depending on the degree of modification. The self-assembly of these molecules at the air/water interface into monolayers can be one possible study of interest to further validate our claim on the stability of fully modified and partially modified dendrimers. To equilibrate such structures is not an easy task, and to be able to fill this gap in the literature can provide a sophisticated explanation to further their uses in biological and technological matter [2].

Atomistic molecular dynamics simulations of Pluronics varying the molecular weight and amphiphilicity fully adsorbed into a model membrane and their effects on the internal structure of the membrane has been identified in chapter 3. To evaluate the insertion mechanism of these Pluronic copolymers from the aqueous phase translocating across the membrane, can benefit in providing further knowledge from the effect of the copolymers moving across the interfaces. The effect of more than one copolymer chain on the system is another interesting phenomenon for future work observing interactions between themselves and the membrane. This work is currently in progress with preliminary results already existent.

7.2.2 Coarse-grain Model

The coarse grain model for Pluronics developed in chapter 6 opens many areas of research for which molecular dynamics simulations can be further used to study block copolymers. One area of research for the Pluronic coarse grain model is to determine the self-assembly process of these amphiphilic copolymers, identifying the molecular mechanism underpinning it. To construct a phase diagram of the Pluronics, illustrating the molecular properties associated to the copolymer in this process, can definitely fill a part in the literature, clarifying experimental observations [3]. The interactions of the Pluronic self-assembled microstructures with biological membranes at a larger scale than the ones used in the atomistic simulations [4] may also be observed at a coarse grain level. This can assist in further recognising the molecular interaction associated with experimental results seen in vitro, where larger molecular weight block copolymers have shown to perturb the membrane [5].

7.3 References

1. Marrink, S.J., et al., *The MARTINI Force Field: Coarse Grained Model for Biomolecular Simulations*. The Journal of Physical Chemistry B, 2007. **111**(27): p. 7812-7824.
2. Bo, Z., et al., *The synthesis of dendrimers bearing alkyl chains and their behavior at air-water interface*. Polymer Bulletin, 1997. **38**(3): p. 257-264.
3. Zhang, K. and A. Khan, *Phase Behavior of Poly(ethylene oxide)-Poly(propylene oxide)-Poly(ethylene oxide) Triblock Copolymers in Water*. Macromolecules, 1995. **28**(11): p. 3807-3812.
4. Nawaz, S., et al., *Interactions of PEO-PPO-PEO block copolymers with lipid membranes: a computational and experimental study linking membrane lysis with polymer structure*. Soft Matter, 2012.
5. Redhead, M., et al., *Relationship between the Affinity of PEO-PPO-PEO Block Copolymers for Biological Membranes and Their Cellular Effects*. Pharmaceutical Research, 2012. **29**(7): p. 1908-1918.

Appendix A

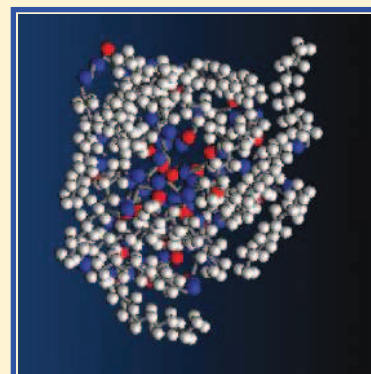
Reprint: Stability of Amphiphilic Dendrimers at the Water/Air Interface

Stability of Amphiphilic Dendrimers at the Water/Air Interface

Selina Nawaz and Paola Carbone*

School of Chemical Engineering and Analytical Science, The University of Manchester, Oxford Road, M13 9PL, United Kingdom

ABSTRACT: By means of atomistic molecular dynamics simulations, we investigate the structure and stability of alkyl-modified polyamido-amide (PAMAM) dendrimers at the air/water interface as a function of the number and the relative position of the modified end groups. We find that the PAMAM dendrimer with all terminal groups functionalized is more stable at the interface than the Janus dendrimer where only half the amine groups are modified. This result is explained in terms of softness of the dendrimer molecule which adapts its conformation to maximize the favorable amide–water contacts segregating the alkyl chains and increasing the structural order of the “hydrophilic core”. We interpret the stability of the molecule at the interface also in terms of particle wettability and energy components. We verify that the atomistic model follows the prediction of the thermodynamic analytical theory adopting an oblate or prolate shape and orientating its longest axis parallel to the normal to the interface. These results indicate that monolayers of fully functionalized molecules could be as stable as (or more stable than) those self-assembled from proper Janus molecules.



INTRODUCTION

In recent years, amphiphilic dendrimers have shown to be promising building blocks for a large range of interfacial materials. In fact, tailor-made dendrimers show interesting self-assembly properties when strong dispersive, polar, or hydrogen bonding intermolecular forces are present.^{1,2} In particular, alkyl-modified hydrophilic dendrimers such as poly(amino amide) (PAMAM) or poly(propylene imine) form a Langmuir–Blodgett monolayer at the surface or interface that, due to the large number of functionalities present in their hydrophilic core, can show high stability. Indeed, amphiphilic dendrimers can bind at the interface more efficiently than classical surfactants, and because of dendrimers' unique topology, their monolayers find a wide number of applications such as surface-based sensors or surface nanopatterning.^{3,4} Recently, the physical characterization of the Langmuir–Blodgett monolayer formed at the air–water interface by amphiphilic PAMAMs fully functionalized with long aliphatic chains has been the subject of intensive experimental investigations.^{5–7} Amphiphilic dendrimers can also self-assemble in aqueous media forming micelles whose stability is a function of the shape of the functionalized dendrimer molecules.² Moreover, through a specific synthetic route, dendrimers can also be modified targeting specifically one side of the molecule. This type of synthetic procedure allows the preparation of amphiphilic “Janus” dendrimers, where the hydrophobic chains are attached only to part of the end monomers, breaking the symmetry of the macromolecule (see Figure 1).^{8–11} In this case, the bipolar nature of the molecules allows the formation in water of a large variety of self-assembled structures that can be exploited for several applications such as encapsulation or delivery of drugs. The Janus dendrimers can be seen as an example of a Janus nanoparticle whose properties and applications have been foreseen as very innovative due to the dual nature of the particle that, especially at interfaces, can bind different substrates.¹²

Computer simulations can help in predicting the behavior of amphiphilic molecules both in bulk and at the interface. Using simplified models, it is possible for example to calculate the free energy profile of ideal nanoparticles at the interface, predicting their stability as a function of shape, orientation, and distance from the interface.^{13–15} Similar simplified models have also been used to study the strength of the interaction between a spherical model Janus nanoparticle at an ideal fluid interface studying how the particle–interface stability is controlled by changing the difference in affinities between the two particle regions and their relative sizes.¹⁶ Moreover, in the particular case of dendrimers, using simplified models it has been predicted that amphiphilic dendrimers interacting via a purely repulsive Gaussian potential crystallize into a cubic lattice with density-independent lattice constants.¹⁷ However, while simplified models are very useful to gain properties common to a large family of molecules,¹⁸ atomistic models are needed when one wants to investigate the specific chemical interactions responsible, for example, for molecular aggregation¹⁹ or intramolecular rearrangements.^{19,20} Despite this, besides the simplified models that idealize the nanoparticle as a compact impenetrable sphere, simulations of nanoparticles at the interface that use an atomistic description of molecules are almost absent in the literature. The only work we are aware of is that of Tay and Bresme²¹ who reported the results of atomistic molecular dynamics simulations performed on an alkythiol passivated gold nanoparticle adsorbed at the air–water interface predicting the contact angle, particle shape, and orientational order of the water molecules.

Received: June 22, 2011

Revised: August 19, 2011

Published: September 14, 2011

Reprint: Interactions of PEO-PPO-PEO block copolymers with lipid membranes: a computational and experimental study linking membrane lysis with polymer structure

Cite this: *Soft Matter*, 2012, **8**, 6744

www.rsc.org/softmatter

PAPER

Interactions of PEO–PPO–PEO block copolymers with lipid membranes: a computational and experimental study linking membrane lysis with polymer structure†

Selina Nawaz,^a Martin Redhead,^b Giuseppe Mantovani,^b Cameron Alexander,^b Cynthia Bosquillon^b and Paola Carbone^{*a}

Received 13th February 2012, Accepted 13th April 2012

DOI: 10.1039/c2sm25327e

Poly(ethylene oxide) (PEO) and poly(propylene oxide) (PPO) block co-polymers (PEO–PPO–PEO, sold as Pluronics, Poloxamers, Tetronics) are a widely used class of amphiphilic materials for different biological applications. In fact for certain members of the Pluronics series, the interactions of block segments with living cells alter the lipid membrane properties and facilitate the permeation of drugs. A fuller understanding of the molecular mechanisms underpinning these interactions is essential for ensuring their safety and efficacy in biomedical applications and to inform the design of new amphiphilic copolymers for potential use in a clinical setting. In this paper, by means of atomistic molecular dynamics simulations and membrane lysis assays, we investigate the relationship between the molecular conformations of a subset of the Pluronic copolymers (L31, L61, L62 and L64) and their haemolytic activity. Our computational studies suggest that the hydrophilic blocks in these copolymers interact with the polar head groups of lipid molecules, resulting in a predicted modification of the structure of the membranes. Parallel membrane lysis assays in human erythrocytes indicate differences in the rates of haemolysis, as a result of incubation with these polymers, that correlate well with the predicted interactions from the atomistic simulations. The computational data thus provide a putative mechanism to rationalize the available experimental data on membrane lysis by these copolymers and quantitatively agree with haemoglobin release endpoints measured when copolymers with the same molecular weight and structure as of those modelled are incubated with erythrocytes. The data further suggest some new structure–function relationships at the nanoscale that are likely to be of importance in determining the biological activity of these otherwise inert copolymers.

Introduction

The development of self-assembled nanostructures formed by amphiphilic macromolecules and their evaluation as nano-devices or as means to alter the cell membrane properties have dramatically increased in recent years.^{1,2} Such amphiphiles can interact strongly with the cell membrane and, depending on their concentration and molecular structure, modify its mechanical properties.³ Block copolymers sold as PluronicsTM are a specific class of triblock amphiphilic copolymers whose structure consists of hydrophilic, poly(ethylene oxide) (PEO), and hydrophobic, poly(propylene oxide) (PPO), blocks arranged in an A–B–A (PEO–PPO–PEO) tri-block structure. These polymers can be

used as surface coating for nanoparticles,⁴ or, exploiting their ability to self-assemble in polar solvents, as drug or gene “nano carriers”.^{5,6} Recently, some PEO–PPO–PEO copolymers within the Pluronic class also have been shown to elicit biological responses both *in vitro* and *in vivo* increasing the susceptibility of multi-drug resistant cancer cells to chemotherapeutic agents such as doxorubicin⁷ and in enhancing gene transcription.⁸ Because these copolymers are designed to interact with and target specific organs within the human body, it is important to understand the molecular mechanism underpinning their association with lipid bilayers in order to avoid toxicity and to inform future rational polymer design. Although numerous experimental studies have been conducted to understand the association and incorporation of selected Pluronics with the lipid membrane, a detailed picture of the interaction mechanism has not been achieved. Indeed, the complex interplay between the chemical interactions can be assessed by the fact that experimental studies employing different models of the lipid membrane such as monolayers,⁹ bilayers¹⁰ or unilamellar vesicles¹¹ have shown contradictory results. The data have suggested that in some cases the amphiphilic copolymers

^aSchool of Chemical Engineering and Analytical Science, The University of Manchester, Oxford Road, M13 9PL Manchester, UK. E-mail: paola.carbone@manchester.ac.uk

^bDivision of Drug Delivery & Tissue Engineering, School of Pharmacy, University of Nottingham, NG7 2RD Nottingham, UK

† Electronic supplementary information (ESI) available. See DOI: 10.1039/c2sm25327e

Reprint: Biological Effects of PEO-PPO-PEO Block Copolymers: Relationship between Polymer Composition and their Interactions with Biological Membranes

Relationship between the Affinity of PEO-PPO-PEO Block Copolymers for Biological Membranes and Their Cellular Effects

Martin Redhead · Giuseppe Mantovani · Selina Nawaz · Paola Carbone · Dariusz C. Gorecki · Cameron Alexander · Cynthia Bosquillon

Received: 10 January 2012 / Accepted: 20 February 2012 / Published online: 3 March 2012
© Springer Science+Business Media, LLC 2012

ABSTRACT

Purpose The interactions of poly(ethylene oxide)-co-poly(propylene oxide) tri-block copolymers (PEO-PPO-PEO block copolymers, Pluronic®, Synperonic®, Poloxamers) of differing chemical composition with cell membranes were systematically investigated in order to clarify the mechanisms behind their previously reported various cellular responses.

Methods Relationships between the structural components of a defined series of PEO-PPO-PEO block copolymers and i) their interactions with biological membranes; ii) their cytotoxic potential were probed using a combination of haemolysis studies and cytotoxicity assays in the Caco-2 and HMEC-1 cell lines.

Results The length of the PPO block as well as the PEO/PPO ratio were determinants of their membrane binding constant and cytotoxicity endpoints measured in the MTS and LDH assays. Similar 2D parabolic relationships were found between polymer composition and their affinity for membranes or their cytotoxicity potential. Cytotoxicity was related to the ability of the copolymers to form ion transversable pores within the cell membrane.

Conclusions The data suggest a link between the affinity of certain Pluronic for biological membranes and their cellular adverse effects. This first cell-based investigation of the interactions of Pluronic with biological membranes is an important step towards unravelling the complex mechanisms which govern the biological effects of widely used amphiphilic materials.

KEY WORDS biocompatibility · drug delivery · haemolysis · membrane · pluronic

INTRODUCTION

PEO-PPO-PEO block copolymers (synonyms: Pluronic®, Synperonic®, Poloxamers) are ABA triblock copolymers, with a central hydrophobic poly(propylene oxide) (PPO) block flanked by two hydrophilic poly(ethylene oxide) (PEO) blocks. In solution, PEO-PPO-PEO block copolymers can assemble into micelles, with the PPO blocks forming a hydrophobic core and the PEO blocks the surrounding hydrophilic corona (1). The hydrophobic core of these micelles can be used to incorporate poorly water soluble drugs, and thus improve their pharmacokinetics and biodistribution (2,3).

Although PEO-PPO-PEO block copolymers are widely used and many are essentially inert to biological substrates, materials within the overall class have recently been reported to elicit marked biological responses, both *in vitro* and *in vivo*. Copolymers of differing chemical composition have displayed varying cytotoxicity profiles, as well as therapeutically desirable effects (4,5). For instance, they have the

Electronic supplementary material The online version of this article (doi:10.1007/s11095-012-0716-6) contains supplementary material, which is available to authorized users.

M. Redhead · G. Mantovani · C. Alexander · C. Bosquillon
Division of Drug Delivery and Tissue Engineering, School of Pharmacy
University of Nottingham
University Park, Nottingham NG7 2RD, UK

S. Nawaz · P. Carbone
School of Chemical Engineering and Analytical Science
The University of Manchester
Oxford Road, M13 9PL, Manchester, UK

D. C. Gorecki
School of Pharmacy and Biomedical Sciences
University of Portsmouth
White Swan Road, Portsmouth PO1 2DT, UK

C. Bosquillon (✉)
School of Pharmacy, Centre for Biomolecular Sciences
University of Nottingham
University Park, Nottingham NG7 2RD, UK
e-mail: cynthia.bosquillon@nottingham.ac.uk

Appendix D

Radius of gyration values for PEO and PPO homopolymers

Number of PEO Monomers	Radius of gyration Rg (nm) MARTINI
2	0.131±0.00563
3	0.199±0.00647
4	0.250±0.0125
5	0.285±0.0233
6	0.315±0.0317
7	0.341±0.0390
8	0.363±0.0445
9	0.397±0.0534
18	0.707±0.0161
27	0.857±0.092
36	0.981±0.133
43	1.049±0.198
30	0.831±0.111
60	1.34±0.206
90	1.71±0.285
180	2.77±0.486

Number of PPO Monomers	Radius of gyration Rg (nm) MARTINI
2	0.176±0.00544
3	0.261±0.0115
4	0.328±0.0210
5	0.383±0.0351
6	0.430±0.0487
7	0.469±0.0627
8	0.509±0.0747
9	0.539±0.0845
18	0.804±0.149
27	1.049±0.196
36	1.148±0.234
43	1.331±0.305

